공학박사 학위논문

Anti-Fouling Ultrafiltration/Microfiltration (UF/MF) Membranes Based on Interfacial Assembly of Functional Materials to Membrane Surface

계면결합을 통해 기능성 재료들을 표면에 도입시킨

내파울링 기능성 한외/정밀여과 분리막에 관한 연구

2016년 8월

서울대학교 대학원

재료공학부

박 성 용

Anti-Fouling Ultrafiltration/Microfiltration (UF/MF) Membranes Based on Interfacial Assembly of Functional Materials to Membrane Surface

계면결합을 통해 기능성 재료들을 표면에 도입시킨
내파울링 기능성 한외/정밀여과 분리막에 관한 연구

지도교수 곽 승 엽

이 논문을 공학박사 학위논문으로 제출함

2016년 4월

서울대학교 대학원
재료공학부
박 성 용

박성용의 공학박사 학위논문을 인준함

2016년 6월

위 원 장 장 지 영 (인)
부위원장 곽 승 엽 (인)
위 원 안 철 희 (인)
위 원 정 재 우 (인)
위 원 김 종 표 (인)

Abstract

Anti-Fouling Ultrafiltration/Microfiltration (UF/MF) Membranes Based on Interfacial Assembly of Functional Materials to Membrane Surface

Sung Yong Park

Department of Materials Science and Engineering

The Graduate School

Seoul National University

Membrane filtration processes are a relatively simple and cost-effective method to obtain high-quality purified water. Membrane processes are typically classified into four categories *i.e.*, reverse osmosis (RO), nanofiltration (NF), ultrafiltration (UF) and microfiltration (MF) by their pore size and operation pressure. Among them, UF and MF processes have been widely used in various industrial and domestic fields due to purified water productivity and affordable water quality. However, membrane fouling, which is defined as the deposition of contaminants (organic, biological and inorganic materials) on the membrane surface or into membrane pores, decreases the membrane performance and increases operating cost by additional process such as membrane cleaning or replacement. In order to solve membrane

fouling phenomena, a variety of reactive functional materials have been introduced to the UF/MF membranes. Nonetheless, these membranes gradually lose anti-fouling properties by leaking the anti-fouling layers due to lack of interaction between the anti-fouling agent and the membrane surface or accumulating irreversible contaminants on the membrane surface. To overcome these limitations, in this study, anti-fouling materials were introduced onto the membrane surface with strong interactions to prepare sustainable anti-fouling active membrane. In addition, reversibly functionalized surface layers were introduced onto the membrane surface by thermo-responsive covalent bonding in order to provide regenerable and convertible functionalities to the membrane.

First, an anti-scaling membrane was developed by introducing a high-density positive charge to a poly(vinylidene fluoride) (PVDF) membrane to suppress membrane scaling in Ca^{2+}/silica-rich wastewater. Positively charged modifiers were synthesized by conjugating an amphiphilic polymer (Brij S10) and branched poly(ethylene imine) (b-PEI) at various molar ratios, and these were then implanted to PVDF membranes during the phase-inversion process. ATR FT-IR spectra revealed that the positive modifiers successfully anchored onto the surface of the membrane by hydrophilic-hydrophobic phase recognition. As introducing the positive charge on the membrane surface, the membranes showed positive surface charge and their pure water permeability (PWP) increased due to the protonation of b-PEI. Anti-scaling properties were also confirmed to be improved by filtration tests using a Ca^{2+}/silica-rich feed solution, which results from the repulsion of metal ion by the positively charged branch on the membrane. In addition, the water flux recovery by

simple membrane backwashing of the modified membrane was double that of the neat PVDF membrane.

Second, a sustainable anti-biofouling membrane was developed by covalently immobilizing silver nanoparticles (Ag NPs) onto PVDF membrane surface mediated by a thiol-end functionalized linker. FE-SEM and EDXS measurements revealed that the Ag NPs were highly bound and dispersed to the PVDF membrane due to the strong affinity of the Ag NPs with the thiol-modified linkers, which had been anchored to the PVDF membrane. The membrane performed well under water permeability and particle rejection measurements, despite the high deposition of AgNPs on the surface of membrane. The Ag-PVDF membrane nanocomposite significantly inhibited the growth of bacteria on the membrane surface, resulting in enhanced anti-biofouling property. Importantly, the Ag NPs were not released from the membrane surface due to the robust covalent bond between the Ag NPs and the thiolated PVDF membrane.

Third, a regenerable anti-fouling membrane was developed via the formation of a dynamic peel-and-stick of hydrophilic poly(ethylene glycol) (PEG) layer onto the surface of a poly(tetrafluoroethylene) (PTFE) membrane, using thermo-responsive reversible covalent bonding. In order to attach a peelable-and-stickable hydrophilic layer onto a membrane surface, a maleimide end-modified PEG layer was coupled with a furan-modified PTFE membrane by reversible Diels-Alder (DA) cycloaddition reaction. The combined results of ATR FT-IR, XPS and FE-SEM measurements clearly revealed that the maleimide end-modified PEG was successfully coupled with the furan-modified PTFE membrane surface by DA reaction. In addition, the

hydrophilic PEG layer was readily and repeatedly reformed on the membrane surface by a thermally driven dynamic peel-and-stick process. The PEG-coupled PTFE membrane showed effective anti-fouling performance against a highly concentrated silica colloidal aqueous solution. In particular, the anti-fouling property was remarkably recovered after regeneration of the hydrophilic layer through the peel-and-stick process.

Finally, a convertible membrane platform was verified by changing membrane surface introduced materials using dynamic peel-and-stick process. SiO_2 and Ag NPs were selected as membrane surface modifying materials to prepare inorganic and metallic nanomaterials surface functionalized membrane, respectively. The combined results of FT-IR and ^1H NMR analyses showed that the maleimide derivatives were successfully synthesized. They were effectively functionalized at the surface of SiO_2 and Ag NPs for introducing maleimide moiety. The various surface analyses results indicated that the SiO_2 and Ag NPs were successfully coupled with the furan-modified PTFE membrane by DA reaction. As expected, the inorganic and metallic layers were repeatedly regenerated on the surface of the membrane through the peel-and-stick process, which was verified by ATR FT-IR, XPS, FE-SEM/EDXS results. In particular, surface chemical and morphological analyses were disclosed that the surface introduced functionalities were converted into desired other functionalities by the peel-and-stick process.

In this study, sustainable anti-fouling membranes have been developed by introducing various anti-fouling materials *i.e*, cationic, biocidal, hydrophilic materials, to UF/MF membranes with strong attractive force. In particular, anti-fouling membrane prepared though thermo-reversible bonding can

overcome irreversible membrane fouling which is considered as a limitation for conventional anti-fouling membranes and convert surface functionality. Therefore, it is expected that this approach opens up the possibility a novel platformable membrane separating system.

Keywords: Water treatment membrane, Ultrafiltration/microfiltration, Anti-fouling, Anti-scaling, Regeneration, Convertible functionality, Covalent assembly, thermo responsive dynamic bonding, Diels-Alder reaction

Student Number: 2007-22951

Contents

List of Tables

List of Figures

(middle), SiO_2-PTFE converted from Ag-PTFE (bottom), (d) XPS spectra for Si 2p of SiO_2-PTFE converted from Ag-PTFE

CHAPTER I

INTRODUCTION

I-1. General Description of Water Treatment Membrane

Global water shortage will be more severe because of increasing global population and expend of economics of developing countries. In the next 40 years, it is expected that the global population grows about 40% and the demand for water resources continually grow in domestic, agriculture and industrial use[1]. From estimation of the World Water Council, about 3.9 billion people will live in “water scare” region in 2030. In addition, the World Health Organization (WHO) reported that 1.1 billion people have lack of access to clean water and 2.6 billion people rarely use proper sanitation[2]. In particular, about 2.2 million people die by waterborne diseases every year. Therefore, the clean and fresh water needs to be protected from contamination and new clean water resources must be obtained by development of water treatment technologies for the world’s growing demand of clean water. Among water treatment methods, membrane purification is greatly being spotlighted as a technology to substitute conventional water treatments such as gravity sedimentation, chemical-assisted coagulation, chlorine disinfection and microbial-mediated decomposition because the membrane process can successively produce high-purified water without requirement of chemical, biological and thermal treatments.

The membrane can be defined essentially as a barrier, which

separates two phases and restricts transport of various chemicals in a selective manner[3] (see Figure I-1). The selective transport of membrane is achieved by control of the permeation rate of various chemical species. The driving forces for the membrane separation are a concentration, pressure, temperature or electric potential gradient. The membrane can be made from various materials *e.g.*, metal, ceramic, polymer. Typically, the polymeric material based on membranes have been widely used in water treatment fields because polymeric materials can make various performance-level membrane products by controlling surface morphology and it can apply for mass production with standard quality. In addition, the pressure-driven membrane processes are most widely used membrane water treatment applications[4-5]. The pressure-driven membrane are typically classified into four categories *i.e.*, reverse osmosis (RO), nanofiltration (NF), ultrafiltration (UF) and microfiltration (MF). The classification criteria of the membrane are characteristic of surface pore size or their intended applications[4-6]. Therefore, the membrane separation has been widely applied to various fields such as purification of wastewater, desalination of sea water, concentration of nutrient materials and etc.

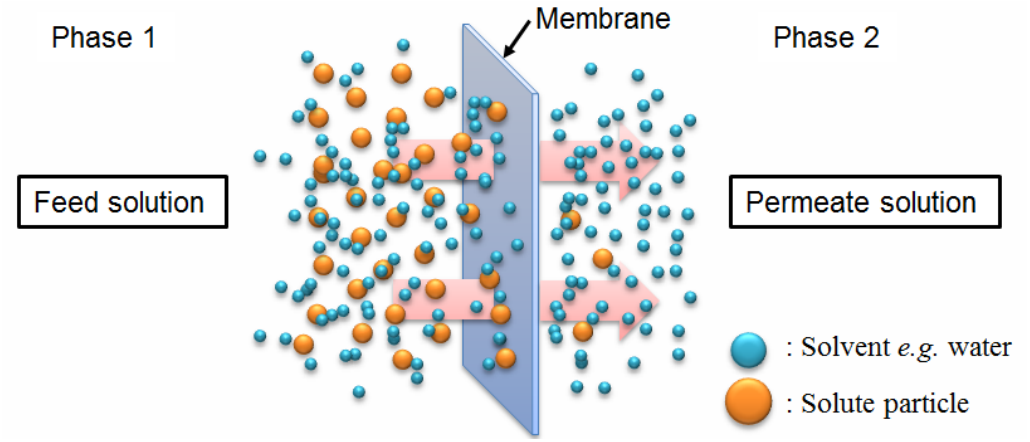

Figure I-1. Schematic representation of a two-phase system separated by a membrane

I-1-1. Historical development of membranes

In eighteenth century, Abbé Nolet used the word ‘osmosis’ for explain of water permeation through a diaphragm kind of a semipermeable membrane, which was firstly described membrane phenomena. After few decades, electro-osmotic flow was reported in 1809 by F. F. Reuss. He found flow of water in electric field. Thomas Graham made fundamental discoveries related to dialysis in 1861. In 1866, Fick and Traube firstly developed synthetic membrane using cellulose nitrate[7]. Bechhold devised a technique for preparation of nitrocellulose synthetic membranes with graded pore size in 1907[8]. Over the next 20 years, microfiltration (MF) membrane technology was expanded to other polymers. In particular, membrane was firstly attempted to make drinking water at the end of World War II. However, until 1960, membranes were still used in only a few laboratories and specialized industrial applications because the membrane could not meet the desired standards such as reliable quality, flux, selectivity and price.

On the other hand, Membrane technology was also applied to medical separation processes. W. J. Kolf had demonstrated the first successful artificial kidney in 1945[9]. The development of artificial kidney was completed by the early 1960s. Nowadays, the membrane based artificial organs have become a key medical device in therapy.

In the early 1960s, Loeb and Sourirajan developed high performance and defect-free reverse osmosis (RO) membrane which consist of an ultrathin selective surface layer and a thicker microporous support layer[10]. The surface thin layer provides selective permeation. In other hand, the microporous support layer provides mechanical strength only. This anisotropic structure

dramatically enhanced the membrane performance which was 10 times higher than that of previously available membrane.

The Loeb-Sourirajan technique inspires the new membrane fabrication technologies. The new membrane forms including, thin active surface layer by interfacial polymerization and multilayer surface by composite or coating methods were developed for achievement of high membrane performance during the period 1960-1980. In addition, various membrane package methods were developed such as plate-and-frame, spiral-wound, tubular, and hollow-fiber modules in this period.

Table I-1. Historical discovery of driving forces for membrane separation and development of membranes

year	Developer	Description
1748	Abbé Nollet	Discovery of the phenomenon of osmosis in natural membranes
1809	Reuss	Discovery of electro-osmosis
1861	T. Graham	Discovery of dialysis
1866	Fick, Traube	Creation of cellulose nitrate membrane as the first synthetic membrane
1907	Bechhold	Preparation of cellulose nitrate membranes of graded pore size
1945	Kolff	Application of membrane to artificial kidney
1927	Satorius	Manufacturing of commercial membrane
1956	Samuel Yuster	Prediction of advent of RO using Gibbs equation
1958-1960	Loeb, Sourirajan	Development of cellulose asymmetric membrane
1963	General atomics	First spiral-wound module
1972	Cadotte	Development of composite membrane fabricated by interfacial polymerization

I-1-2. Classification of membrane process

Membrane processes are typically classified into four categories *i.e.* RO, NF, UF, and MF by surface pore size and operation pressure, which is summarized in Figure I-2[3]. The MF membranes can reject colloidal particles and bacteria about the range diameter 0.1–10 μm. The UF membranes can be filtered for dissolved macromolecules such as polysaccharide, proteins, fat, hydrophilic polymers and virus. The mechanism of MF and UF processes is sieving effect. In contrast, the penetration phenomena of RO and NF processes are quite different because the surface pores are too small. All most solutes are rejected by these filtration processes. The difference between RO and NF membranes is penetration of monovalent ions. The NF membrane selectively penetrates monovalent ions through rejection penetration of di- and multivalent ions. The ions exclusion mechanism at the membrane surface is explained by a combination of steric hindrance and Donnan exclusion effect[11-12].

The RO membranes can only penetrates water molecule. The accepted mechanism of transport for RO process is called the solution-diffusion model[13]. From this theory, solute penetration by dissolving in the membrane material and diffusing down a concentration gradient. The separation is determined by the difference of solubilities and mobilities in the membrane materials.

As the surface pore sizes become smaller in the membrane process, it is required the more transmembrane pressure across membrane. Typically, the RO and NF process requires high operation pressure exceeding 10 atm. On the other hand, the UF and MF membranes can operate with low

transmembrane pressure.

The membrane processes have been widely applied various water treatment fields. The RO membrane can produce ultra-pure water by rejection of almost water dissolved solutes. The application areas of RO membrane are sea water desalination and production of ultra-pure water. The NF process effectively rejected di- or multivalent ions, which can applied purification of ground water and selective recovery process. The UF and MF processes apply to waste water treatment, membrane bioreactor (MBR) and pre-treatment process for RO or NF processes.

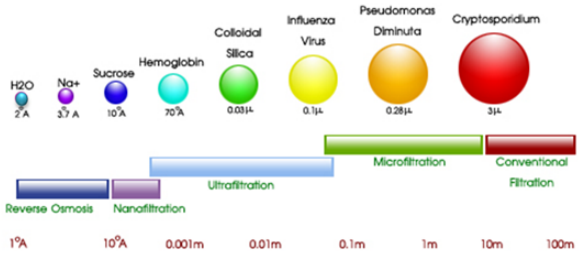

	RO	NF	UF	MF
Pore size	0.1 ~ 1 nm	1 ~ 10 nm	10 ~ 100 nm	100 ~ 1000 nm
Rejection materials	monovalent ions	sugar, pesticides, herbicides, divalent anions	proteins, starches, colloids, silica, organics, dye, fat	clay, bacteria, large viruses, suspended solids
Permeates	Water	monovalent ions	ions, small molecules	colloids, proteins
Operation pressure	14~69 bar	3.5~16 bar	1~7 bar	0.7 bar
Application	water desalination,	advanced water purification for ground water	pretreatment of RO or NF, Water purification	MBR, pretreatment of RO or NF

Figure I-2. Schematic illustration of membrane process about reverse osmosis (RO), nanofiltration (NF), ultrafiltration (UF) and microfiltration (MF), and their rejected materials, operation conditions and applications

I-1-3. Preparation of membrane

The vast majority of membranes are commercially prepared by polymer materials due to high productivity with stable quality for all membrane processes. Inorganic based membranes *i.e.*, ceramic, metal, are used in specific applications such as high solvent resistance membrane process and gas separation. The types of membranes are divided into symmetric and anisotropic membranes (see Figure I-3). The symmetrical membranes include isotropic microporous, non-porous dense and electrical charged membranes. The anisotropic membranes are composed of thin surface layer and microporous support layer. The roles of thin surface layer and microporous support are separation function and endowment of enough mechanical strength, respectively. Generally, symmetrical membranes have low membrane performance due to long penetration path length. In contrast, the thin surface layer in the anisotropic membrane improves permeation velocity. Thus, the almost commercialized membranes have been prepared by anisotropic structure. The preparation techniques for symmetrical and anisotropic membranes are described below.

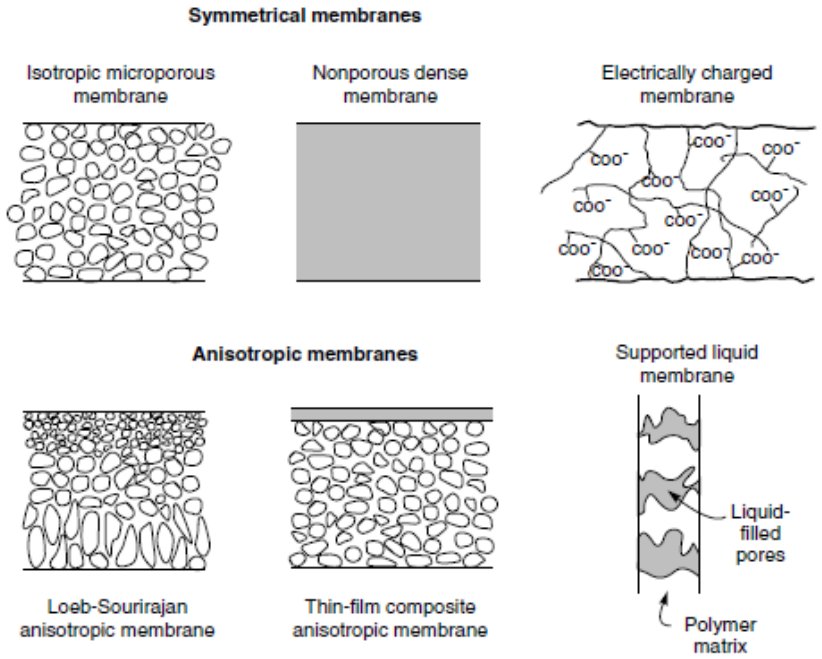

Figure I-3. Schematic diagrams of the principle types for membranes[7]

I-1-3-1. Symmetrical membranes

Dense nonporous isotropic membranes are widely used in laboratory research. In contrast, they are scarcely used in commercial membrane separation process due to low permeation property.

The isotropic nonporous membranes are typically fabricated by solution casting and melt extrude methods. The solution casted membrane is prepared by evaporation of solvent of casted viscous polymer solution in the range 15–20 wt%. Preferred solvents are moderately volatile chemicals such as acetone, cyclohexane and ethyl acetate. In the preparation of melt extrude film method, polymer is melted with pressure and heat using hot press machine. The melted extrude polymer solution is cooling down solidification of membrane. The appropriate polymers are non-soluble in suitable solvents at room temperature such as polyethylene, polypropylene and nylon, so membranes cannot be prepared by the solution casting method.

The isotropic porous membranes are fabricated by track-etch methods[14] expanded-film[15], and template leaching[16-17]. (see Figure I-4) The track-etched membranes are prepared by making constant holes to thin polymer film, which is typically carried out by irradiation of fission particles to the thin polymer film. The fission particles are obtained from nuclear reactor or other radiation sources. The advantage of this method is the preparation of high quality membrane with uniform cylindrical pore diameter. The track-etched membranes are almost a perfect screen filter. Thus, they are widely used to measure the number and type of suspended particles in water or air. The expanded-film membranes are made from crystalline polymers by an orientation and annealing process. A variety of commercialized membranes

are prepared by this technique. In the first step of this process, melted crystalline polymer is extruded with a very rapid drawdown. Next, the crystallites in the polymer are aligned in the orientation direction. After cooling and annealing process, the film is rapidly stretched. The pore size of the membrane can be controlled via the rate and extent of stretching step. The expanded-film formation process is illustrated in Figure I-4(b). In the template leaching method, the homogeneous polymer melt is prepared by adding a leachable component. After formation of the thin film by extrusion of the polymer melt, the leachable materials can be removed by a suitable solvent. Finally, the isotropic microporous membrane is obtained.

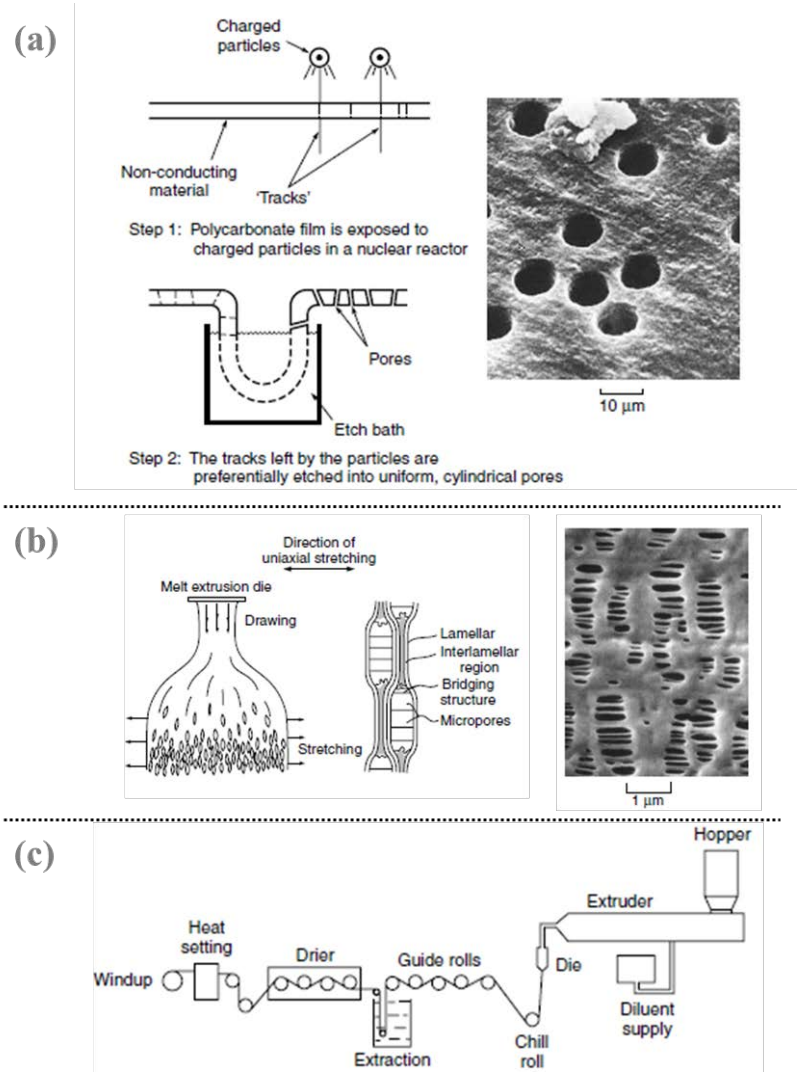

Figure I-4. Preparation diagrams of isotropic porous membranes for (a) track-etched membrane, (b) expanded-film membrane, and (c) template leaching membrane. This figure was modified from ref 7

I-1-3-2. Anisotropic membranes

Anisotropic membranes have layered structures. Typically, they consist of a very thin surface layer and a thicker microporous support layer. Three kinds of techniques *i.e.*, phase separation, interfacial polymerization, solution-coated composite membranes generally used in order to prepare asymmetric membrane structure.

Phase separation method is one of the representative preparation processes for an anisotropic membrane through precipitation of liquid polymer solution induced by immersion in nonsolvent, water vapor absorption, thermal gelation and evaporation of solvent, which is summarized in Table I-2. In all phase separation processes, a liquid polymer solution is precipitated into a solid phase and a liquid phase. The solid phase that is polymer-rich region forms the matrix of the membrane and a liquid phase that is polymer-poor region forms the membrane pores.

Non-solvent induced phase separation (NIPS) is the most important membrane fabrication technique among precipitation methods because this method can control pore-size and form large membrane area without defects. The NIPS process is composed of four steps which are casting, evaporation, precipitation and annealing. First, the viscous polymer solution is cast as a thin film on a plate. For a period of time, the casted film is left to stand to evaporate some of solvent. Next, the film is immediately immersed in a non-solvent (typically water) bath to precipitate the film and form the membrane. The prepared membrane is immersed in hot nonsolvent bath for annealing process.

Typically used polymer in this process are cellulose acetate (CA),

polysulfone (PSf), poly(vinylidene fluoride) (PVDF), and polyacrylamide (PAM). The specification for these polymers are tough, amophorous, high molecular weight and soluble in a suitable water-miscible solvent.

The suitable casting solvents are aprotic solvents with high solubility parameter. The most widely used solvents are Dimethyl formamide (DMF), N-methyl pyrrolidone (NMP), dimethyl acetamide (DMAc) and dimethyl sulfoxide (DMSO) which dissolve various polymers and casting polymer solutions precipitate rapidly in the water as a non-solvent to form porous, anisotropic structure[10, 18-20]. The casting polymer concentrations are in the range 15 – 20 wt% for ultrafiltration membrane. For preparation of RO and gas separation membranes, the concentration of the casting solution is generally higher about 25%.

I-1-3-3. Theoretical approach to phase separated membrane formation

Michaels, Strathmann and Smolders described phase diagram involved polymer-solvent-precipitation medium[18-19, 21-25]. This diagram showed change in composition of the casted solution as immersion into non-solvent bath. Figure I-5 shows a typical three-component phase diagram for the components used to prepare Loeb–Sourirajan membranes. The corners of the phase diagram indicates three components of polymer, solvent, and nonsolvent (generally, water); points in the diagram represent mixtures of the three components. The phase separation diagram has two types of phase regions: a one-phase region, where all components are miscible; and a two-phase region, where the system separates into a solid (polymer-rich) phase

and a liquid (polymer-poor) phase. During NIPS process, the polymer solution loses solvent and gains non-solvent. The casted polymer solution moves from a composition in the one-phase region to a composition in the two-phase region.

During the precipitation process, the casting solution enters the two-phase region (binodal boundary) of the phase diagram. This brings the casting solution into a metastable two-phase region. In this region, compositions of polymer solution are thermodynamically unstable but will not normally precipitate unless well nucleated. As more solvent leaves the casting solution and nonsolvent enters the solution, the composition crosses into another region of the phase diagram in which a one-phase solution is always thermodynamically unstable. In this region, polymer solutions spontaneously separate into two phases. The boundary between the metastable and unstable regions is called the spinodal boundary. Thus, the membrane precipitation process is a series of steps. First, solvent exchange with the precipitation medium occurs. Then, as the composition enters the two-phase region of the phase diagram, phase separation or precipitation begins. The time taken for solvent–water exchange before precipitation occurs can be measured because the membrane turns opaque as soon as precipitation begins. Depending on the casting solution composition, the time to first precipitation may be almost instantaneous to as long as 30–60 s. In the final step of the precipitation process, desolvation of the polymer phase converts the polymer to a relatively solid gel phase, and the membrane structure is fixed. The solid polymer phase forms the matrix of the final membrane, and the liquid solvent–nonsolvent phase forms the pores. The precipitation behavior of polymer–solvent

mixtures is further complicated by slow kinetics caused by the viscosity of polymer solutions and by thermodynamic effects that allow metastable solutions to exist for a prolonged time without precipitating.

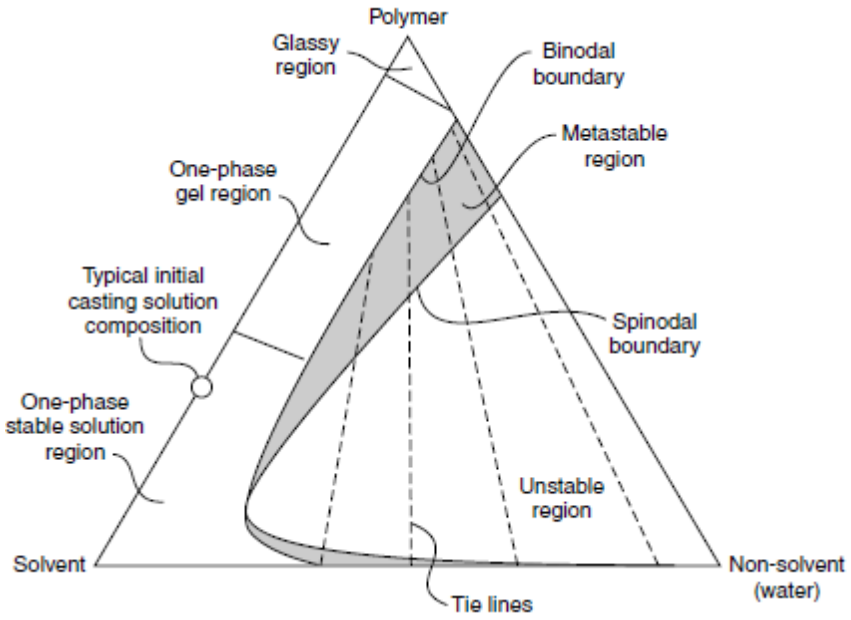

Figure I-5. Schematic diagram of the three-component phase diagram often used to rationalize the formation of water-precipitation phase separation membranes[7]

Thermal gelation method, called thermally induced phase separation (TIPS) is the simplest solution precipitation method for membrane preparation[26-27]. A file is cast form a hot with one-phase polymer solution. As cooling the cast film, the polymer solidified and the solution separates into solid phase including dispersed pores. Generally, more rapid cooling forms smaller membrane pores enhances membrane anisotropy. TIPS process can apply the various polymers, but this method is typically used to form membranes from polyethylene (PE) and polypropylene (PP) because these polymers cannot be made into a microporous membrane via NIPS process.

Solvent evaporation method is one of the earliest methods for fabrication of microporous membranes, which was developed in the 1920s[28-30]. A polymer is a two-type solvent mixture comprising of a volatile solvent and less volatile non-solvent. The preferred solvents are dichloromethane and acetone for volatile solvent and water and alcohol for less volatile non-solvent. An anisotropic microporous membrane is prepared by different solvent evaporation rate. As the volatile solvent evaporates, the casting polymer is concentrated in the less volatile non-solvent. Thus, the polymer solidifies and forms the membrane structure. Many factors affect the pore size and porosity of membranes in this method. These variables are ratio of volatile/non-solvents, evaporation time and polymer concentration. In particular, increase in the nonsolvent ratio in the polymer casting solution, or decrease in the polymer concentration, increases membrane porosity.

Water vapor absorption method is exposure of polymer casting film to high humidity to form microporous membrane by precipitation[31]. This method has been generally used by combination of solvent evaporation

method, which is an important process for formation of microfiltration membrane.

Table I-2. Preparation processes for phase separation membranes

Types of preparations	Process
Non-solvent precipitation	The cast polymer solution is immersed in a non-solvent bath (typically water). Absorption of water and loss of solvent cause the film to rapidly precipitate from the top surface down
Thermal gelation	The polymeric solution is cast hot. Cooling causes precipitation
Solvent evaporation	A mixture of solvents is used to form the polymer casting solution. Evaporation of one of the solvents after casting changes the solution composition and causes precipitation
Water vapor absorption	The cast polymer solution is placed in a humid atmosphere. Water vapor absorption causes the film to precipitate

I-1-3-4. Interfacial polymerization membranes

Interfacial polymerization membranes are made by reaction between amine and acid chloride at the membrane surface, which is formed a densely cross-linked, extremely thin membrane surface layer (see Figure I-6). The amine-loaded support is then immersed in a water-immiscible solvent solution including a reactant, *e.g.*, diacid chloride in hexane. The amine and acid chloride reacted at the interface of the two immiscible solutions to form a densely cross-linked, thin membrane layer. The interfacial membrane has very finely porous surface and much higher performance compared with the best cellulose acetate Loeb-Sourirajan membrane. The first interfacial polymerization membrane was developed by Cadotte et al. via polyethyleneimide cross liked with toluene-2,4-diisocyanate at the membrane surface[32]. After several years, high performance membrane was prepared by reaction of phenylene diamine with trimesoyl chloride[33-35]. This membrane has a high water flux and consistent salt rejections over 99.5% for seawater. This rejection property can make single-pass seawater desalination. One of drawbacks of the interfacial polymerization membrane is weak bonding stability of amide in the presence of chlorine. The chlorine which is commonly used as an antimicrobial agent in water could dissolve the amide bonds of membrane surface, resulting in loss of rejection property. Today, the almost commercialized RO and NF membranes are produced by this technique due to excellent water flux with high rejection property.

I-1-3-5. Solution-coated composite membranes

Another approach for production of anisotropic composite

membranes is solution-coating method [36]. This technique forms a thin selective layer on a microporous support. Water casting method has been widely used in this method. The polymer casing solution added to the surface of the water bath spreads as a thin film and picked up on the moving microporous support membrane. The selective layer is formed the thin thickness about 0.1 ~ 0.2 μm. the requirement of this method are clean, defect-free and very finely microporous.

I-1-4. Membrane modules

In order to effectively apply membrane purification to industrial scale plant, it requires hundreds to thousands of square meters of membrane area. Thus, large area or number of membranes should be effectively packed into a suitable container. These membrane packages are called membrane modules. Membrane modules are typically classified into four categories: plate-and frame module, spiral-wound module, tubular module and hollow fiber module.

Plate-and-frame modules were the earliest type of membrane system due to a simple package method using a plate membrane[37-38]. As shown in Figure I-7(a), membrane, feed spacers and product spacers are layered together between two end plates. The feed solution is forced across the surface of the membrane. Generally, the plate-and-frame modules are used in limited application areas because they are expensive, low membrane permeability and low packing density compared to the other module systems. Thus, plate-and-frame modules are now applied to elecrodialysis, pervaporation, and in a limited number of RO and UF applications with high

fouling feeds.

Spiral-wound modules are constructed from similar flat membranes but in the form of a “pocket” containing two membrane sheets separated by a highly porous support plate [39]. Figure I-7(b) shows the schematic illustration of spiral-wound module. This module consist of a membrane envelope of spacers and membrane wound around a perforated central collection tube; the module is placed inside a tubular pressure vessel, feed passes axially down the module across the membrane envelope, where it spirals towards the center and exits through the collection tube. Spiral-wound-modules have many advantages for application to membrane process such as high pressure operation, low fouling tendency and fabrication from various membrane materials. Thus, spiral-wound-modules are applied various membrane areas including RO, NF and UF process.

In the tubular modules, tube shape membranes are formed on the inside of the tube shape porous paper or fiber glass support. The tube geometry effectively suppresses the concentration polarization at the membrane surface by good fluid hydrodynamics, which endows resistance to membrane fouling. In contrast, tubular modules do not typically used in membrane process due to low packing density and relatively high preparation cost.

Hollow fiber modules have been widely used in membrane process owing to high packing density. The hollow fiber modules can contain up to 10,000 hollow fiber membranes with the diameter 200 – 2500 μm. The main advantage of hollow fiber modules is very large surface area within an enclosed volume, increasing the efficiency of the separation process. In

contrast, hollow fiber modules have low fouling resistance because high packing density endows more attractive force between foulants and membrane surface.

The selection of membrane module type is considered by a number of factors such as types of membrane process, fouling tendency of feed solution, permeate-side pressure drop, operation pressure, membrane material, and manufacturing cost, which are summarized in Table I-3.

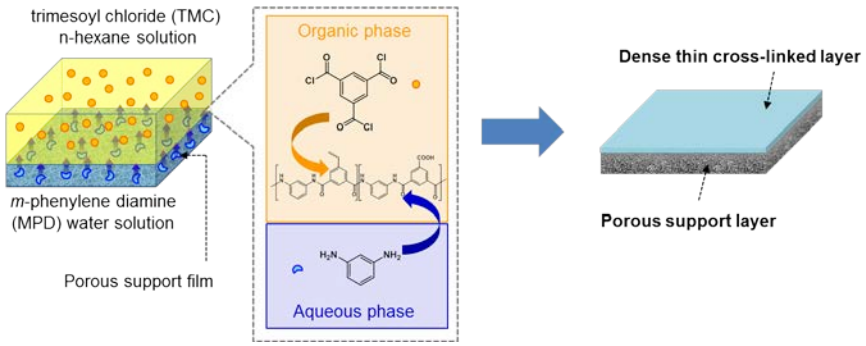

Figure I-6. Schematic illustration of the interfacial polymerization process[32]

Table I-3. Factors for membrane module design

Factors	Plate-and-frame	Spiral-wound	Tubular	Hollow fiber membrane
Fouling resistance	Good	Intermediate	Excellent	Poor
Permeate-side pressure drop	Low	Intermediate	Low	High
Suitability for high pressure operation	Yes	Yes	Marginal	Yes
Limited to specific types of membrane material	No	No	No	Yes
Manufacturing cost (USD/m^2)	50-200	5-100	50-200	5-20

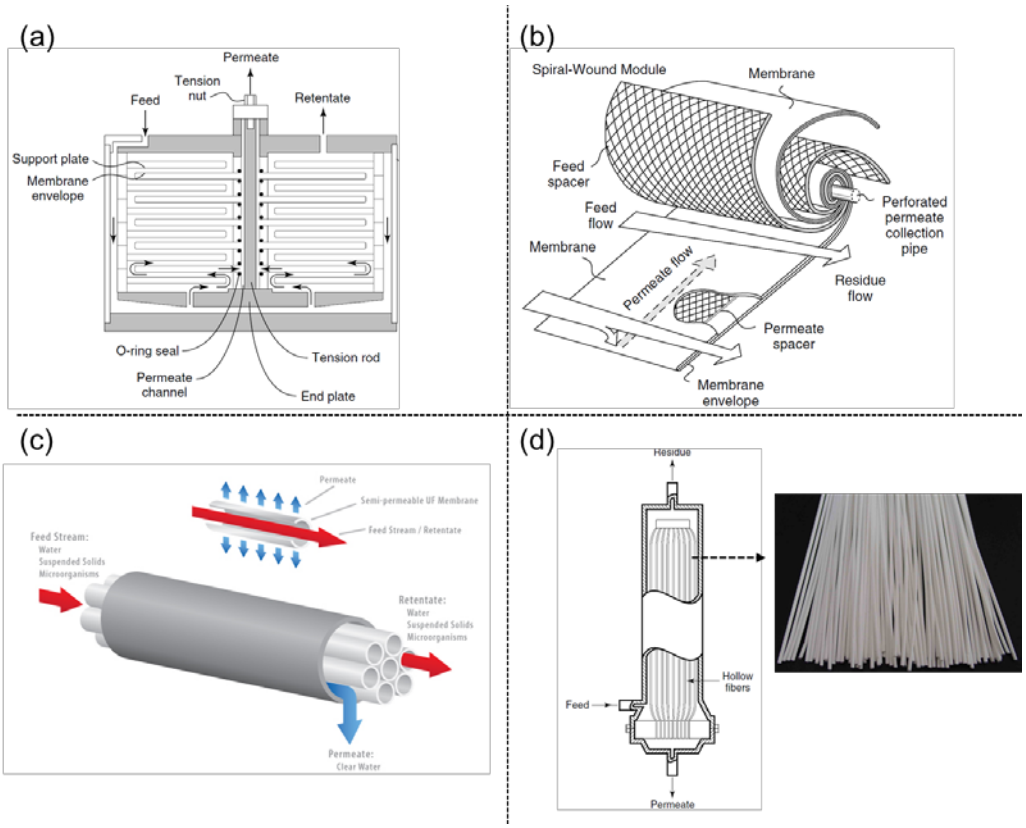

Figure I-7. Schematic illustration of membrane modules: (a) plate-frame module, (b) spiral-wound module, (c) tubular module and (d) hollow fiber module, which are modified from ref 7 and 37

I-2. Membrane Fouling

Fouling is defined as the accumulation of unwanted deposits on the surface or inside the pore of the membrane that degrade its permeability and increase operation cost by additional processes such as membrane cleaning and replacement[40-43]. Fouling formation mechanism can be understood by examining the forces of interaction between the foulants and membrane surface. Derjaguin-Landau-Verwey-Overbeek (DLVO) theory can explain the fouling mechanism by the net particle-surface (particle) interaction which is derived from a summation of the van der Waals and the electrical doble layer forces[44-47]. According to this theory, the particles which have different charge about membrane surface can more easily attach on the membrane surface by an electrostatic attractive force. In order to minimize fouling, the surface and the particle should be kept repulsive of each other or reduce the interaction between them. In addition, the hydrophobic particles tend to cluster or group together to form colloidal particles because this lowers the interfacial free energy (surface tension) due to exposure surface area results in this shape while limiting exposure to the hydrophilic environment.

Fouling is a complex phenomenon, which is influenced by various factors such as foulant characteristics, *e.g,* solubility, hydrophobicity, charge, size, concentration, membrane properties, *e.g.*, morphology, pore size, surface chemistry, surface charge, operation conditions, *e.g.*, trans membrane pressure, cross-flow velocity, temperature and feed solution properties *e.g.*, pH, ionic strength, solution chemistry[48-50].

The fouling generated sites are divided into external surface fouling

and internal fouling (pore blocking fouling)[51-53]. The external surface fouling refers to the build-up, formation of deposits or cake/gel-like layers on the outer surface of the feed-side of the membrane. The internal fouling (pore blocking) happens when foulants are formed inside the pores of the membrane by partial, gradual narrowing, or completely pore blockings. The external surface fouling is usually reversible and can be removed by physical/chemical cleaning process. In contrast, the internal fouling is in most cases, irreversible, due to compaction of foulants and membrane degradation.

The foulants in membrane process can be classified into three broad groups: inorganic fouling, organic fouling and biological fouling[54]. Inorganic fouling, which is often called scaling, is generated from the deposition of inorganic colloidal particles and particulates, precipitation and/or crystallization of mineral salts from the feed solution such as $CaCO_3$, $CaSO_4$, silicate, $BaSO_4$ and so on. Organic fouling is occurred by deposition of organic matters such as humic acid, proteins, polysaccharides, and high molecular organic compounds. Biological fouling is mainly occurred by growth of microorganisms such as bacteria, fungi, algae, yeast and so on. However, in most cases, membrane fouling is not caused by single fouling mechanism. In real membrane purification process, complicated membrane foulings are generated from combination of different fouling materials and mechanisms.

I-2-1. Inorganic fouling (scaling)

Inorganic fouling often called scaling is defined to deposition of precipitated hard minerals from the feed solution that involves both

crystallization and transport mechanisms[55]. Furthermore, inorganic colloidal particles and precipitates such as silica, silt, clays, corrosion products are also mainly contribute to inorganic fouling[56]. Several factors affect the rate of scaling such as the degree of supersaturation, flow conditions, membrane surface property (roughness, morphology) and solution temperature. Among them, a super-saturated condition occurs nucleation and growth of crystals such as $CaCO_3$, $CaSO_4$, SiO_2, $BaSO_4$, $MgCO_3$, and $Ca_3(PO_4)_2$ in the feed solution and membrane surface[57]. Calcium carbonate ($CaCO_3$) is one of the most common foulants found in various feed solution. Increase in the concentration of calcium cation ions and carbonate anion at the membrane surface leads to the scaling formation of $CaCO_3$ due to exceed its solubility. The reactions leading to $CaCO_3$ precipitation are as following equations[58].

$$HCO_3^-{}_{(aq)} \leftrightarrow OH^-{}_{(aq)} + CO_{2\,(aq)}$$

$$OH^-{}_{(aq)} + HCO_3^-{}_{(aq)} \leftrightarrow CO_3^{2-}{}_{(aq)} + H_2O$$

$$Ca^{2+}{}_{(aq)} + CO_3^{2-}{}_{(aq)} \leftrightarrow CaCO_{3\,(s)}$$

I-2-2. Organic fouling

Organic fouling is the adsorption and/or deposition of dissolved and colloidal organic materials onto the membrane surface such as humic acid, proteins, polysaccharides, and high molecular organic compounds. These materials can be adsorption at the molecular level or formation of gel layer on the membrane surface. In most case, the organic foulings are rarely to remove without use of chemical cleaning. The most common organic fouling is due to the deposition of natural organic matters (NOM)[59-60]. NOM are mainly

composed of humic substances and are especially abundant in natural waste water. NOM can adsorb on the membrane surface by various interactions between membrane surface and NOM such as electro static interaction, hydrophobic interaction, and specific chemical affinity.

I-2-3. Biological fouling (biofouling)

Biological fouling (or biofouling) is the accumulation and growth of biological species on the membrane surface, which affects decline permeability and membrane life time. Microorganisms are the most common materials of the biofouling. They tend to form a dense biofilm that blocks membrane function. Microorganisms present in water then adhere on the membrane surface and bind nutrient materials such as proteins, lipids, polysaccharides, humic acids and nucleic acids[61-62]. Microorganisms can multiply on the membrane surface and form dense biofilm layer. The microorganisms are more resistant when they are embedded in a biofilm as compared to those in a dispersed state[63-65] . Biofilm is composed of multiplied microorganisms and extracellular polymeric substances (EPS) with amphiphilic properties which are created from microorganisms. In addition, biofilm formation could partially or completely block the pores of the membrane, so that the diffusive transport is largely reduced.

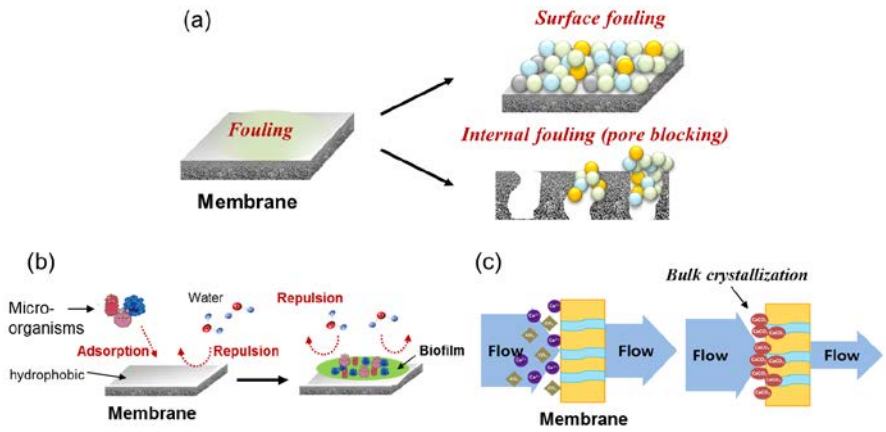

Figure I-8. Schematic illustration of membrane foulings; (a) the fouling sites on a membrane can be divided into membrane surface (external) and internal fouling (pore blocking), (b) formation of biological foulings derived from microorganisms, (c) formation of membrane scaling (inorganic fouling) generated from bulk crystallization of calcium carbonate

I-3. Surface Modification of Membrane

Membrane fouling significantly declines water permeability and membrane lifetime. In order to solve membrane fouling phenomena, many efforts have been tried to remove fouling layer on the membrane. Eliminable foulings such as external fouling and concentrated polarization can removed by back-washing, hydraulic cleaning, chemical cleaning and adjusting cross flow velocity because these foulants are loosely attached on the membrane surface or pores. Selection of suitable membrane module type is also effective for reducing membrane fouling to suppress adherence of foulants on the membrane surface. However, these attempt cannot be a fundamental solution for membrane fouling because some foulants robustly attached on the membrane surface and into membrane pores by chemical interactions. The irreversible or permanent fouling is hardly removed by post-treatment methods.

Membrane surface modification is one of a fundamental route to develop anti-fouling membrane. Thus, many researchers and membrane companies have been paid much attention for development of anti-fouling membrane for endowment of hydrophilic, degradation, and self-cleaning properties using various surface modification methods such as coating, grafting and incorporation.

I-3-1. Surface coating

Surface coating is a convenient and efficient method for membrane surface modification, which has been widely used to adjust surface properties

of water treatment membrane. Various materials have been adopted in this method such as hydrophilic polymer (water-insoluble polymer, cross-linked water soluble polymer), charged polymer and reactive nanoparticles. Surface coating layer acts as a protective layer to reduce or remove the adherenced foulants on the membrane surface. Coating method is a simple and easily applied to conventional membrane, and achieves reasonable anti-fouling performance. On the other hand, physically attached coating layer on the membrane surface may be gradually deteriorated due to the loss or leaching of coating layer during continual membrane operation.

I-3-2. Chemical modification

Direct coupling of anti-fouling materials to membrane surface is an effective method to develop anti-fouling layer without loss of surface property. This method can be achieved by divergence and convergence approaches. Grafting is the typical divergent approach for preparing anti-fouling layer. In this process, specific functional polymer materials are growth on the membrane surface. The advantage of this method is direct attachment of various functional polymers on the membrane surface such as hydrophilic, negatively charged, positively charged and zwitterionic polymers. Chemical coupling is a representative route for the convergence approach. Functional materials *e.g.*, commercialized functional materials, size/shape controlled functional polymer, reactive inorganic materials, and etc., are directly bound to membrane surface via chemical reaction. The advantage of this method is direct and robust assembly of the desired functionalities on the membrane surface.

I-3-3. Incorporation

Incorporation method has been widely applied to develop antifouling membrane by introducing various functional materials during membrane fabrication process. Typically, anti-fouling membranes are prepared through phase separation process using polymer dope solution including the functional materials. The advantage of this method is preparation of anti-fouling membrane using conventional fabrication process without post treatment and variety of functional materials such polymer, metal, inorganic materials which can introduce to membrane with the same fabrication process. However, the incorporated functional materials were partially located on membrane surface due to absence of interaction between membrane surface and functional materials. In addition, they may loss during long-term membrane operation by leaching owing to absence or weak interaction.

One of solution of this drawback is incorporating amphiphilic materials into the membrane. Incorporation of amphiphilic copolymer into the membrane using this method is able to prepare surface functionalized anti-fouling membrane by hydrophobic-hydrophilic phase recognition separation during membrane fabricating process because hydrophilic part of the amphiphilic copolymer tends to migrate upon membrane surface during phase separation process owing to hydrophilic affinity, on the other hand, hydrophobic part can be anchored with hydrophobic membrane polymer material.

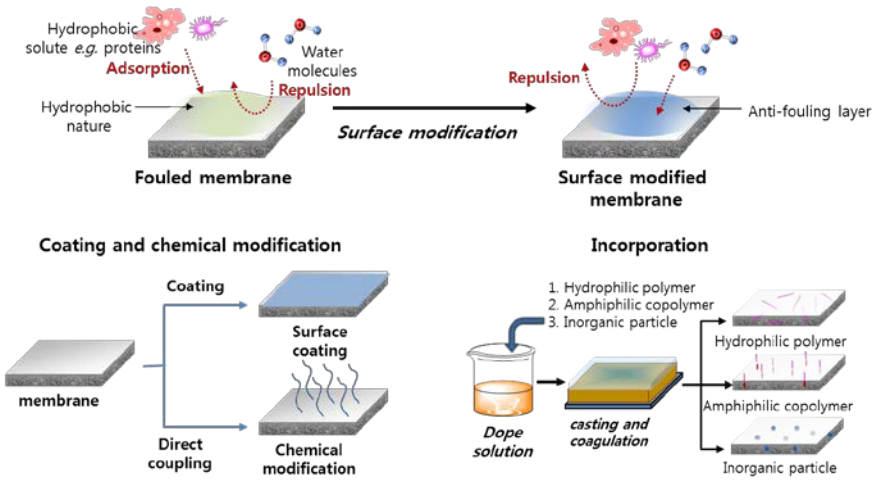

Figure I-9. Schematic illustration of membrane surface modification for endowment anti-fouling properties (bottom left) coating and chemical modification method (bottom right) incorporation method

I-4. Thermo Reversible Dynamic Bond

Anti-fouling layer on the membrane surface can hinder the adsorption of foulants onto the membrane surface and can even render any adsorbed contaminants easily removed by a simple washing process. Nevertheless, water contaminants continually and permanently accumulate on membrane surfaces and in membrane pores, and this brings about a gradual deterioration of membrane performance. Accumulated irreversible membrane foulings does not effectively remove by conventional membrane cleaning approaches.

Dynamic bonding can be one of the solutions for the deteriorated anti-fouling membranes by endowment regeneration or alteration of surface properties. Dynamic bond-incorporated membrane can selectively undergo reversible breaking and reformation of the anti-fouling layer to endow the membrane surface with the desired properties. Such dynamic bonds have been extensively utilized for stimuli-responsive smart materials, such as a self-healing material[66-68], a smart adhesive[69-70] and an actuator[71-72] Dynamic bondings are defined as any class of bonding that can selectively undergo reversible breaking and re-formation controlled by external stimuli such as light, ion strength, pH and temperature[73]. Figure I-10 shows the classification of dynamic bondings by response to external stimuli.

Among dynamic bondings, Diels-Alder (DA) cycloaddition between furan and maleimide functional groups is a representative dynamic bond to form a covalently thermo-reversible cyclic coupling which can be restored to their original forms by controlling temperature[69, 74]. The furan and maleimide

functional groups are reacted together and formed their cyclic adduct by DA reaction from room temperature to 60 °C. The furan-maleimide cyclic adduct restores its original form at treatment with high temperature exceeding 100 °C. Furthermore, DA cycloadditions for furan-maleimide groups have been reported to have high and feasible reversible efficiencies[68]. Thus, it is expected that membrane anti-fouling properties are regenerable or conversion by changing a surface functional layer using the thermo-reversible covalent bonding.

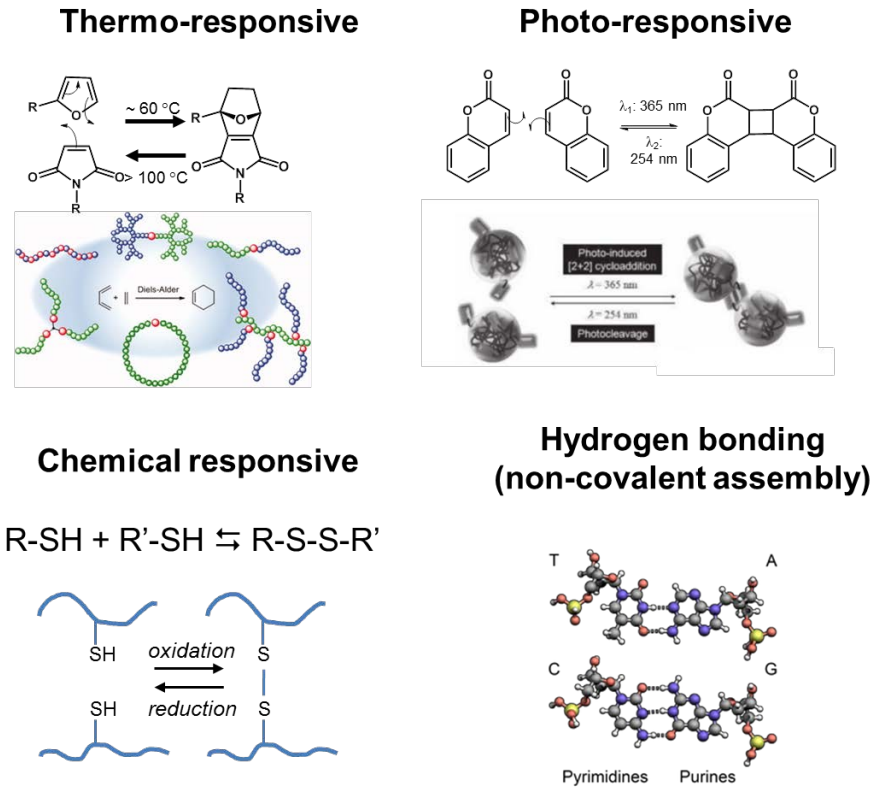

Figure I-10. Classification of dynamic bondings by response external physical and chemical stimuli

I-5. Research Objects

The main objective of this research is development of anti-fouling UF/MF membranes by robust assembly and reversible attachment of various functional materials onto the membrane surface. In the conventional route for fabrication of anti-fouling membranes, the anti-fouling properties were gradually and completely degraded by leaking the anti-fouling layers or accumulating irreversible contaminants on the membrane surface due to lack of interaction between the anti-fouling agent and the membrane surface. To overcome this limitation, anti-fouling materials were introduced onto the membrane surface with strong physical and chemical interactions. Furthermore, reversibly functionalized surface layers were introduced onto the membrane surface by thermo-responsive covalent bonding in order to provide regenerable and convertible functionalities to the membrane.

In chapter II, positively charged branched poly(ethylene imine) (b-PEI) was introduced to PVDF membrane by a physical anchoring method to suppress membrane scaling. To robustly anchor b-PEI to membrane, b-PEI was connected with an amphiphilic agent to endow a hydrophobic segment. The modified b-PEI was then anchored onto the PVDF membranes by hydrophobic-hydrophilic phase recognition separation during membrane fabrication process. The surface introduced positive charge can effectively repel cation ions and suppress membrane scaling at the membrane surface, indicating that the b-PEI implanted membrane is applied to waste water treatment containing a high content of metal ions.

In chapter III, biocidal silver nanoparticles (Ag NPs) were directly

assembled onto the PVDF membrane surface via silver-sulfur interaction. The Ag NPs covalently bound membrane showed excellent anti-biofouling performance. Furthermore, the introduced Ag NPs did not released from membrane surface during successive membrane filtration process. This membrane can applied sustainable anti-biofouling membrane without loss of biocidal property.

In chapter IV and V, reversibly functionalized surface layers were introduced onto the PTFE membrane surface by thermo-responsive covalent bonding in order to endow regeneration and conversion of surface functionalities. In chapter IV, the maleimide modified hydrophilic PEG layer was coupled with the furan modified PTFE membrane by DA coupling reaction. The PEG layer was able to peel by adjusting temperature and the fresh PEG layer was then re-stuck with the membrane surface by DA reaction. This peel-and-stick process regenerated an anti-fouling property without membrane replacement. In chapter V, three types of maleimide modified functional materials *i.e.,* SiO_2 NPs, Ag NPs, PEG, were reversibly assembled onto the furan modified PTFE membrane surface. The surface introduced functional material can be converted into another functionality by the thermally driven peel-and-stick process. This novel functional membrane platform can solve membrane fouling problem derived from irreversible fouling though replacing degraded anti-fouling layer by fresh anti-fouling layer. In addition, this platform enabled conversion surface functionalities into desired other functionalities.

References and Notes

1. *Coping with Water Scarcity. Challenge of the Twenty-first Century*; United Nations (UN) Water . Food and Agricultural Association (FAO): **2007**.

2. WHO/UNICEF, *Progress on sanitation and drinking-water: 2010 update*. World Health Organization: Geneva and United Nations Children's Fund: New York: **2010**.

3. Nath, K., *Membrane separation processes*. PHI Learning Pvt. Ltd.: **2008**.

4. Ulbricht, M., Advanced functional polymer membranes. *Polymer* **2006,** *47* (7), 2217-2262.

5. Kesting, R. E., Four tiers of structure integrally skinned phase inversion membranes and their relevance to the various separation regimes. *J. Appl. Polym. Sci.* **1990,** *41* (11-12), 2739-2752.

6. Mulder, M., *Basic Principles of Membrane Technology*. Kluwer Academic Publishers: London, **1996**.

7. Baker, R. W., *Membrane technology*. Wiley Online Library: **2000**.

8. Bechhold, Die Filtration von Kolloiden. *Zeitschrift für Analytische Chemie* **1907,** *46* (9), 589-590.

9. Kolff, W.; Berk, H.; WELLE, N. M.; Ley, A.; Dijk, E.; Noordwijk, J., The artificial kidney: a dialyser with a great area. *Acta Medica Scandinavica* **1944,** *117* (2), 121-134.

10. Loeb, S.; Sourirajan, S., *Sea Water Demineralization by Means of an Osmotic Membrane in Saline Water Conversion–II, Advances in Chemistry Series Number 28*. American Chemical Society: Washington, DC, **1963**.

11. Ostwald, W., Elektrische eigenschaften halbdurchlässiger

scheidewände. *Z. phys. Chem* **1890,** *6* (71), 2.

12. Donnan, F. G., Theory of membrane equilibria and membrane potentials in the presence of non-dialysing electrolytes. A contribution to physical-chemical physiology. *J. Membr. Sci.* **1995,** *100* (1), 45-55.

13. Fick, A., Über diffusion. *Poggendorff Annal. Phys. Chem.* **1855,** *94*, 59-86.

14. Fleischer, R.; Alter, H.; Furman, S.; Price, P.; Walker, R., Particle Track Etching Diverse technological uses range from virus identification to uranium exploration. *Science* **1972,** *178* (4058), 255-263.

15. Bierenbaum, H. S.; Isaacson, R. B.; Druin, M. L.; Plovan, S. G., Microporous polymeric films. *Industrial & Engineering Chemistry Product Research and Development* **1974,** *13* (1), 2-9.

16. Ichikawa, T.; Takahara, K.; Shimoda, K.; Seita, Y.; Emi, M. Hollow Fiber Membrane and Method for Manufacture Thereof. US Patent 4,708,800, **1987**.

17. Lopatin, G.; Yen, L. Y.; Rogers, R. R. Microporous membranes from polypropylene. US Patents 4,874,567, **1989**.

18. Michaels, A. S. High flow membrane. US Patent 3,615,024, **1971**.

19. Manjikian, S., Desalination membranes from organic casting solutions. *Industrial & Engineering Chemistry Product Research and Development* **1967,** *6* (1), 23-32.

20. Pinnau, I.; Koros, W. J. Defect-free ultrahigh flux asymmetric membranes. US Patent 4,902,422, **1990**.

21. Altena, F. W.; Smolders, C., Calculation of liquid-liquid phase separation in a ternary system of a polymer in a mixture of a solvent and a

nonsolvent. *Macromolecules* **1982,** *15* (6), 1491-1497.

22. Reuvers, A.; Van den Berg, J.; Smolders, C., Formation of membranes by means of immersion precipitation: Part I. A model to describe mass transfer during immersion precipitation. *J. Membr. Sci.* **1987,** *34* (1), 45-65.

23. Reuvers, A.; Smolders, C., Formation of membranes by means of immersion precipitation: Part II. the mechanism of formation of membranes prepared from the system cellulose acetate-acetone-water. *J. Membr. Sci.* **1987,** *34* (1), 67-86.

24. Strathmann, H.; Scheible, P.; Baker, R., A rationale for the preparation of Loeb-Sourirajan-type cellulose acetate membranes. *J. Appl. Polym. Sci.* **1971,** *15* (4), 811-828.

25. Strathmann, H.; Kock, K., The formation mechanism of phase inversion membranes. *Desalination* **1977,** *21* (3), 241-255.

26. Lloyd, D. R.; Kim, S. S.; Kinzer, K. E., Microporous membrane formation via thermally-induced phase separation. II. Liquid—liquid phase separation. *J. Membr. Sci.* **1991,** *64* (1), 1-11.

27. Lloyd, D. R.; Kinzer, K. E.; Tseng, H. S., Microporous membrane formation via thermally induced phase separation. I. Solid-liquid phase separation. *J. Membr. Sci.* **1990,** *52* (3), 239-261.

28. Ferry, J. D., Ultrafilter Membranes and Ultrafiltration. *Chem. Rev.* **1936,** *18* (3), 373-455.

29. Elford, W., Principles governing the preparation of membranes having graded porosities. The properties of “gradocol” membranes as ultrafilters. *Transactions of the Faraday Society* **1937,** *33*, 1094-1104.

30. Pierce, H. F., Nitrocellulose membranes of graded permeability. *J. Biol. Chem.* **1927,** *75* (3), 795-815.

31. RILEY, R. L.; Lonsdale, H.; LaGrange, L.; Lyons, C., Development of ultrathin membranes. *Office of Saline Water Research and Development Progress Report No. 386* **1969**, PB# 207036.

32. Rozelle, L. T.; Cadotte, J.; Cobian, K.; Kopp Jr, C., Nonpolysaccharide membranes for reverse osmosis: NS-100 membranes. *Reverse osmosis and synthetic membranes* **1977**, 249–262.

33. Kamiyama, Y.; Yoshioka, N.; Matsui, K.; Nakagome, K., New thin-film composite reverse osmosis membranes and spiral wound modules. *Desalination* **1984,** *51* (1), 79-92.

34. Riley, R.; Fox, R.; Lyons, C. R.; Milstead, C.; Seroy, M.; Tagami, M., Spiral-wound poly (ether/amide) thin-film composite membrane systems. *Desalination* **1976,** *19* (1), 113-126.

35. Petersen, R. J., Composite reverse osmosis and nanofiltration membranes. *J. Membr. Sci.* **1993,** *83* (1), 81-150.

36. Ward, W.; Browall, W.; Salemme, R., Ultrathin silicone/polycarbonate membranes for gas separation processes. *J. Membr. Sci.* **1976,** *1*, 99-108.

37. Günther, R.; Perschall, B.; Reese, D.; Hapke, J., Engineering for high pressure reverse osmosis. *J. Membr. Sci.* **1996,** *121* (1), 95-107.

38. Stern, S.; Sinclair, T.; Gareis, P.; Vahldieck, N.; Mohr, P., Helium recovery by permeation. *Industrial & Engineering Chemistry* **1965,** *57* (2), 49-60.

39. Bray, D. T. Reverse osmosis purification apparatus. US Patent

3,417,870, **1968**.

40. Goosen, M.; Sablani, S.; Al-Hinai, H.; Al-Obeidani, S.; Al-Belushi, R.; Jackson, D., Fouling of reverse osmosis and ultrafiltration membranes: a critical review. *Sep. Sci. Technol.* **2005,** *39* (10), 2261-2297.

41. Tijing, L. D.; Woo, Y. C.; Choi, J.-S.; Lee, S.; Kim, S.-H.; Shon, H. K., Fouling and its control in membrane distillation—a review. *J. Membr. Sci.* **2015,** *475*, 215-244.

42. Shi, X.; Tal, G.; Hankins, N. P.; Gitis, V., Fouling and cleaning of ultrafiltration membranes: a review. *Journal of Water Process Engineering* **2014,** *1*, 121-138.

43. Rana, D.; Matsuura, T., Surface modifications for antifouling membranes. *Chem. Rev.* **2010,** *110* (4), 2448-2471.

44. Contreras, A. E.; Kim, A.; Li, Q., Combined fouling of nanofiltration membranes: Mechanisms and effect of organic matter. *J. Membr. Sci.* **2009,** *327* (1–2), 87-95.

45. Chen, K. L.; Mylon, S. E.; Elimelech, M., Aggregation Kinetics of Alginate-Coated Hematite Nanoparticles in Monovalent and Divalent Electrolytes. *Environ. Sci. Technol.* **2006,** *40* (5), 1516-1523.

46. Yuan, W.; Zydney, A. L., Humic Acid Fouling during Ultrafiltration. *Environ. Sci. Technol.* **2000,** *34* (23), 5043-5050.

47. Christenson, H. K., DLVO (Derjaguin–Landau–Verwey–Overbeek) theory and solvation forces between mica surfaces in polar and hydrogen-bonding liquids. *Journal of the Chemical Society, Faraday Transactions 1: Physical Chemistry in Condensed Phases* **1984,** *80* (7), 1933-1946.

48. Belfort, G.; Davis, R. H.; Zydney, A. L., The behavior of suspensions

and macromolecular solutions in crossflow microfiltration. *J. Membr. Sci.* **1994,** *96* (1), 1-58.

49. Faibish, R. S.; Elimelech, M.; Cohen, Y., Effect of Interparticle Electrostatic Double Layer Interactions on Permeate Flux Decline in Crossflow Membrane Filtration of Colloidal Suspensions: An Experimental Investigation. *J. Colloid Interface Sci.* **1998,** *204* (1), 77-86.

50. Wiesner, M. R., Morphology of particle deposits. *J. Environ. Eng.* **1999,** *125* (12), 1124-1132.

51. Zhu, H.; Nyström, M., Cleaning results characterized by flux, streaming potential and FTIR measurements. *Colloids Surf. Physicochem. Eng. Aspects* **1998,** *138* (2–3), 309-321.

52. Knyazkova, T. V.; Maynarovich, A. A., Recognition of membrane fouling: testing of theoretical approaches with data on NF of salt solutions containing a low molecular weight surfactant as a foulant. *Desalination* **1999,** *126* (1–3), 163-169.

53. Hoek, E. M. V.; Allred, J.; Knoell, T.; Jeong, B.-H., Modeling the effects of fouling on full-scale reverse osmosis processes. *J. Membr. Sci.* **2008,** *314* (1–2), 33-49.

54. Meng, F.; Chae, S.-R.; Drews, A.; Kraume, M.; Shin, H.-S.; Yang, F., Recent advances in membrane bioreactors (MBRs): Membrane fouling and membrane material. *Water Res.* **2009,** *43* (6), 1489-1512.

55. He, F.; Gilron, J.; Lee, H.; Song, L.; Sirkar, K. K., Potential for scaling by sparingly soluble salts in crossflow DCMD. *J. Membr. Sci.* **2008,** *311* (1–2), 68-80.

56. Gryta, M.; Tomaszewska, M.; Karakulski, K., Wastewater treatment

by membrane distillation. *Desalination* **2006,** *198* (1–3), 67-73.

57. Darton, T.; Annunziata, U.; del Vigo Pisano, F.; Gallego, S., Membrane autopsy helps to provide solutions to operational problems. *Desalination* **2004,** *167*, 239-245.

58. Snoeyink, V., JenkinsD. Water Chemistry. New York: John Wiley & Sons: **1980**.

59. Buffle, J.; Wilkinson, K. J.; Stoll, S.; Filella, M.; Zhang, J., A Generalized Description of Aquatic Colloidal Interactions: The Three-colloidal Component Approach. *Environ. Sci. Technol.* **1998,** *32* (19), 2887-2899.

60. Gryta, M., Fouling in direct contact membrane distillation process. *J. Membr. Sci.* **2008,** *325* (1), 383-394.

61. Hilal, N.; Kochkodan, V.; Al-Khatib, L.; Levadna, T., Surface modified polymeric membranes to reduce (bio)fouling: a microbiological study using E. coli. *Desalination* **2004,** *167* (0), 293-300.

62. Yang, H.-L.; Lin, J. C.-T.; Huang, C., Application of nanosilver surface modification to RO membrane and spacer for mitigating biofouling in seawater desalination. *Water Res.* **2009,** *43* (15), 3777-3786.

63. Baker, J. S.; Dudley, L. Y., Biofouling in membrane systems — A review. *Desalination* **1998,** *118* (1–3), 81-89.

64. Siboni, N.; Martinez, S.; Abelson, A.; Sivan, A.; Kushmaro, A., Conditioning film and initial biofilm formation on electrochemical CaCO3 deposition on a metallic net in the marine environment. *Biofouling* **2009,** *25* (7), 675-683.

65. Griebe, T.; Flemming, H.-C., Biocide-free antifouling strategy to

protect RO membranes from biofouling. *Desalination* **1998,** *118* (1–3), 153.

66. Syrett, J. A.; Becer, C. R.; Haddleton, D. M., Self-healing and self-mendable polymers. *Polym. Chem.* **2010,** *1* (7), 978-987.

67. Zhang, Y.; Broekhuis, A. A.; Picchioni, F., Thermally self-healing polymeric materials: The next step to recycling thermoset polymers? *Macromolecules* **2009,** *42* (6), 1906-1912.

68. Peterson, A. M.; Jensen, R. E.; Palmese, G. R., Room-temperature healing of a thermosetting polymer using the diels-alder reaction. *ACS Appl. Mater. Interfaces* **2010,** *2* (4), 1141-1149.

69. Tasdelen, M. A., Diels-Alder "click" reactions: Recent applications in polymer and material science. *Polym. Chem.* **2011,** *2* (10), 2133-2145.

70. Hu, J.; Liu, S., Engineering Responsive Polymer Building Blocks with Host–Guest Molecular Recognition for Functional Applications. *Acc. Chem. Res.* **2014,** *47* (7), 2084-2095.

71. Rajagopalan, M.; Jeon, J.-H.; Oh, I.-K., Electric-stimuli-responsive bending actuator based on sulfonated polyetherimide. *Sensors Actuators B: Chem.* **2010,** *151* (1), 198-204.

72. Asoh, T. A.; Matsusaki, M.; Kaneko, T.; Akashi, M., Fabrication of temperature-responsive bending hydrogels with a nanostructured gradient. *Adv. Mater.* **2008,** *20* (11), 2080-2083.

73. Wojtecki, R. J.; Meador, M. A.; Rowan, S. J., Using the dynamic bond to access macroscopically responsive structurally dynamic polymers. *Nature materials* **2011,** *10* (1), 14-27.

74. Domingo, L. R.; Sáez, J. A., Understanding the mechanism of polar Diels-Alder reactions. *Org. Biomol. Chem.* **2009,** *7* (17), 3576-3583.

CHAPTER II

POSITIVE CHARGED MODIFIED POLY(VINYLIDENE FLUORIDE) (PVDF) MEMBRANES BY ANCHORING POSITIVE CHARGED BRANCHED POLY(EHTYLENE IMINE) FOR SUPPRESSION OF MEMBRANE SCALING

II -1. Introduction

Membrane scaling is generated from the deposition of inorganic particular materials, precipitation and/or crystallization of inorganic salts derived from feed solution. The most common mineral deposits are $CaCO_3$, $CaSO_4$, SiO_2, $BaSO_4$, $MgCO_3$, and $Ca_3(PO_4)_2$[1-2]. The combination of these minerals especially accelerates formation of scale on the membrane surface[3]. This phenomenon decreases membrane performance and life time, shortening membrane replacement cycles and increasing maintenance costs[4-5]. Especially, some industrial wastewater such as that produced during the manufacture of glass substrates for thin-film-transistor liquid-crystal displays (TFT-LCD), contains significant amounts of metal ions, and this causes scaling problems during membrane wastewater treatment

To reduce membrane scaling, many researchers have attempted to decline concentration polarization at the membrane surface by diluting metal ion concentration in the feed solution using chemical additives to coordinate or neutralize them before membrane treatment[6-9]. However, this approach not only requires an additional process before membrane purification but also produces additional waste. Other approaches involved control of cross-flow velocity[1, 10-11], high membrane operating temperature[12], and elimination of adhered scalants at the membrane surface using strong acidic or basic chemicals[13]. Increased cross-flow velocity can suppress the adsorption of metal ions on the membrane surface, and a high operating temperature improves the solubility of precipitates in the feed solution, both of which reduce scaling. However, although these methods can delay the occurrence of membrane scaling, metal salt precipitates are eventually deposited on the membrane surface when there is no interfacial anti-adhesive force acting against the metal ions. In the case where chemicals were used to remove scalants from the membrane surface, membrane lifetime could be reduced through destruction of membrane chemical structure by strong acids or bases. Thus, in terms of membrane materials, it is necessary to introduce an anti-adhesive force on the surface of membrane to repel metal ions and precipitates.

In an attempt to solve membrane scaling, positively charged membranes synthesized by introducing cationic materials to the membrane were reported[14-18]. They prepared a positively charged nanofiltration (NF) membrane by crosslinking positively charged polyethylene imine (PEI) on the surface[19]. The modified NF membrane containing the cross-linked PEI layer showed improved pure water permeability (PWP) and enhanced cation

rejection efficiency. These properties were attributed to the hydrophilicity of PEI and the repulsive electrostatic forces between cations and the positive charge of PEI. Despite such examples of high membrane performance, the NF membrane process is not suitable for industrial scale wastewater treatment because of its low water flux and high energy consumption. In addition, the cross-linked PEI layer may become separated from the membrane surface during membrane operation because of the lack of interfacial interactions between the PEI and the membrane. On the other hand, ultrafiltration/microfiltration (UF/MF) membranes have relatively large surface pores, high water permeability and their operations require low energy consumption, so they are more suitable for industrial wastewater purification processes. Thus, it is necessary to develop a positively charged UF/MF membrane with good anti-scaling properties. Moreover, the positive charges should be maintained during membrane operation.

Here, this study describes an anti-scaling UF/MF membrane fabricated by implanting a high-density positively charged polymer, *i.e.*, branched PEI (b-PEI), on membrane surface. To robustly introduce the b-PEI to the membrane surface, the end-groups of b-PEI were modified to alkyl chains, and the modified b-PEI was then anchored onto the PVDF UF/MF membranes by hydrophobic-hydrophilic phase recognition of the modified b-PEI during membrane fabrication process. As expected, the resulting membranes had a high surface positive charge, enhanced water permeability, and significantly suppressed scaling in highly concentrated Ca^{2+}/silica wastewater. This membrane can be applied in eco-friendly and economical purification processes for wastewater containing a high content of metal ions.

II-2. Experimental Section

II-2-1. Materials

Poly(vinylidene fluoride) (PVDF; Mw = 570,000 g mol^{-1}) was purchased from Solvay Chemicals. Poly(ethyleneimine) (PEI; branched Mw = 800 g mol^{-1}), poly(ethylene glycol) octadecyl ether (Brij® S10, Fw=711) and epichlorohydrin (C_3H_5OCl, 99.9%) were purchased from Sigma-Aldrich. Poly(vinylpyrrolidone) (PVP; M_w = 40,000 g mol^{-1}) was supplied by Daejung Chemicals & Metals. N-methyl-2-pyrrolidone (NMP; > 99%) and acetonitrile (C_2H_3N, >99 %) were supplied by Tokyo Chemical Industry. All chemicals were used as received, without further purification. Aqueous solutions were prepared with deionized (DI) water with a resistivity exceeding 18 MΩ cm.

II-2-2. Preparation of positive modifier

To introduce branched PEI (b-PEI) as a positive anti-scale agent onto the membrane surfaces, the b-PEI was modified with Brij® S10, which is composed of a hydrophobic octadecyl alkyl chain and hydrophilic poly(ethylene glycol). First, the hydroxyl end group of the Brij S10 was converted into an epoxy functional group by reaction with epichlorohydrin under basic conditions. The epoxy-end functionalized Brij S10 was denoted as S10E. Next, the S10E was reacted with b-PEI at various molar ratios S10E/b-PEI. In this study, three types positively charged amphiphilic copolymers were prepared. They were denoted as positive modifiers and encoded as PX, where X is the S10E/b-PEI molar ratio (S10E/b-PEI = 1, 2, and 5). Briefly,

2.84 g of Brij S10 (4 mmol) was added to 3.7 g of epichlorohydrin (40 mmol) with 0.48 g of NaOH (12 mmol). The reaction was run for 2 hours at 50 °C. The above solution was then slowly dropped into a large amount of acetonitrile to obtain precipitate. The supernatant was separated and evaporated. The products of S10E were dried overnight in a vacuum oven at 50 °C. The above three molar ratios of S10E/b-PEI were used for synthesis of positive modifiers with various numbers of alkyl chains. The S10E was injected into 4 g of b-PEI (5 mmol) with vigorously stirring and the reaction maintained at room temperature for 24 hours. The final product was obtained by evaporation and dried overnight under vacuum. The S10E and positive modifiers were analyzed by Fourier-transform infrared spectroscopy (FT-IR; Thermo Scientific Nicolet 6700 FT-IR spectrometer) with a spectral resolution of 4 cm^{-1} over the range 4000–400 cm^{-1} and ^{1}H nuclear magnetic resonance (^{1}H NMR, Bruker Avance 600) spectroscopy using CD_3OD as a solvent.

II-2-3. Preparation of positively charged PVDF membrane

Positively charged PVDF membranes were prepared via phase-inversion of a PVDF dope solution containing positive modifiers. The formulation of PVDF dope solution was 16 wt% PVDF, 5 wt% PVP, 78 wt% NMP and 1.6 wt% positive modifier (10 wt% per PVDF). The dope solution was prepared by dissolving PVDF, PVP and positive modifier in NMP solvent at 40 °C with mechanical stirring overnight. To remove bubbles, the resulting dope solution was stored in a 40 °C oven, without stirring, for 4–6 hours. The dope solution was cast on a glass plate with a 200 μm gap casting knife and the glass plate then immediately immersed into a DI water bath as the

nonsolvent. The resulting membrane was rinsed with DI water to remove the solvent and unanchored positive modifier. The series of positively charged membranes were named PVDF-PX, where PX indicates the types of positive modifier. Figure II-1 shows a schematic illustration of the preparation procedure for the positively charged PVDF membranes. The prepared membranes were stored in a DI water bath before use.

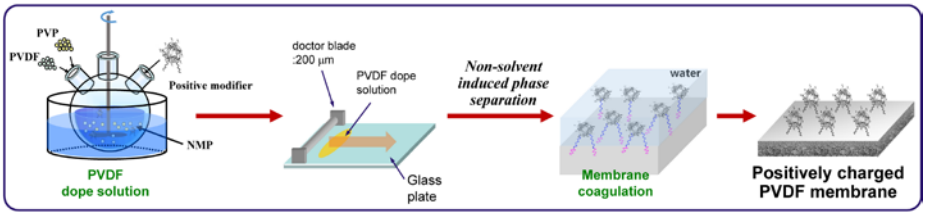

Figure II-1. Schematic illustration of the preparation procedure for positively charged PVDF flat membranes via phase-separation

II-2-4. Membrane Characterization

The positively charged PVDF membranes were analyzed by attenuated total reflection (ATR) FT-IR with a spectral resolution of 4 cm^{-1} over the scan range 4000–650 cm^{-1}. The morphology of membranes was observed by field-emission scanning electron microscopy (FE-SEM; JEOL JSM-7800F), with membrane samples coated by Pt sputtering.

To evaluate the surface charge of the prepared membranes, the surface zeta potentials of the membranes were measured with a SurPASS electrokinetic analyzer (Anton-Paar GmbH) in the pH range 3–11. The surface zeta potential (ζ) of the membranes was calculated by the Helmholtz–Smoluchowski equation [20],

$$\zeta = \frac{\Delta E_{sp}}{\Delta P} \times \frac{\eta \kappa}{\varepsilon_0 \varepsilon_r} \qquad (1)$$

where $\Delta E_{sp}/\Delta P$ is the change in streaming potential with pressure, η is the viscosity of the electrolyte, κ is the conductivity of the electrolyte, and ε_r and ε_0 are the permittivity of the electrolyte and free space, respectively.

Pure water permeabilities were measured using an Amicon 8050 dead-end stirred cell (Millipore Corp.) at a constant pressure (1 bar). PWP was calculated from the following equation (2),

$$PWP = \frac{Q}{t \cdot A \cdot \Delta P} \qquad (2)$$

where Q is the volume of the permeate (L), t is the filtration time (h),

A is the effective area of the membrane (m^2) and ΔP is the transmembrane pressure (bar).

The pore size distribution in the membrane was analyzed using a capillary flow porometer (CFP-1500AEL, Porous Material Inc.). The membranes were wetted by SilWick silicone fluid with a surface tension of 19.1 dynes cm^{-1}. The completely wetted membrane was placed in a sample chamber. N_2 gas was then applied and the pore sizes calculated by the following equation (3),

$$D = 4\,\gamma \cos\theta / P \qquad (3)$$

where D is the pore diameter, γ is the surface tension of the wetting liquid, θ is the contact angle of the wetting liquid and P is the differential gas pressure applied to the wetting liquid in the pores.

In order to evaluate anti-scaling property for the positively charged PVDF membrane, scaling resistance test was carried out using high concentrated ion feed solution containing $CaCl_2$, NaCl, and colloidal silica. The configuration of feed solution was 3 mM $CaCl_2$, NaCl and 250 ppm colloidal silica. In addition, CO_2 gas was supplied to the pressurized vessel for dissolving CO_3^{-2} anion to feed solution. The carbonate anion forms the $CaCO_3$ precipitate to react with calcium ion.

The scaling resistance evaluation was composed of 5 cycles of permeation of pure water and high concentrated ion feed solution. After permeation of high concentrated ion feed, the membranes were back-washed by pure water for 5 min at 1 bar to eliminate loosely bound foulants on the

membrane surface.

All fluxes were recorded using an analytic mass balance. The degree of membrane scaling was confirmed by calculation of normalized flux values for the scaled and backwashed membrane,

$$N = F_t / F_i, \quad (4)$$

where N is the normalized flux, F_t is the flux value, and F_i is the PWP. Equations (5)–(6) give the decrease in total flux caused by membrane scaling,

$$r_{rev}(\%) = (N_w - N_f) \times 100, \quad (5)$$

$$r_{ir}(\%) = (1 - N_w) \times 100, \quad (6)$$

where r_{rev}, and r_{ir} are the percentages of reversible and irreversible foulings, respectively. N_f and N_w are the normalized flux values of the scaled and backwashed membrane, respectively.

After filtration evaluation, membrane surface was observed by FE-SEM equipped with energy dispersive x-ray spectroscopy (EDXS) (JEOL JSM-6700F) for analyzing morphology and chemical composition of membrane surface. In addition, permeability of metal ions and silica was analyzed using inductively coupled plasma atomic emission spectrometry (ICP-AES, PerkinElmer Optima-4300 DV) with an argon plasma source operated at 6,000 K.

II-3. Results and Discussion

II-3-1. Positive modifier

b-PEI is classified as a cationic polymer because it contains a large amount of protonable amine groups. To anchor the cationic b-PEI onto the hydrophobic membrane surface effectively, the b-PEI was reacted with amphiphilic Brij S10 composed of hydrophilic PEG block and hydrophobic octadecyl alkyl chains. The PEG block in Brij S10 helps to migrate the b-PEI towards the membrane surface during membrane production, while the octadecyl alkyl chain in Brij S10 helps to tightly anchor the b-PEI onto the membrane.

From the FT-IR results (Figure II-2), the C-O stretch of the epoxy ring at 765 cm^{-1} was appeared in the epoxy-end modified Brij S10 (S10E) and this IR band was then eliminated after reaction with b-PEI in the IR spectra of amphiphilic positive modifiers (P1, P2, P5), indicating successful conjugation between Brij S10 and b-PEI moieties through the epoxy ring opening reaction. ^{1}H NMR analysis shows more detailed results regarding the reaction progress for the positive modifier. As shown in Figure II-3, the ^{1}H NMR spectra of S10E showed new NMR peaks at 2.5, 2.75, 3.4 and 3.8 ppm, corresponding to the epichlorohydrin, indicating the successful epoxy ring functionalization to Brij S10. The degree of substitution (DS) of the epoxy ring in S10E was 100%. However, the epichlorohydrin peaks were completely absent from the amphiphilic positive modifier spectra (P1, P2, P5). Furthermore, ^{1}H NMR peaks at 2.6–2.7, 2.85 and 3.85 ppm corresponding to N-C$\underline{H_2}$-C$\underline{H_2}$-N, (for

2.6–2.85 ppm) and –C<u>H</u>(OH)-CH_2-N (for 3.85 ppm) were observed in P1, P2, P5 samples. These results clearly show that the amphiphilic positive modifiers composed of Brij S10 and b-PEI were successfully synthesized. The molar ratios S10E/b-PEI obtained from ^{1}H NMR were calculated as 1.03 for P1, 2.02 for P2 and 4.91 for P5 and the b-PEI contents in the positive modifiers were 51.0% for P1, 34.2% for P2 and 17.2% for P5, which are consistent with the b-PEI/S10E reaction molar ratios (Table II-1).

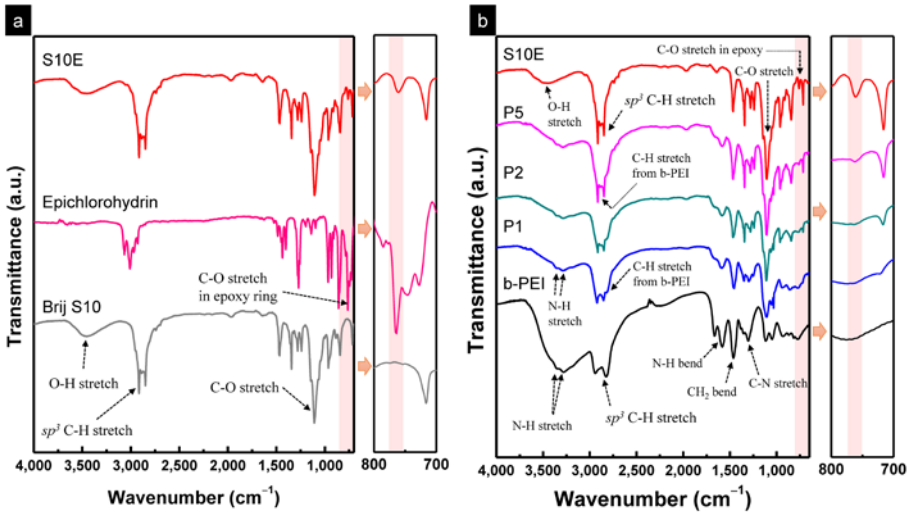

Figure II-2. FT-IR spectra of (a) Brij S10, epichlrohydrin and epoxy end-modified Brij S10 (S10E), and (b) S10E, branched PEI (b-PEI) and positive modifier (P1, P2, P5), (a, b) right inset FT-IR spectra collected over the range 700-800 cm^{-1} corresponding as C-O stretch of epoxy ring

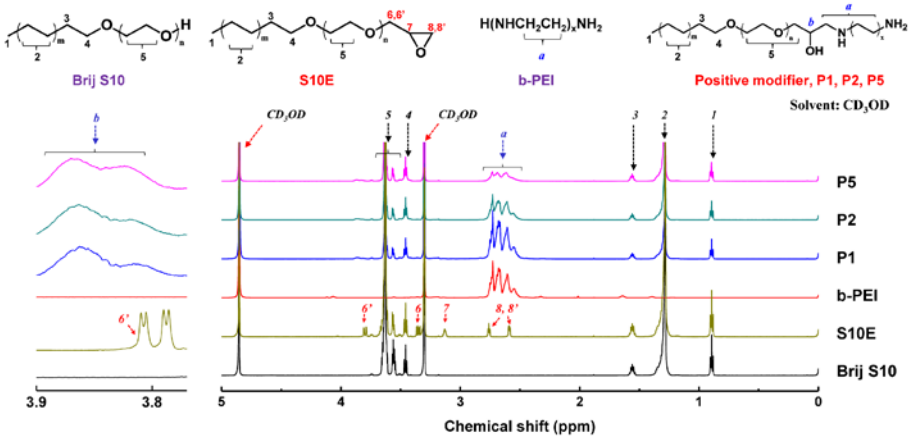

Figure II-3. ^{1}H NMR spectra of Brij S10, epoxy end-modified Brij S10 (S10E), branched PEI (b-PEI) and positive modifiers (P1, P2, P5), degree of substitution (DS) was calculated from the ratio of the integral over '1' and 'a' in the ^{1}H NMR spectra of P1, P2, and P5

Table II-1. Recipe and degree of substitution (DS) of the positive modifier, calculated from ^{1}H NMR analysis

Sample ID	Recipe for positive modifier		Degree of substitution by ^{1}H NMR	Content of b-PEI (%)
	b-PEI	S10E		
P1	4 g (5 mmol)	3.83 g (5 mmol, 1 eqv.)	1.03	51.0
P2		7.67 g (10 mmol, 2 eqv.)	2.02	34.2
P5		19.2 g (25 mmol, 5 eqv.)	4.91	17.2

II-3-2. Positively charged PVDF membrane

The positively charged PVDF membranes, PVDF-P1, PVDF-P2, and PVDF-P5, were fabricated by nonsolvent induced phase-separation (NIPS) of a dope solution containing 10 wt% of the amphiphilic positive modifier per PVDF material. Figure II-4 shows ATR FT-IR spectra of the neat PVDF membrane, the positively charged PVDF membranes, and the amphiphilic positive modifiers. The IR band for sp^3 C-H stretch (2850–2930 cm^{-1}) corresponding to the C-H stretch of the positive modifier appeared in the modified membrane. This indicates that the positive modifier was presented onto the PVDF membrane surface during membrane fabrication process. In addition, as shown in Figure II-5, the zeta potential values for the modified PVDF membranes exhibited a positive surface charge below pH 9. On the other hand, the neat PVDF membrane showed negative zeta potential values over the whole pH range because the C-F moiety in the neat PVDF membrane has a negative charge. The PVDF membrane incorporating neutral charged Brij S10 without b-PEI (PVDF-S10, more detailed characterization: Figures II-6, II-7) showed constant zeta potential values within ± 4 mV over the whole pH range and the neutral isoelectric point (IEP). These results suggest that the desired positive charge moiety was successfully introduced onto the PVDF membrane by anchoring the amphiphilic positive modifier. Interestingly, the IR spectra of the top and bottom surfaces of the positively charged PVDF membranes showed different intensities of the sp^3 C-H stretch corresponding to the amphiphilic positive modifiers over the range 2850–2930 cm^{-1}. As can be seen in Figure II-4, the intensity of the sp^3 C-H stretch for the top surface was higher than that for the bottom surface, indicating that

the positive modifiers were more located at the top surface of the membrane. This was thought to be attributed to migration of the amphiphilic positive modifier towards the membrane top surface during the NIPS process. When the cast thin dope solution was exposed to the water as nonsolvent, the hydrophilic part (b-PEI) of the positive modifier migrated towards the membrane top surface because of the hydrophilic affinity of the b-PEI segment with water, whereas the alkyl chain was consolidated within the hydrophobic PVDF layer. These migrations resulted in positive moieties anchored onto the surface of the PVDF membranes. Complete migration of the positive modifier towards the membrane surface was not likely to be achieved during the NIPS process because there was insufficient time for the modifier to fully undergo phase separation. Nonetheless, the difference in IR intensities between top and bottom surfaces verified that the ionic b-PEI mainly existed near the membrane top surface. Thus, this method provided the membrane surface with positive charge moieties by tightly anchoring the positive modifier.

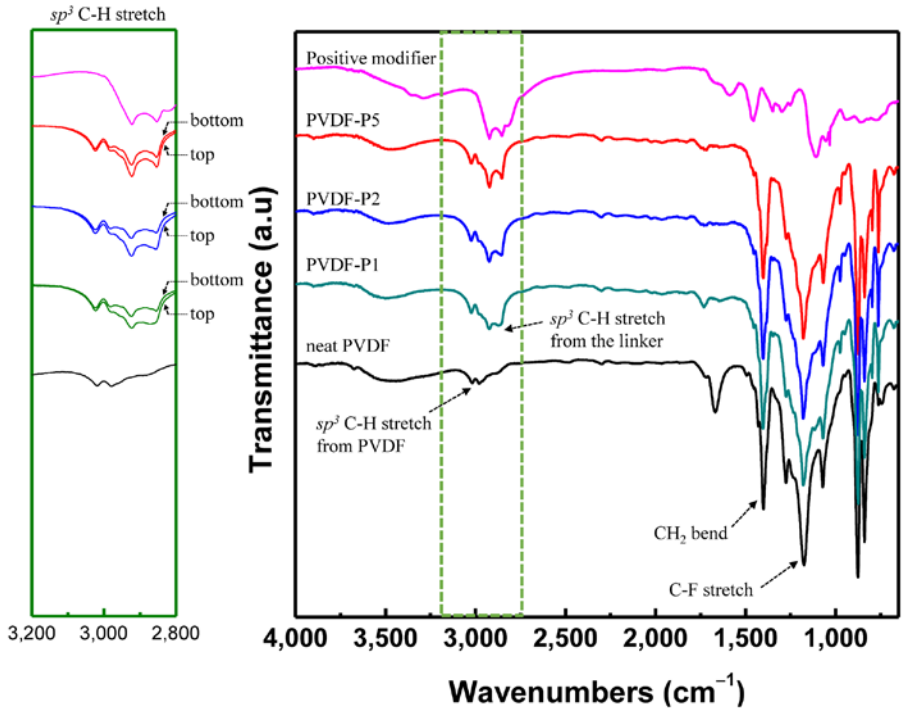

Figure II-4. FT-IR spectra of (right) the positive modifier, top surface of the positively charged and neat PVDF membranes and (left) both surfaces (top and bottom) of the positively charged PVDF membrane, collected over the range 3200–2800 cm^{-1}, corresponding to the C-H stretch of the positive modifier

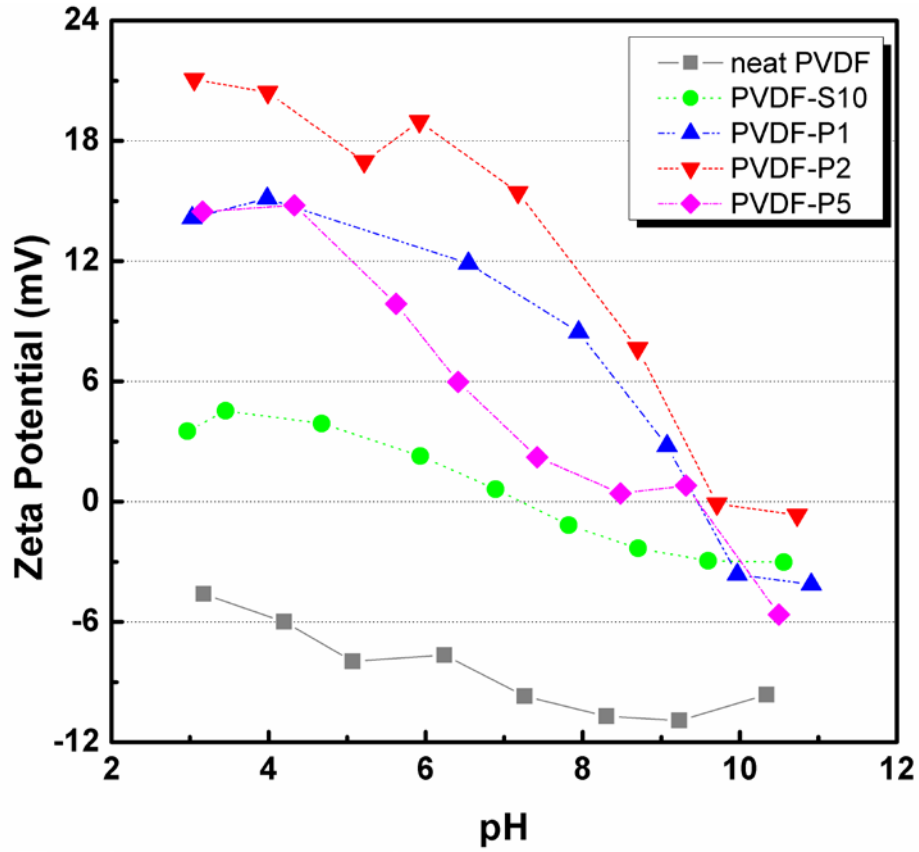

Figure II-5. Zeta potential results for neat, neutral and the positively charged PVDF membranes over the pH range 3–11

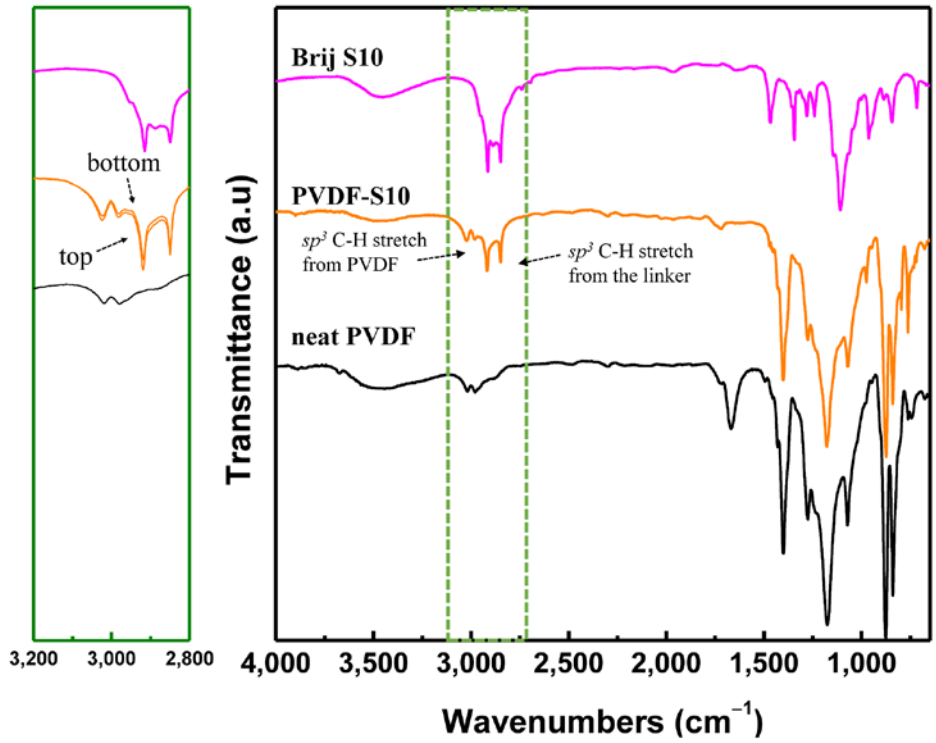

Figure II-6. (right) FT-IR spectra of the Brij S10, top surface of the PVDF-S10 membrane and neat PVDF membrane (left) FT-IR spectra of both surfaces (top and bottom) of the PVDF-S10 membrane, collected over the range 3200-2800 cm^{-1} corresponding as C-H stretch of the positive modifier

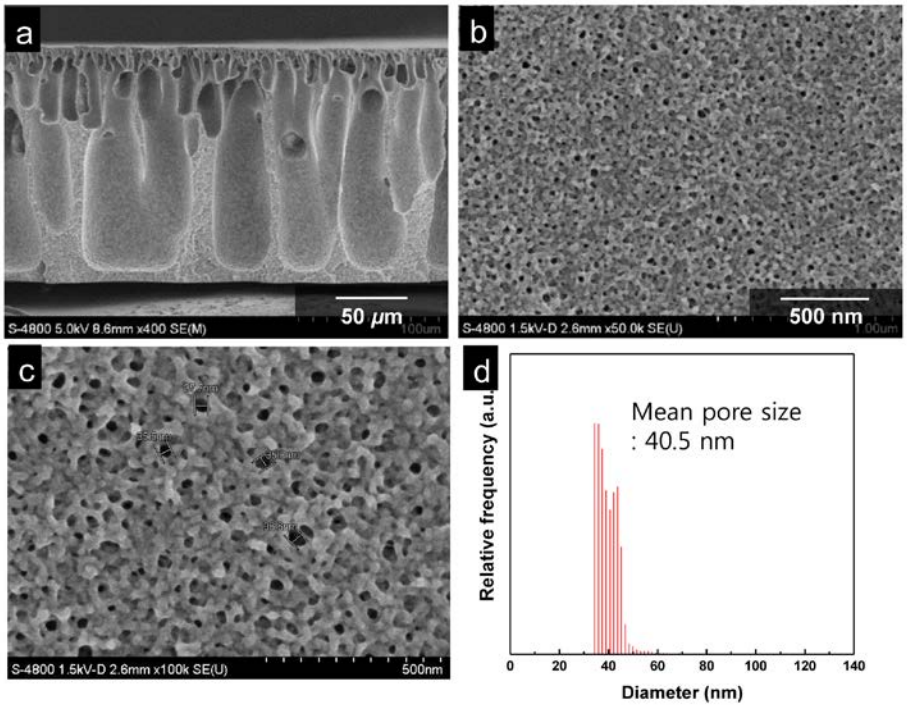

Figure II-7. FE-SEM images for (a) cross-section (b-c) top surface morphologies of the PVDF-S10 membrane, (d) the result of the pore-size and distribution of the PVDF-S10 membrane obtained from capillary flow porometer

Figure II-8 shows FE-SEM images for the top surface and cross-section morphologies of the neat PVDF and the positively charged PVDF membranes. All membranes had a similar morphology, typical of asymmetric membranes prepared by the NIPS process. The pore sizes at the top surface of the membrane were in the range 20–60 nm in all membrane samples (Figure II-9). The results of capillary flow porometry also showed that all membranes had a similar mean pore diameter (*ca*. 40 nm) and size distribution(see bottom of Figure II-8). These results show that the positive modifiers were well anchored onto the PVDF membrane surface without significantly affecting membrane morphology or pore sizes.

Figure II-10 shows the PWP values for the neat PVDF and positively charged PVDF membranes. The measured PWP values ranged from 1200 to 1650 L m^2 h^{-1} bar^{-1}. The PWP values for the positively charged PVDF membranes were higher than that for the neat PVDF membrane, which can be attributed to the ionic segment of b-PEI anchored on the membrane surface. Interestingly, the PVDF-P2 membrane had the highest PWP values (1654 ± 19 L m^2 h^{-1}) compared with the other positively charged PVDF membranes (PVDF-P1, PVDF-P5). It might be associated with the b-PEI content on the membrane surface. In the previous results about surface charge, the zeta potential value of the PVDF-P2 membrane was higher than for the other positively charged membranes over the whole pH range, suggesting that the b-PEI content on the membrane surface in the PVDF-P2 membrane was higher than that of the other membranes. The roles of b-PEI and the octadecyl group in the modifier are the positive charge moiety and the anchoring group within the PVDF membrane, respectively. As a result, an increase in the molar

ratio of Brij S10 in the positive modifier enhances the anchoring on the membrane surface but reduces the positive charge density at the membrane surface because of a decrease in the quantity of b-PEI. That is, anchoring efficiency and positive charge contents of the modifier is reciprocal, which was verified by the ^{1}H NMR results (b-PEI contents: 51.0% for the P1, 34.2% for P2 and 17.2% for P5). Thus, it was thought that the content ratio between b-PEI and octadecyl group in the modifier is a key factor to govern the positive charge strength at the membrane surface. The positive modifier P1 had the highest b-PEI content but may have had low anchoring efficiency because of low hydrophobic alkyl content. On the other hand, the positive modifier P5 was well-anchored but would not provide the membrane surface with increased positive moieties because of its low b-PEI content. Although the positive modifier P2 had the intermediate b-PEI and hydrophobic alkyl contents, it gave the highest positive density at the membrane surface in the modified membranes. This was attributed to the optimal content ratio for cationic b-PEI/hydrophobic anchoring group of the positive modifier P2 compared with the other positive modifiers. The combined results for ATR FT-IR, FE-SEM, capillary porometry, and zeta potential analysis showed that positive charges were successfully anchored onto the membrane surface by the hydrophilic-hydrophobic recognition phase-separation. In particular, the PVDF-P2 membranes had the highest membrane performance and the positive charge density through highly efficient surface anchoring of b-PEI.

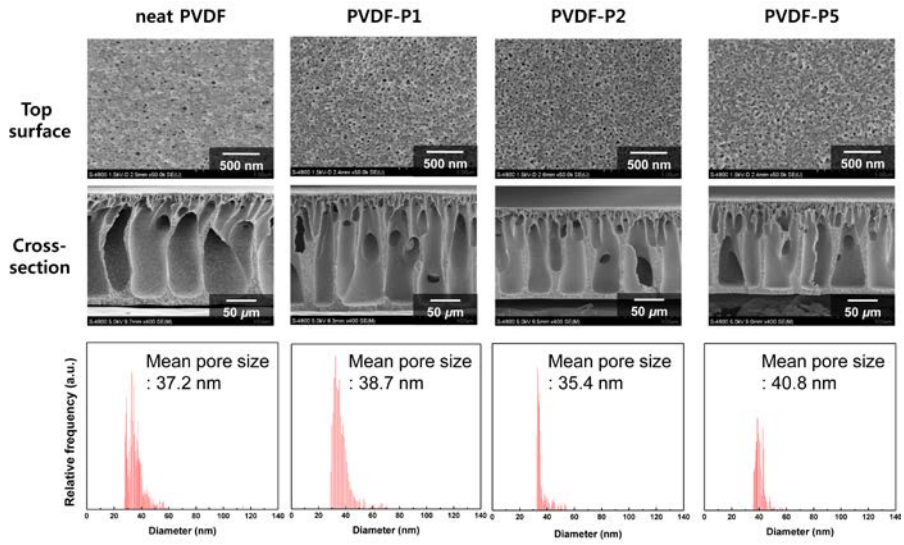

Figure II-8. FE-SEM images of the top surface (upper line) and cross-section (middle line) morphologies of the neat (row 1) and positively charged (rows 2–4) PVDF membrane (lower line), the results of pore size distribution of the neat and positively charged PVDF membranes obtained from the capillary flow porometer

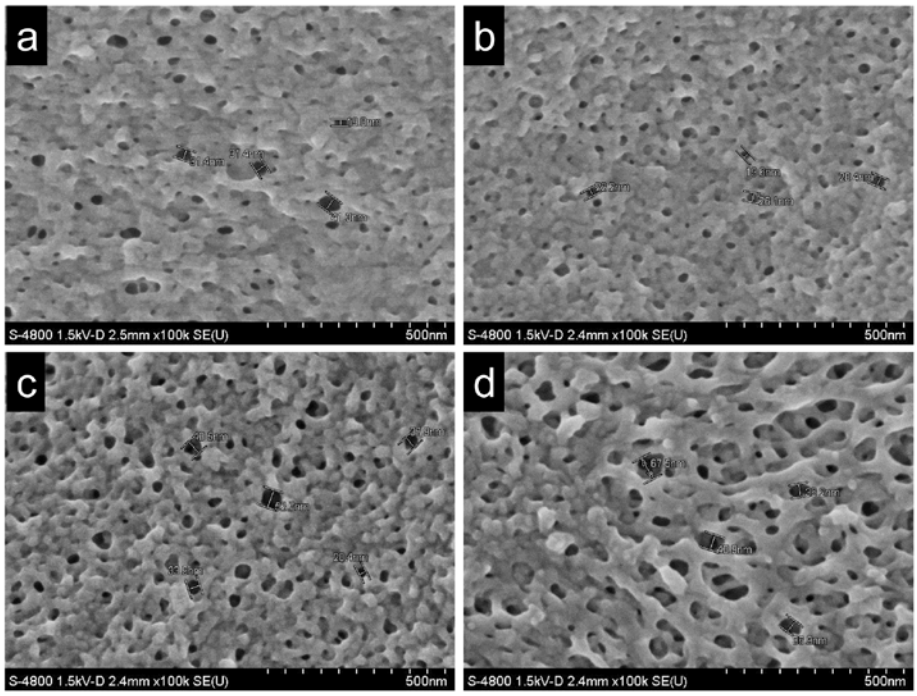

Figure II-9. FE-SEM images for enlarged top surface morphologies of (a) neat PVDF, (b) PVDF-P1, (c) PVDF-P2 and (d) PVDF-P5 membranes

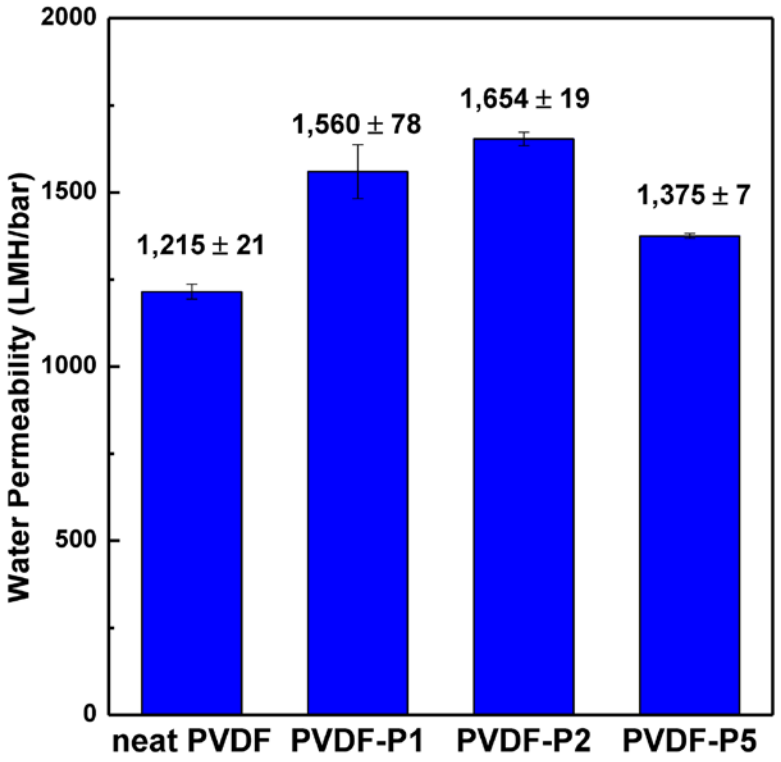

Figure II-10. Pure water permeability at 1 bar of the neat and positively charged PVDF membranes, the bars showing standard deviation represent the average of three test results

II-3-3. Evaluation of scaling resistance

To investigate the resistance to scaling by the positively charged PVDF membrane, scaling resistance tests were carried out using a high concentrated ion feed solution including Ca^{2+}, Na^{+} ions and colloidal silica to form precipitates on the membrane surface. CO_2 gas was supplied to dissolve carbonate anion which forms $CaCO_3$ precipitate with Ca^{2+} ion. The PVDF-P2 membrane was selected to this evaluation due to the highest surface positive charge density. As can be seen in Figure II-11, the water fluxes for the both neat PVDF and PVDF-P2 membranes were dramatically declined by passage of the high concentrated ion and colloidal silica containing feed solution. However, the positively charged membrane, *i.e.*, PVDF-P2, showed much higher recovered water fluxes after simple membrane back-washing that that for the neat PVDF membrane. Especially, this recovery tendency for the PVDF-P2 membrane was stably maintained by repeated fouling evaluation. On the other hand, in the neat PVDF membrane, the recovered water fluxes were gradually reduced by repeated fouling tests. The flux for high concentrated ion feed solution was also declined by increase in cycles. The recovered flux, indicating reversible fouling, of the PVDF-P2 membrane was 24-36% for whole filtration cycles. On the other hand, the neat PVDF membrane was recovered its performance around 5-15% for whole filtration test.

To analyze scaling reason, surface morphology and chemical composition analysis was carried out using FE-SEM/EDXS for filtrated membrane samples (see Figure II-12). In the neat PVDF membrane, the surface of membrane was completely covered with precipitates which were

composed of silica and calcium precipitates. By contrast, the PVDF-P2 membrane was partially covered with precipitates. The composition of the almost precipitates was silica. A Ca element was not found on the surface of membrane through EDXS analyzing. Furthermore, metal ion permeability of the PVDF-P2 membrane was much higher than that for the neat PVDF membrane (see Table II-2). The permeability of metal ions was around 36% (Na^+), 41% (Ca^{2+}) for the neat PVDF membrane and 75% (Na^+) and 78% (Ca^{2+}) for the PVDF-P2 membrane. These results indicate that the metal ions were more preferred to absorb on the neat PVDF membrane surface due to its negatively charged surface property. Although the performance of membrane was decreased in high colloidal silica content in the feed solution, the surface positive charge of PVDF-P2 membrane suppressed adsorption of metal ions onto membrane surface. This indicates that enhancement of scaling resistance property was directly related to a higher surface positive density. Consequently, it is expected that the positively charged PVDF membrane can be applied as a scale-resistant membrane for wastewater containing high concentrations of metal ions.

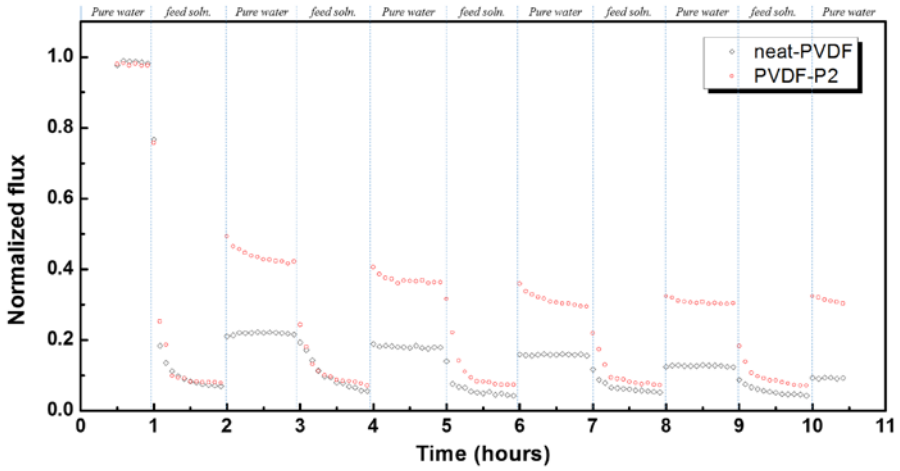

Figure II-11. Filtration tests of neat and PVDF-P2 membranes using a 3 mM $CaCl_2$, 3 mM NaCl aqueous solution containing 250 ppm silica particles

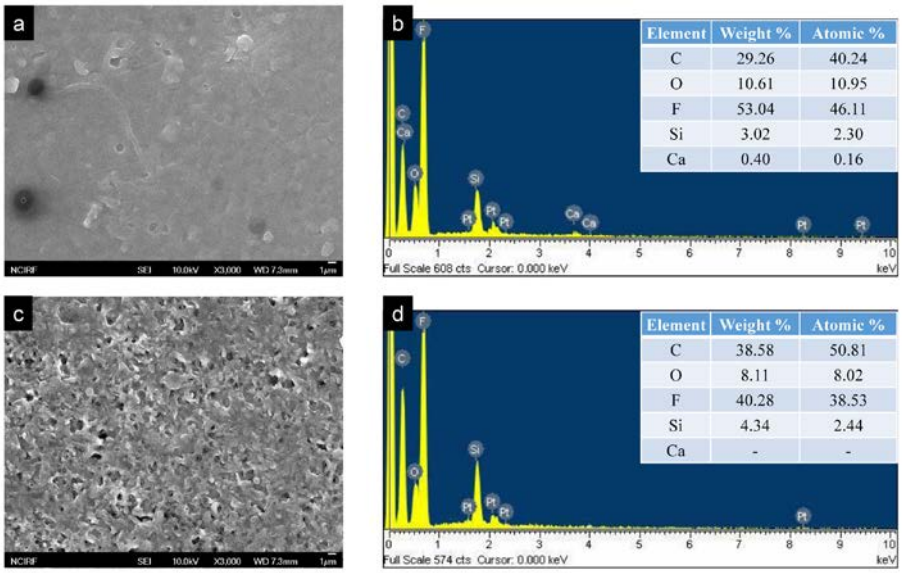

Figure II-12. FE-SEM images for top surface morphologies after filtration test of (a) neat PVDF and (c) PVDF-P2 membrane, EDXS spectra of (b) neat PVDF (d) PVDF-P2 membranes (inset table) chemical composition of membrane surface

Table II-2. Concentration of sodium, calcium and silicon in retention and permeate for the neat and the PVDF-P2 membranes during scaling resistance evaluation

neat PVDF	Cycle	1	2	3	4	5
Retention ($mg\ L^{-1}$)	Na	69.93	66.85	71.51	70.25	79.66
	Ca	85.27	81.56	89.50	86.89	84.80
	Si	45.40	45.21	42.50	42.30	44.93
Permeate ($mg\ L^{-1}$)	Na	27.62	24.89	23.78	23.97	28.79
	Ca	37.27	32.43	36.07	36.46	34.48
	Si	1.45	1.32	1.49	1.45	1.83
Permeability (%)	Na	39.50	37.23	33.25	34.12	36.14
	Ca	43.71	39.76	40.30	41.96	40.66
	Si	3.19	2.92	3.51	3.43	4.07
PVDF-P2	Cycle	1	2	3	4	5
Retention ($mg\ L^{-1}$)	Na	68.50	72.97	71.14	73.36	68.02
	Ca	86.50	88.85	84.95	89.43	84.13
	Si	42.48	44.45	47.19	45.61	48.16
Permeate ($mg\ L^{-1}$)	Na	46.97	51.83	58.11	56.21	55.04
	Ca	61.91	65.21	73.36	70.75	68.17
	Si	1.34	1.36	1.46	1.67	1.75
Permeability (%)	Na	68.57	71.03	81.68	76.62	80.92
	Ca	71.57	73.39	86.36	79.11	81.03
	Si	3.15	3.06	3.09	3.66	3.63

II-4. Conclusions

In this chapter, positively charged UF/MF membranes have been developed for enhancement of anti-scaling property by surface anchoring an amphiphilic positive modifier onto a PVDF membrane. The ATR FT-IR spectra and zeta potential analysis showed that cationic b-PEI was successfully anchored onto the membrane surface via hydrophilic-hydrophobic mediated phase-separation assembly. The membrane morphology and mean pore size were not significantly altered, despite the introduction of positive charges onto the membrane surface with high density. The combined results of evaluating PWP and scaling resistance showed that a higher density of positive surface charges on the membrane led to an enhancement in water permeability and scaling resistance for highly concentrated metal ions/silica wastewater. An advantage of this membrane is that the positive charge was robustly introduced to the membrane by simply adding the amphiphilic positive modifier during the membrane fabrication process. The enhanced anti-scale property of this membrane makes them attractive for eco-friendly and economical purification of an industrial wastewater containing high metal ion content.

References and Notes

1. Lee, S.; Kim, J.; Lee, C.-H., Analysis of CaSO4 scale formation mechanism in various nanofiltration modules. *J. Membr. Sci.* **1999,** *163* (1), 63-74.

2. Lin, C.; Shirazi, S.; Rao, P., Mechanistic Model for CaSO4 Fouling on Nanofiltration Membrane. *J. Environ. Eng.* **2005,** *131* (10), 1387-1392.

3. Song, L.; Singh, G., Influence of various monovalent cations and calcium ion on the colloidal fouling potential. *J. Colloid Interface Sci.* **2005,** *289* (2), 479-487.

4. Seidel, A.; Elimelech, M., Coupling between chemical and physical interactions in natural organic matter (NOM) fouling of nanofiltration membranes: implications for fouling control. *J. Membr. Sci.* **2002,** *203* (1–2), 245-255.

5. Lee, S.; Lee, C.-H., Effect of operating conditions on CaSO4 scale formation mechanism in nanofiltration for water softening. *Water Res.* **2000,** *34* (15), 3854-3866.

6. Hasson, D.; Semiat, R.; Bramson, D.; Busch, M.; Limoni-Relis, B., Suppression of CaCO3 scale deposition by anti-scalants. *Desalination* **1998,** *118* (1–3), 285-296.

7. Karakulski, K.; Gryta, M., Water demineralisation by NF/MD integrated processes. *Desalination* **2005,** *177* (1–3), 109-119.

8. Kim, J. O.; Choi, S. P.; Yoon, H.; Kim, G. T., Fouling and scaling reduction by pulsed electric field treatment as pretreatment for desalination. *Desalination and Water Treatment* **2012,** *43* (1-3), 118-123.

9. Gill, J. S., A novel inhibitor for scale control in water desalination.

Desalination **1999,** *124* (1–3), 43-50.

10. Hoek, E. M. V.; Kim, A. S.; Elimelech, M., Influence of crossflow membrane filter geometry and shear rate on colloidal fouling in reverse osmosis and nanofiltration separations. *Environmental Engineering Science* **2002,** *19* (6), 357-372.

11. Koyuncu, I., Reactive dye removal in dye/salt mixtures by nanofiltration membranes containing vinylsulphone dyes: effects of feed concentration and cross flow velocity. *Desalination* **2002,** *143* (3), 243-253.

12. Shirazi, S.; Lin, C.-J.; Chen, D., Inorganic fouling of pressure-driven membrane processes — A critical review. *Desalination* **2010,** *250* (1), 236-248.

13. Jung, Y.-J.; Kiso, Y.; Yamada, T.; Shibata, T.; Lee, T.-G., Chemical cleaning of reverse osmosis membranes used for treating wastewater from a rolling mill process. *Desalination* **2006,** *190* (1–3), 181-188.

14. Du, R.; Zhao, J., Positively charged composite nanofiltration membrane prepared by poly(N,N-dimethylaminoethyl methacrylate)/polysulfone. *J. Appl. Polym. Sci.* **2004,** *91* (4), 2721-2728.

15. Huang, R.; Chen, G.; Sun, M.; Hu, Y.; Gao, C., Studies on nanofiltration membrane formed by diisocyanate cross-linking of quaternized chitosan on poly(acrylonitrile) (PAN) support. *J. Membr. Sci.* **2006,** *286* (1–2), 237-244.

16. Du, R.; Zhao, J., Properties of poly (N,N-dimethylaminoethyl methacrylate)/polysulfone positively charged composite nanofiltration membrane. *J. Membr. Sci.* **2004,** *239* (2), 183-188.

17. Su, Y.; Jian, X.; Zhang, S.; Wang, G., Preparation and

characterization of quaternized poly(phthalazinone ether sulfone ketone) NF membranes. *J. Membr. Sci.* **2004,** *241* (2), 225-233.

18. Huang, R.; Chen, G.; Sun, M.; Gao, C., Preparation and characterization of composite NF membrane from a graft copolymer of trimethylallyl ammonium chloride onto chitosan by toluene diisocyanate cross-linking. *Desalination* **2009,** *239* (1–3), 38-45.

19. Cheng, S.; Oatley, D. L.; Williams, P. M.; Wright, C. J., Positively charged nanofiltration membranes: Review of current fabrication methods and introduction of a novel approach. *Adv. Colloid Interface Sci.* **2011,** *164* (1–2), 12-20.

20. Kumar, M.; Ulbricht, M., Advanced ultrafiltration membranes based on functionalized poly(arylene ether sulfone) block copolymers. *RSC Adv.* **2013,** *3* (30), 12190-12203.

CHAPTER III

SILVER NANOPARTICLES LINKED POLY(VINYLIDENE FLUORIDE) (PVDF) MEMBRANES FOR ENDOWMENT OF SUSTAINABLE ANTI-BIOFOULING PROPERTY

III-1. Introduction

Membrane biofouling derived from microorganism is a major obstacle to successful membrane operation because the microorganisms that accumulate on a membrane surface not only grow over time, they tend to form a dense biofilm that blocks membrane function[1-2]. The biofouling rapidly deteriorates the membrane performance and increases the maintenance costs by requiring regular membrane cleaning or replacement[3-4].

To solve the membrane biofouling problems, a variety of reactive functional materials, such as hydrophilic[5-8], charged[9-11], photocatalytic[12-15], or biocidal materials[16-20] have been introduced into the ultra- and micro-filtration membranes. These materials can reduce membrane biofouling by adhesion inhibition of hydrophobic foulants or decomposition of microbial foulants. Although these material's properties endow a good anti-fouling properties to the water treatment membrane, a number of limitations have

been associated with these materials, including stability, pH dependence and membrane degradation[21-23]. Exceptionally, among the biocidal materials, silver nanoparticles (Ag NPs), display strong inhibitory and a biocidal properties against a variety of microorganism types with long period time[23-27]. Significant efforts have been devoted to introducing Ag NPs into polymeric membrane substrates to form Ag NP/membranes nanocomposite. Ag NP/membranes nanocomposite are usually prepared through a non-solvent induced phase separation (NIPS) process using an Ag NPs-included dope solution[16, 18-20]. Ag NPs have also been coated directly onto polymer membrane substrates to form Ag NP/membranes nanocomposite[17]; however, the practical utility of these methods has been limited by the low efficiency of Ag NP deposition onto the membrane surfaces. Furthermore, the immobilized Ag NPs can be released (or leached) from the membranes owing to the lack of interaction between Ag NP and membrane. Indeed, Alvarez and coworkers reported that the Ag NPs which were located on the membrane surface were readily removed during water filtration process[16]. The unwanted loss of the Ag NPs from the membrane brings about the deterioration in the desired properties such as an anti-biofouling property and a membrane life time. Most problematic of all, the Ag NPs released from the membrane can penetrate easily into the human body, can produce cell damage and cancer[28-30].

Recently, Mauter and coworkers described the preparation of Ag NPs/membrane nanocomposites in which the Ag NPs were electrostatically assembled on the membrane. The membrane was prepared by means of the assembly between the Ag NPs encapsulated with the positively charged polyethyleneimine (PEI) and the polysulfone (PSF) membrane functionalized

with the negative charged carboxylic acid[31]. Electrostatic interactions were useful for depositing the Ag NPs on the membrane substrate; however, the Ag NPs were eventually released from the membrane due to the weakness of the electrostatic attraction between the Ag NPs and the membrane[16]. Stable and robust bonds between the Ag NPs and the membrane are important for ensuring the preparation of safe, eco-friendly, stable, anti-biofouling, and high-efficiency membranes. Metal-sulfur interaction is one of the solution for strong attachment of Ag NPs onto membrane surface because sulfur group has high affinity and formation of covalent bond with noble metals such as silver, gold, platinum and etc. which have large ionic radius and low oxidation station. It is expected that introduction of metal-sulfur linkage can develop sustainable anti-biofouling membrane by suppression of leaching biocidal Ag NPs onto membrane surface.

This study describes the Ag NP-poly(vinylidene fluoride) (Ag-PVDF) membrane nanocomposites having a sustainable anti-biofouling property through the covalent assembly of the Ag NPs onto the PVDF membrane surface via a thiol end-functionalized amphiphilic block copolymeric linker. To this end, the thiol end-functionalized amphiphilic block copolymer as a covalent linker between the Ag NPs and the membrane were physically anchored onto the membrane via hydrophilic–hydrophobic phase recognition of the amphiphilic linkers during the NIPS membrane fabrication process, resulting in the thiolated PVDF membrane. Ag NPs then covalently bound to the thiolated PVDF membrane via a simple impregnation process. Surprisingly, the resulting Ag-PVDF membrane nanocomposite did not release detectable amounts of Ag NPs from the membrane, and the

membrane displayed excellent anti-biofouling property. This makes them tremendously attractive in applications ranging from high-efficient membrane to eco-friendly water purification systems.

III-2. Experimental Section

III-2-1. Materials

Polyvinylidene fluoride (PVDF, M_w = 570,000 g mol^{-1}) was supplied from Solvay Chemicals. Silver nitrate ($AgNO_3$, 99%), trisodium citrate ($C_6H_5Na_3O_7$, analytic grade), sodium borohydride ($NaBH_4$, 98.5%), polyethylene-*block*-polyethylene glycol (P(E-*b*-EO), M_n = 2,250 g mol^{-1}, PEO: 80%), toluene (C_7H_8, 99.5%), and mercaptoacetic acid ($C_2H_4O_2S$, 98%) were purchased from Sigma-Aldrich. *N, N*-Dimethylacetamide (C_4H_9NO, 99%) was purchased from Tokyo Chemical Industry (TCI). Polyvinylpyrrolidone (PVP, M_w = 40,000 g mol^{-1}) and diethyl ether ($C_4H_{10}O$, analytic grade) were supplied from Daejung Chemicals & Metals. All chemicals were used as received without further purification. The aqueous solutions were prepared from deionized (DI) water having a resistivity exceeding 18.0 MΩ cm.

III-2-2. Preparation of amphiphilic thiol linker

The linker used for the covalent assembly of Ag NPs with the PVDF membrane was prepared by converting the hydroxyl group of the P(E-*b*-EO) to a thiol group through an esterification reaction using mercaptoacetic acid.

A 11.3 g sample of P(E-*b*-EO)was dissolved in 50 mL dry toluene at 80 °C. After complete dissolution of the P(E-*b*-EO), the mixture containing 1.38 g mercaptoacetic acid and 0.5 mL concentrated sulfuric acid was slowly added dropwise to the P(E-*b*-EO) solution. The solution was vigorously stirred at 110 °C for 2 hours. The solution was then dropped into cold diethyl ether with vigorous stirring, and the crude product was filtered out. To remove the unreacted reactants, the crude product was washed several times with diethyl ether and filtered. The final product was dried in a vacuum at room temperature for overnight. The thiol-modified P(E-*b*-EO) was characterized by Fourier-transform infrared spectroscopy (FT-IR, Thermo Scientific Nicolet 6700 FT-IR spectrometer) with a spectral resolution of 4 cm^{-1} over the range 4000 – 400 cm^{-1} and by ^{1}H nuclear magnetic resonance (^{1}H NMR, Bruker AVANCE 600) spectroscopy using $CDCl_3$ as a solvent.

III-2-3. Preparation of thiolated PVDF membrane

The thiolated PVDF membrane was prepared via hydrophilic–hydrophobic phase recognition between the thiol-modified amphiphilic linker and the PVDF polymer during a NIPS process. The membrane dope solution was prepared by dissolving 15 wt% PVDF, 5 wt% PVP, and 0.75–2.25 wt% thiol-modified P(E-*b*-EO) (5–15 wt% per PVDF raw material) in a DMAc solution at 40 °C for overnight using a mechanical stirrer. The dope solution was put in an oven at 40 °C for two hours to remove any bubbles. The dope solution was cast onto a glass plate using a 200 μm casting applicator, and the cast film was immediately immersed in DI water, which acted as a non-solvent, to produce a PVDF flat sheet membrane incorporating the linkers

having thiol functional groups. The thiolated membrane was then carefully rinsed with DI water to remove the solvent, pore-forming agent, and unanchored linker. The thiolated PVDF membrane was denoted PVDF-SHX, where X indicates the weight percentage of the thiol-modified P(E-*b*-EO) relative to the PVDF in the dope solution. For comparison, a neat PVDF membrane was prepared using the protocol described above except that the thiol-modified P(E-*b*-EO) was not added. All membranes were stored in DI water prior to use.

III-2-4. The preparation of Ag NPs-covalently assembled PVDF membrane nanocomposite

The colloidal Ag NPs were synthesized according to previously reported protocols[32-33]. Briefly, 20 mL of a 1 mM $AgNO_3$ aqueous solution was mixed with an equal volume of a 1 mM trisodium citrate solution. A 0.6 mL volume of 0.1 M $NaBH_4$ solution was quickly injected into the $AgNO_3$/trisodium citrate mixture with vigorous stirring at room temperature. The color of the solution immediately changed from dark gray to yellow, indicating the successful formation of Ag NPs. The size of as-synthesized Ag NP was ca. 5-8 nm (see Figure III-1). The Ag NPs were covalently bound to the thiolated PVDF membrane by immersing a sample of the prepared thiolated PVDF membrane (10×8 cm^2) into the colloidal Ag NP aqueous solution under mildly basic conditions. The solution was then agitated gently at room temperature in an orbital shaker for 1 day. The specimen was then carefully rinsed several times with DI water to remove loosely bound Ag NPs, and the sample was stored in a DI water bath prior to use. The Ag NP–PVDF

membrane nanocomposite was denoted Ag-PVDF. The overall procedure used to prepare the Ag-PVDF membrane nanocomposite is schematically illustrated in Figure III-2. For comparison, the neat PVDF membrane was treated with the Ag NP colloid in the same manner used for the production of Ag-PVDF. The neat PVDF membrane into which non-covalently bound Ag NPs had been introduced was denoted Ag/PVDF.

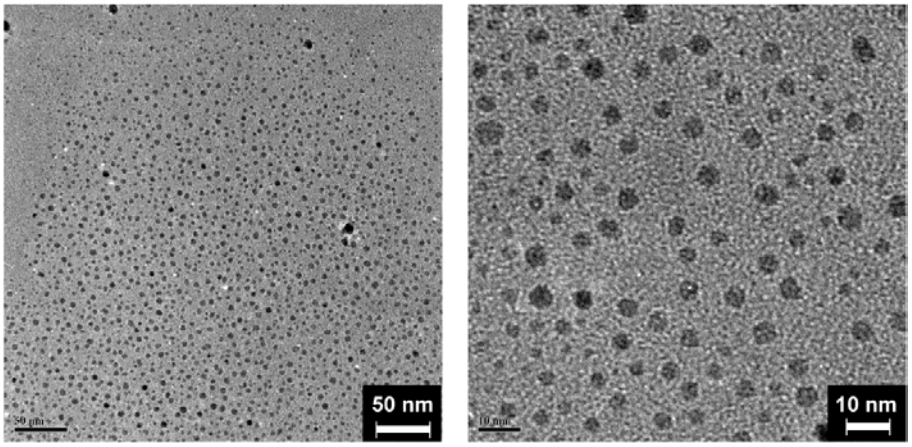

Figure III-1. TEM images of as-synthesized Ag NPs; (left) low and (right) highly magnified TEM image

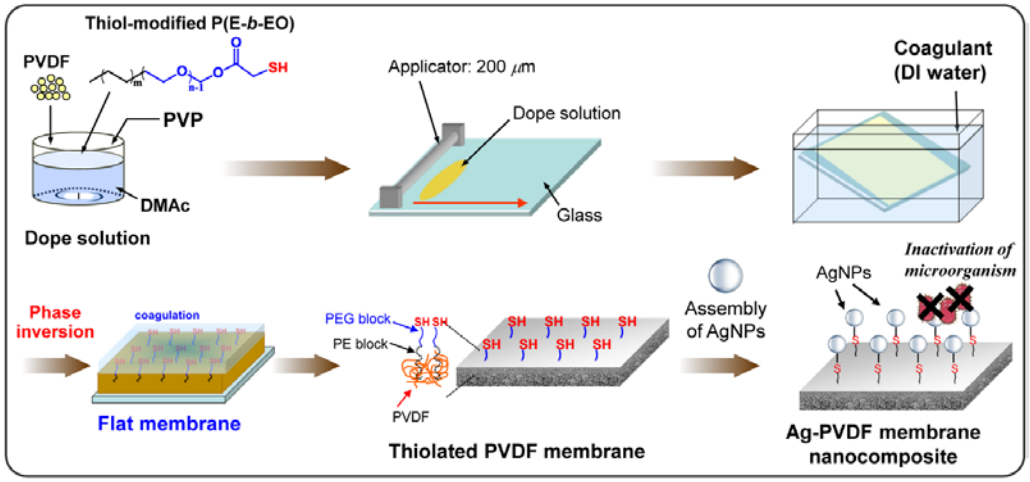

Figure III-2. Schematic illustration of the procedure for the formation of the Ag NPs covalently assembled on the PVDF membrane (Ag-PVDF membrane nanocomposite)

III-2-5. Membrane characterization

The thiolated PVDF membrane was analyzed by attenuated total reflection Fourier-transform infrared (ATR FT-IR, Thermo Scientific Nicolet 6700 FT-IR spectrometer) spectroscopy with a spectral resolution of 4 cm^{-1} over the scan range from 4000–650 cm^{-1}. The surface and cross-sectional morphologies of the membranes were observed by field-emission scanning electron microscopy (FE-SEM, Carl Zeiss SUPRA 55VP, JEOL 7800F) and energy-dispersive X-ray spectroscopy (EDXS, Bruker X-flash-4010). The samples used for FE-SEM imaging were coated with a thin Pt layer (ca. 20 nm thick). The Ag loading in the Ag-PVDF was determined using inductively coupled plasma atomic emission spectrometry (ICP-AES, PerkinElmer Optima-4300 DV) with an argon plasma source operated at 6,000 K. The pure water permeability (PWP) of each membrane was measured using an Amicon 8050 dead-end stirred cell (Millipore corp.) connected to a pressure vessel filled with DI water. The PWP was measured continuously by collecting the permeate on an analytic mass balance (CAS CUW 420H) at constant pressure (1 bar), and the value was calculated using the following equation (*1*),

$$PWP = Q/(t \cdot A \cdot \Delta P), \qquad (1)$$

where Q is the volume (L) of the permeate, t is the filtration time (h), A is the effective membrane area (m^2), and ΔP is the transmembrane pressure (bar).

The membrane pore size was analyzed by filtering an aqueous suspension of polystyrene (PS) latex beads (diameter: 0.06 μm and 0.1 μm)

and γ-globulin (diameter: 20–30 nm at pH 7) through the membrane. The rejection value of each particle was calculated using the following equation (*2*),

$$R(\%) = \left(1 - \frac{C_p}{C_f}\right) \times 100 \quad (2)$$

where R(%) is the rejection percentage of these particles, and C_p and C_f are the particle concentrations in the permeate and feed solutions, respectively. The particle concentration in the feed (C_f) and permeate (C_p) solutions were determined using standard concentration curves for the PS latex bead and the γ-globulin, plotted using the turbidity value of each PS latex particle and the UV absorbance intensity at λ_{max} (279 nm) of γ-globulin, respectively. The concentration of each filtrate was determined using a linear regression of the standard curves. The turbidity of the PS latex suspended solution and the UV absorbance of the γ-globulin suspensions were measured using a turbidity analyzer (HACH 2100 AN) or a UV-visible spectrometer (PerkinElmer Lambda 25), respectively.

The binding stability between the Ag NPs and the membrane was tested by conducting a Ag NP release test in which DI water was continuously filtered through the Ag-PVDF membrane nanocomposite (effective membrane area: 13.4 cm^2) using the Amicon dead-end stirred cell. The degree of Ag NP release from the membrane was quantitatively analyzed by evaluating the concentration of Ag in the filtrate using ICP-AES. The amount of Ag present on the membrane surface was analyzed by X-ray photoelectron spectroscopy

(XPS), and the patterns were recorded using a Kratos AXIS-HSi spectrometer featuring a monochromatic Mg $K_{\square}$ X-ray source operated at 10 mA.

Membrane anti-adhesion and biofouling resistance tests were conducted using an aqueous suspension of *Escherichia coli* (*E. coli*). The *E. coli* TOP10 strain (purchased from Invitrogen) was first cultured in a (250 mL) flask in Luria-Bertani (LB) broth (1% bactotryton, 0.5% yeast extract, 1% NaCl) in a 37 °C incubation shaker for 20 hours to obtain a suspension of stationary phase bacteria (~ 10^9 CFU/mL). Prior to the bacterial adhesion and filtration experiments, all membranes were rinsed with 70% ethanol aqueous solution for 30 minutes and then incubated for 30 minutes in each of a series diluted aqueous ethanol solutions (50, 25, 0% aqueous ethanol solution) to remove ethanol from the membrane. The bacteria adhesion to the resulting membrane surface was evaluated by incubating the stationary phase bacteria in the presence of neat PVDF and Ag-PVDF membranes (1 × 1 cm^2) in a 37 °C incubation shaker for 4 hours. The membranes were then removed from the *E. coli* suspension solutions and carefully rinsed several times with phosphate buffered saline (PBS). The bacteria that adhered to the membrane were observed by FE-SEM imaging. Prior to FE-SEM observation, the bacteria adhered to the membrane were fixed in a 4% (v/v) glutaraldehyde solution[34], and the resulting membranes were dehydrated with ethanol and dried at room temperature.

The resistance due to biofouling during filtration was assessed by conducting a filtration test using *E. coli* as a biofoulant. The membranes were inoculated by applying 6 mL of an *E. coli* suspension solution (~10^7 CFU/mL) to the membrane using a vacuum filter cell. LB broth solution (concentration:

0.5 g/L) was then filtered over the inoculated membrane for 24 hours to provide a feed solution. The feed solution temperature was kept at 25 °C using a laboratory-grade constant temperature water bath. The flux was recorded using an analytic mass balance. After 24 hours, the membrane was rinsed with DI water for 10 minutes to remove unattached *E. coli* and its byproducts from the membrane surface. The flux recovery was assessed by flushing the membrane with DI water using the filtered cell and re-measuring the PWP. The filtration test results are reported in terms of the normalized flux, which was calculated using the following equation (*3*),

$$N = F_t / F_{i,} \quad (3)$$

where N is the normalized flux, F_t is the flux value, and F_i is the initial flux value. Equations (*4*)–(*6*) give the decrease in total flux due to membrane fouling:

$$r_t(\%) = (1 - N_f) \times 100, \quad (4)$$

$$r_{rev}(\%) = (N_w - N_f) \times 100, \quad (5)$$

$$r_{ir}(\%) = (1 - N_w) \times 100, \quad (6)$$

where r_t, r_{rev}, and r_{ir} are the degree of decrease in the total, reversible, and irreversible fluxes, respectively. N_f and N_w are the normalized flux values of the fouled membrane and pure water-flushed membrane, respectively.

III-3. Results and Discussion

III-3-1. Amphiphilic thiol linker

The thiol-modified amphiphilic block copolymer linker was prepared via an esterification reaction between the hydroxyl end group of P(E-*b*-EO) and the mercaptoacetic acid. The reaction progress was monitored by FT-IR spectroscopy (see Figure III-3). The IR transmittance spectrum of the thiol-modified P(E-*b*-EO) was indistinguishable from that of the neat P(E-*b*-EO), with the exception of a peak consistent with a carbonyl stretch at 1739 cm^{-1}. The carbonyl stretching for the thiol-modified P(E-*b*-EO) was observed to the higher wavenumber than that for mercaptoacetic acid (1716 cm^{-1}). The peak shift was attributed to the esterification reaction between the hydroxyl group of the P(E-*b*-EO) and mercaptoacetic acid, which further indicates that the thiol functional group was successfully introduced onto the end of the P(E-*b*-EO) molecule via an esterification reaction between the hydroxyl end group of the P(E-*b*-EO) and the mercaptoacetic acid. In addition to FT-IR studies, ^{1}H NMR measurements of the thiol-modified P(E-*b*-EO) were collected to quantify the degree of thiol modification. As shown in Figure III-4, new peaks appeared at 4.3, 3.3, and 2.0 ppm in the thiol-modified P(E-*b*-EO), which corresponded to –C*H*$_2$OOC–CH$_2$–SH (4.30 ppm), –CH$_2$OOC–C*H*$_2$–SH (3.29 ppm), and –CH$_2$OOC–CH$_2$–S*H* (2.01 ppm), and were attributed to the substitution of the P(E-*b*-EO) hydroxyl group with the thiol functional group. The degree of thiol modification was calculated from the ratio of the integrals of the PEO methylene protons (at 4.30 ppm) adjacent to the ester functionality and the PE methylene protons (at 3.46 ppm) adjacent to

the ether functionality, assigned as 6 and 4 in Figure 2, respectively. The calculated degree of thiol modification in the thiol-modified P(E-*b*-EO) was 99%, indicating that nearly all of the P(E-*b*-EO) hydroxyl end groups had been converted to thiol groups and that the preparation of the thiol-modified amphiphilic block copolymer linker was successful.

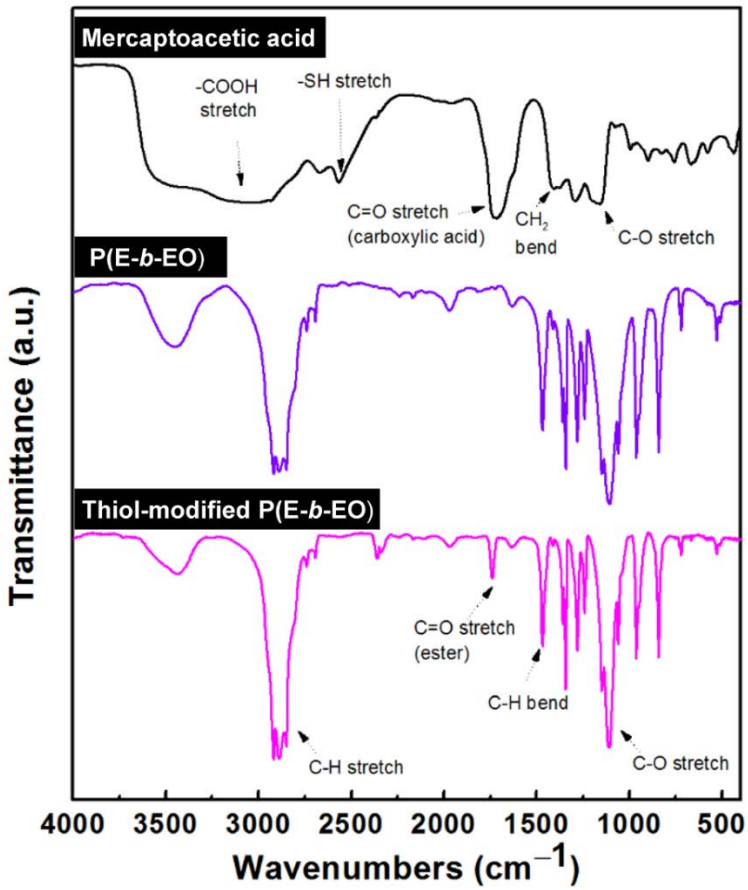

Figure III-3. FT-IR spectra of mercaptoacetic acid, polyethylene-*block*-polyethylene glycol, and the thiol-modified polyethylene-*block*-polyethylene glycol copolymer

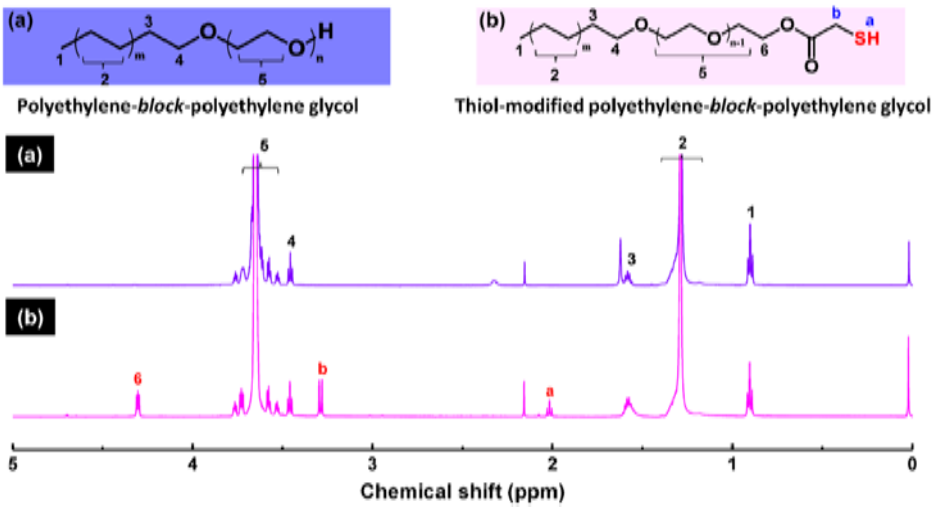

Figure III-4. ^{1}H NMR spectra of (a) the polyethylene-*block*-polyethylene glycol and (b) the thiol-modified polyethylene-*block*-polyethylene glycol copolymer, the degree of thiol-modification was calculated from the ratio of the integrals over 4 and 6 in the ^{1}H NMR spectrum of the thiol-modified polyethylene-*block*-polyethylene glycol

III-3-2. Thiolated PVDF Membrane

The thiolated PVDF membrane was fabricated through a non-solvent induced phase separation (NIPS) process of the PVDF dope solution including the varied amount of the amphiphilic thiol-modified P(E-*b*-EO) linker. Figure III-5 shows the ATR FT-IR transmittance patterns of the thiol-modified linker, the neat PVDF membrane, and the thiolated PVDF membranes. As shown in Figure III-5(a), the IR bands corresponding to the sp^3 CH stretch of the linker (between 2850 and 2920 cm^{-1}) were more pronounced in the thiolated PVDF membranes prepared with a larger amount of the linker in the PVDF dope solution. The C-O stretch at 1150 cm^{-1} in the FT-IR spectra of the thiolated PVDF membranes, which was attributed to the PEO ether linkage in the linker molecule, gradually grew in as the amount of linker in the dope solution increased. These results indicate that the linkers have been successfully incorporated into the membrane. The mechanism by which the linkers were introduced into the membrane during the NIPS process was investigated by analyzing the IR transmittance through the top and bottom surfaces of the thiolated PVDF membrane. Here, the top surface corresponds to the water contact side and the bottom surface corresponds to the glass contact side. As shown in Figure III-5(b), the intensity of the sp^3 CH stretch (between 2850 and 2920 cm^{-1}) for the top surface was higher than that for the bottom surface. The C-O stretch at 1110 cm^{-1} was also slightly stronger for the top surface than for the bottom surface. In addition, the XPS spectra of O 1s (Figure III-5(c)) showed the difference intensity and concentration of oxygen between top and bottom surfaces of the thiolated PVDF membrane. Oxygen species in the thiolated PVDF membrane were

derived from the PEO block. Therefore, the degree of surface thiol functionalization can be calculated by analysis of oxygen amount in the membrane surface. From the XPS spectra, the intensity of O 1s of the top surface (3.45 wt%) was much bigger than that of the bottom surface (1.37 wt%). These oxygen amounts can be converted into the amount of sulfur element, and the sulfur elements calculated from the amount of oxygen were 0.16 wt% for the top surface and 0.06 wt% for the bottom surface. This reveals that the thiol linker were located at the top surface ca. 2.5 times more than at the bottom surface. As a result, the silver loading mount on the top surface were much higher than that on the bottom surface (see Figure III-6). Thus, the combined results of the ATR FT-IR and the XPS suggest that the thiol-modified P(E-*b*-EO) linker migrated toward the top surface during the NIPS process due to the hydrophilic affinity of the PEO segment in the linker with the water contacted with the top surface of the membrane. In water, the hydrophilic–hydrophobic phase recognition of the linker during the membrane formation most likely exposed the thiol functional group attached to the end of the PEO segment of the linker to the membrane surface, whereas the hydrophobic PE moiety was inserted into the consolidated hydrophobic PVDF layer. These migrations resulted in a self-assembled thiol-functionalized PVDF membrane. Perfect phase separation by the amphiphilic linker was not likely to occur during the PVDF consolidation process in water, as the NIPS process was far too rapid to provide sufficient time for the linker to fully undergo phase separation. Some of the linker may remain present on the inside of the membrane. Nevertheless, the IR spectra from the top and bottom surfaces of the thiolated PVDF membrane show that the linker was mainly

present near the membrane surface, thereby allowing the thiol functional linker on the PVDF membrane to covalently bond to the Ag NPs.

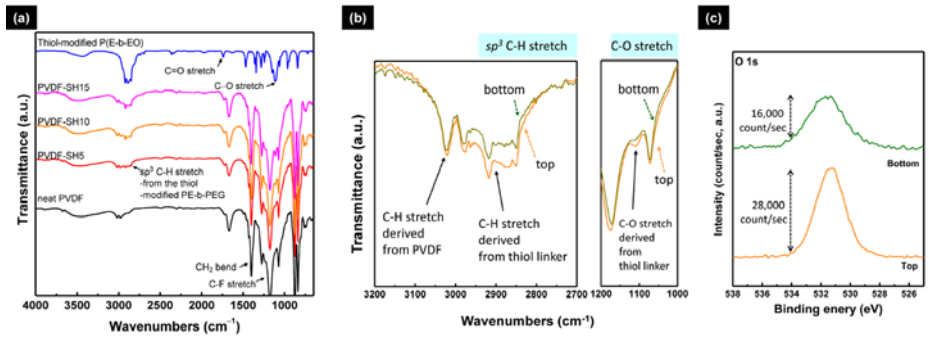

Figure III-5. (a) FT-IR spectra of the neat PVDF membrane, thiolated PVDF membranes and the thiol-modified amphiphilic copolymer linker; and (b) ATR FT-IR spectra of both surfaces (top and bottom) of the thiolated PVDF membrane, collected over the range 3200–2700 cm^{-1} and 1200–1000 cm^{-1}, corresponding to the C-H and C-O stretches of the linker, respectively; (c) XPS spectra of O 1s of both top and bottom surfaces

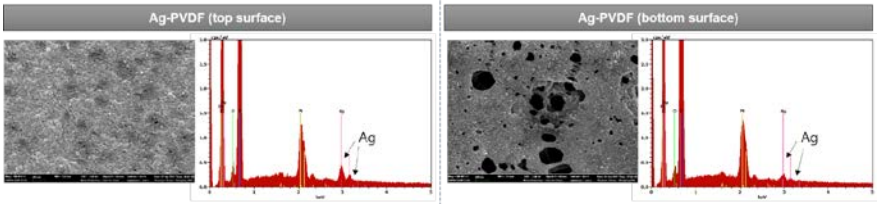

Element	Series	Atomic conc. (at.%)	Error
Carbon	K-series	49.13	14.31
Oxygen	K-series	3.07	1.93
Fluorine	K-series	47.05	19.80
Silver	L-series	0.75	0.63
Total		100	

Element	Series	Atomic conc. (at.%)	Error
Carbon	K-series	50.35	14.32
Oxygen	K-series	2.22	1.38
Fluorine	K-series	47.17	19.65
Silver	L-series	0.26	0.29
Total		100	

Figure III-6. The SEM images and the EDXS spectra of top (left) and bottom (right) surfaces of the Ag-PVDF membrane nanocomposite, quantitative results of elements composed of the Ag-PVDF membrane nanocomposite were summarized in tables

The effects of the linker on the PVDF membrane structure were characterized by measuring the morphologies of the thiolated PVDF membranes prepared with various amounts of the linker, *i.e.*, neat PVDF (PVDF-SH0), PVDF-SH5, PVDF-SH10, and PVDF-SH15 membranes. The PWP values of each membrane were also measured. FE-SEM (Figure III-7) showed that the neat and thiolated PVDF membranes displayed similar morphologies typically observed in asymmetric membranes composed of a dense top layer and a porous bottom layer. The thiolated PVDF membrane thickness was found to increase and the number of pores on the top surface layer decreased as the amount of linker in the membrane increased. Indeed, as listed in Table III-1, the thiolated PVDF membranes produced from the dope solution containing more than 1.5 wt% linker in the dope solution, *i.e.*, PVDF-SH10 and PVDF-SH15, exhibited the most dramatic decreased in the PWP values compared to the neat PVDF membrane due to a higher membrane thickness and a reduced number of surface pores. This can be attributed to the presence of PE moiety in the linker. Basically, PE moiety is insoluble in DMAc solution. Thus, excess of PE moiety can reduce the thermodynamic stability of the membrane dope solution and inhibit the pore formation in the PVDF membrane. On the other hand, the PWP and morphology of the PVDF-SH5 membrane were nearly indistinguishable from the corresponding properties of the neat PVDF membrane. These results clearly demonstrated that the membrane formation was not affected by the presence of less than 0.75 wt% linker in the dope solution. Therefore the PVDF-SH5 membrane was selected for the preparation of the Ag-PVDF membrane nanocomposite.

Table III-1. The pure water permeability (PWP) values obtained from the neat PVDF and the thiolated PVDF membranes with different loadings of the thiol-modified linker

Sample name	**neat PVDF**	**Thiolated PVDF**		
		PVDF-SH5	**PVDF-SH10**	**PVDF-SH15**
Pure water permeability (PWP) ($L\ m^{-2}\ h^{-1}\ bar^{-1}$)	1742 ± 35	1696 ± 65	418 ± 41	345 ± 24

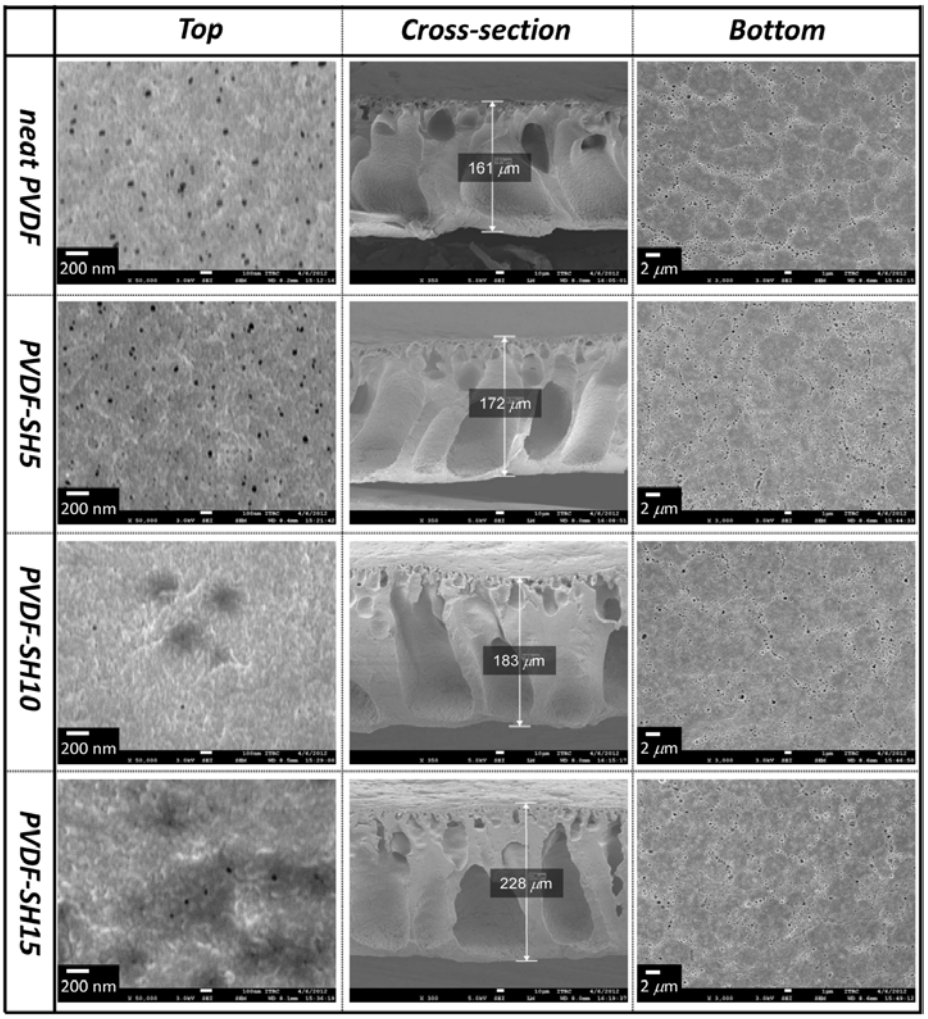

Figure III-7. Top surface (left), cross-sectioned (center) and bottom surface (right) morphologies of the neat (1st line) and the thiolated (2-4 lines) PVDF membranes, collected using FE-SEM observation

III-3-3. Ag-PVDF membrane nanocomposite

Thiol functional groups form strong coordination bonds with noble metals, *e.g.*, Ag and Au, that have a relatively large ionic radius and a low oxidation state. According to Pearson's hard and soft acids and base (HSAB) theory[35], the sulfur atom in a thiol group and a noble metal tend to share the valence electrons to form a covalent bond. Alkyl sulfide anions, in particular, which form through the removal of a proton from a thiol group, have a stronger affinity toward these metals than a thiol group. Mildly basic conditions, therefore, favored deprotonation of alkyl thiol and the formation of covalent bonds between the colloidal Ag NPs and the thiolated membrane (PVDF-SH5), when the PVDF-SH5 membrane was immersed in the colloidal Ag NP solution under the mildly basic condition. As anticipate, the color of the membrane changed from white to reddish-yellow (Figure III-8), indicating that the Ag NPs were successfully immobilized on the surface of the membrane due to the formation of strong sulfur–metal bonds mediated by the thiol-modified linker embedded in the membrane, yielding the self-assembled Ag NPs-PVDF (Ag-PVDF) membrane nanocomposites. Figures III-9(a) and (b) show the surface morphology and elemental analysis of the Ag-PVDF membrane nanocomposite measured by FE-SEM and EDXS, respectively. The FE-SEM image (Figure III-9 (a)) showed that the spherical Ag NPs were directly attached to the surface of the membrane. The EDXS spectra of the Ag-PVDF membrane nanocomposite (Figure III-9(b)) distinctly revealed that the Ag NPs were present on the surface of the Ag-PVDF membrane nanocomposite. As can be seen Figure III-9(a), the size of attached Ag NP on the membrane surface is seem to increase compared to the as-synthesized Ag

NP (below 10 nm). This can be attributed to a breakdown of the electronically repulsive stabilizing structure of Ag NP by introducing the covalent bond at the nanoparticle surface and a subsequent partial aggregation between Ag NPs on the surface of the membrane[36]. The extent of Ag NP loading in the Ag-PVDF membrane nanocomposite was evaluated using ICP-AES to quantitatively analyze the effects of the thiol functionality in the membrane on the deposition of Ag NPs to the membrane. The Ag elemental loading was 10,266 mg kg^{-1} in the Ag-PVDF membrane nanocomposite. By contrast, the Ag/PVDF membrane nanocomposite prepared without the thiolated linkers yielded a Ag elemental loading that was approximately 5 times lower (2,124 mg kg^{-1}) than that of the Ag-PVDF membrane nanocomposite. These results indicate that the presence of the thiolated linker in the membrane played a key role in stabilizing the Ag NPs on the membrane surface.

The PWP value and rejection properties of the Ag-PVDF membrane nanocomposite were characterized as a measure of the membrane performance. Figure III-9(c) shows that the Ag-PVDF membrane nanocomposite (1768 ± 37 L m^{-2} h^{-1}) had a PWP value comparable to that of the neat PVDF membrane (1742 ± 36 L m^{-2} h^{-1}), indicating that the two membranes provided similar water treatment efficiencies. The rejection properties of the two membranes were similar as well. Both membranes yielded a high rejection (exceeding 99%) of 0.1 μm and 0.06 μm PS latex particles, although the Ag-PVDF membrane nanocomposite exhibited a slightly lower rejection of 20-30 nm γ-globulin relative to the neat PVDF membrane (Figure III-9(d)). This means that the largest surface pore size in both membranes appeared to be within the range 30–60 nm. It is seemed that

the introduced Ag NPs to the membrane did not reducing the surface porosity because the small sized Ag NPs can pass through surface pore then bind a highly porous support layer rather than clogging surface pore. Thus, the assembly of Ag NPs to the PVDF-SH5 membrane did not significantly affect the structure and performance of the membrane, which anticipate that the Ag-PVDF membrane nanocomposite well apply to real water purification system.

Figure III-8. Photographic image of the Ag-PVDF membrane nanocomposite

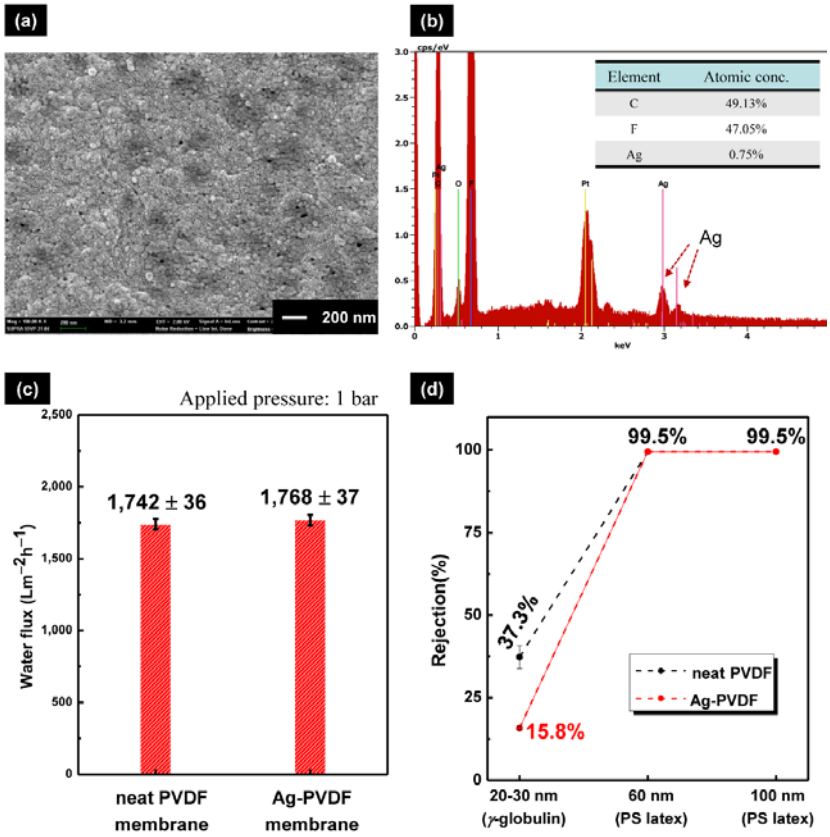

Figure III-9. Characteristics of the Ag-PVDF; (a) Top surface morphology observed by FE-SEM and (b) chemical composition of the membrane surface obtained by EDXS, membrane performances of the neat PVDF membrane and the Ag-PVDF membrane nanocomposite; (c) Pure water permeability and (d) rejection of the standard sized particles (γ-globulin, 0.06 μm and 0.1μm polystyrene latex beads), the bars with the standard deviation represent the average of three filtration results

III-3-4. Release of Ag from the membrane

The stable and robust bond between the Ag NPs and the membrane is important for ensuring the maintenance of anti-biofouling performance for high-efficient and eco-friendly membrane system. The quantity of Ag NPs released from the membrane was evaluated during continuous membrane operation using 2 L pure water. Figure 6 shows the release of Ag element from the Ag/PVDF and Ag-PVDF membrane nanocomposites during deionized water filtration. Figure III-10(a) shows that approximately 52% of the Ag was released from Ag/PVDF membrane nanocomposite and into the filtrate after filtering 2 L water. A significant fraction of the Ag (43.6%) was released from the Ag/PVDF membrane nanocomposite during even the initial stages of filtration, up to 500 mL. On the other hand, the Ag-PVDF membrane nanocomposite did not lose a detectable amount of Ag NPs during the entire water filtration process, even though the membrane had a 5-fold greater Ag loading compared to the Ag/PVDF membrane nanocomposite.

The XPS data (see Figures III-10(b) and (c)) revealed that the peak intensity corresponding to the Ag $3d_{5/2}$ orbital binding energy in the Ag-PVDF membrane nanocomposite was present without a loss of the intensity after filtering 2 L water. The intensity of the Ag XPS peaks in the Ag/PVDF membrane nanocomposite, by contrast, was markedly reduced, indicating a loss of the Ag NPs from the surface of membrane. The stable covalent bond between the Ag NPs and the membrane prevented the release of Ag NPs from the Ag-PVDF membrane nanocomposite due to the formation of the sulfur-metal covalent interaction.

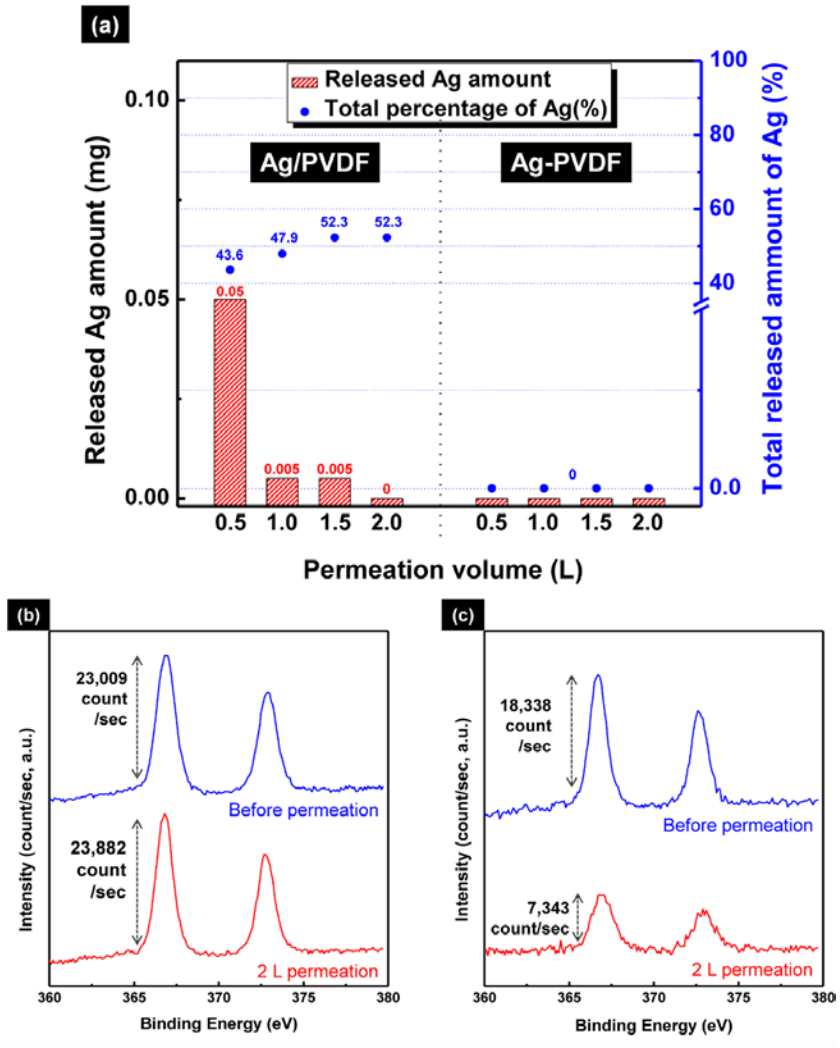

Figure III-10. (a) The amount of Ag released into the filtrate from the Ag/PVDF and the Ag-PVDF membrane nanocomposites, XPS spectra of the Ag 3d orbital from (b) the Ag-PVDF and (c) the Ag/PVDF membrane nanocomposites, before and after pure water filtration

III-3-5. Biofouling resistance

Previous studies[16-17, 31] have reported that Ag may be released from a Ag/membrane composite as Ag^+ ions, which then act as biocidal agents. These reports concluded that the release of Ag^+ ions is required for realizing high anti-biofouling properties; however, the Ag-PVDF membrane nanocomposite released no elemental Ag or Ag^+ ions. Biofouling resistance for the Ag-PVDF membrane nanocomposite was evaluated using *E. coli* as a biofoulant. The degree of resistance to biofouling was evaluated by incubating membrane samples in the presence of a stationary phase cell suspension of *E. coli* at 37 °C for 4 hours. The cultured membranes were then imaged by FE-SEM to observe the bacteria-adhered membrane surface. As shown in Figure III-11, the membrane surface images of the cultured neat and Ag-PVDF membranes were distinctly different. Debris from dead *E. coli* could be observed on the Ag-PVDF membrane nanocomposite surface (Figure III-11(d–f)), whereas intact live *E. coli* were observed on the neat PVDF membrane surface (Figure III-11(a–c)). The assembled Ag NPs effectively killed the bacteria on the membrane surface. The strong antibacterial effects of the Ag-PVDF membrane nanocomposite may reduce biofouling of the membrane by suppressing the growth and development of bacteria on the membrane surface. As shown in Figure III-12(a), the normalized flux through the *E. coli* inoculated neat PVDF and Ag-PVDF membranes decreased continuously due to membrane fouling as the LB broth solution was passed over. However, the normalized flux through the Ag-PVDF membrane nanocomposite was 3 times higher than that of the neat PVDF membrane after filtering the nutrient solution over 25 h. The normalized flux of the neat

PVDF membrane was 0.038, whereas the normalized flux of the Ag-PVDF membrane nanocomposite was 0.11. These results were attributed to the suppression of microorganism adhesion and growth due to the biocidal properties of the Ag-PVDF membrane nanocomposite. Surprisingly, the normalized PWP value of the biofouled Ag-PVDF membrane nanocomposite was 0.88 after flushing with DI water. The extent of reversible fouling was calculated to be 74% and the extent of irreversible fouling was 12%. These results suggested that nearly all of the foulants that had attached to the membrane surface had been removed by DI water flushing, and the membrane performance was nearly recovered. On the other hand, the normalized flux through the biofouled neat PVDF membrane after DI water flushing was 0.36. The calculated reversible fouling was 29% and the irreversible fouling was 64%, indicating that the neat PVDF membrane lost much of its functionality to irreversible biofouling. The surfaces of the fouled membranes after the filtration test were observed using FE-SEM (Figures III-12(c) and (d)). Almost none of the adhered *E. coli* cells remained present on the surface of the Ag-PVDF membrane nanocomposite, whereas many intact *E. coli* cells were observed on the neat PVDF membrane surface. These results show that covalent assembly of Ag NPs provides PVDF membrane with a sustainable anti-biofouling property without released Ag^+ ions. Thus, it is believe that the covalently assembled Ag-PVDF membrane nanocomposite can well be applied to a high performance and eco-friendly water purification system.

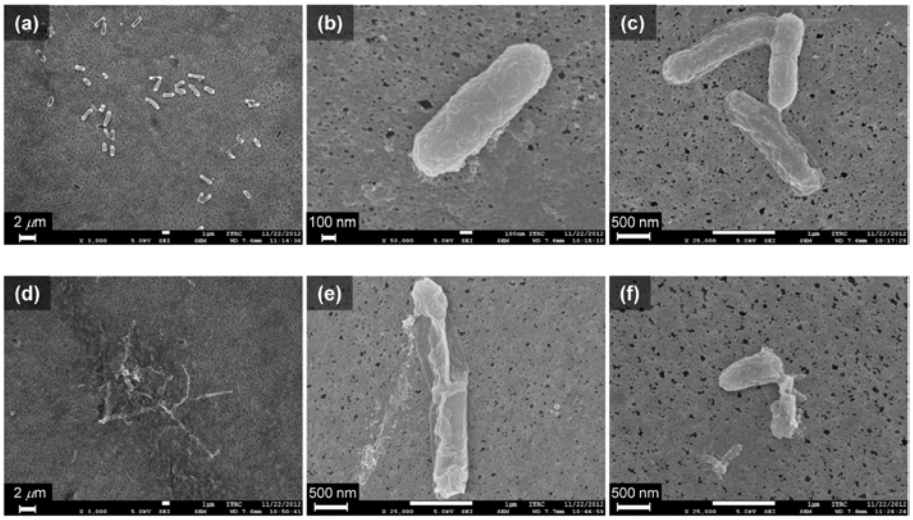

Figure III-11. FE-SEM images of the surface adhered *E. coli* on (a–c) the neat PVDF membrane and (d–f) the Ag-PVDF membrane nanocomposite, both membranes were incubated with stationary phase of *E. coli* suspension for 4 hours at 37 °C

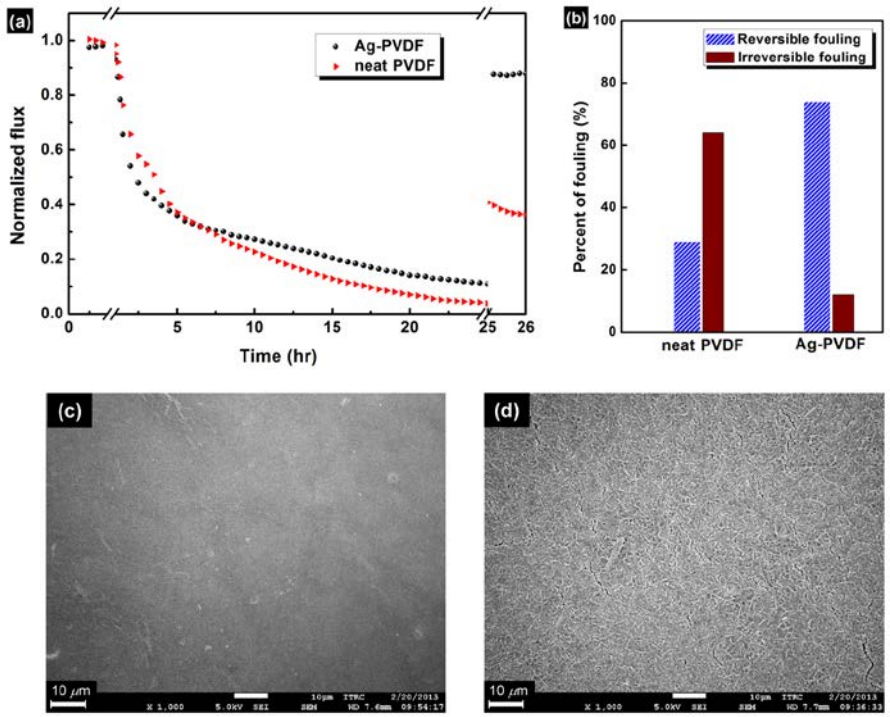

Figure III-12. (a) Filtration test of *E. coli* inoculated neat and Ag-PVDF membranes using a synthetic nutrient media feed solution, and (b) calculated percentage of the reversible and the irreversible fouling of the neat PVDF and the Ag-PVDF membranes. FE-SEM images of membrane top surfaces of (c) the neat PVDF and (d) the Ag-PVDF membranes after the filtration test

III-4. Conclusions

In this chapter, a sustainable anti-biofouling active membrane nanocomposite was developed via the formation of a robust covalent linkage between Ag NPs and a PVDF membrane, mediated by a thiol-end functional amphiphilic block copolymer linker. The thiolated amphiphilic linker was prepared and anchored onto the PVDF membrane via hydrophilic–hydrophobic phase separation assembly of the linker during membrane production using a NIPS process, resulting in the formation of a thiolated PVDF membrane. Immersion of the thiolated PVDF membrane in a pH-controlled colloidal Ag NP aqueous solution yielded the Ag-PVDF membrane nanocomposite, in which the Ag NPs were highly deposited. The membrane morphology and performance were similar to the properties observed in the neat PVDF membrane. ICP-AES and XPS results revealed that the Ag-PVDF membrane nanocomposite displayed excellent binding stability and did not release the Ag from the membrane. In particular, the Ag-PVDF membrane nanocomposite distinctly suppressed the growth of *E. coli* on the membrane surface and showed enhanced and sustainable anti-biofouling properties. These features make the Ag-PVDF membrane nanocomposite quite attractive as an eco-friendly and human-friendly cost-effective water treatment system.

References and Notes

1. Hilal, N.; Kochkodan, V.; Al-Khatib, L.; Levadna, T., Surface modified polymeric membranes to reduce (bio)fouling: a microbiological study using E. coli. *Desalination* **2004,** *167* (0), 293-300.

2. Yang, H.-L.; Lin, J. C.-T.; Huang, C., Application of nanosilver surface modification to RO membrane and spacer for mitigating biofouling in seawater desalination. *Water Res.* **2009,** *43* (15), 3777-3786.

3. McDonogh, R.; Schaule, G.; Flemming, H.-C., The permeability of biofouling layers on membranes. *J. Membr. Sci.* **1994,** *87* (1–2), 199-217.

4. Drews, A., Membrane fouling in membrane bioreactors—Characterisation, contradictions, cause and cures. *J. Membr. Sci.* **2010,** *363* (1–2), 1-28.

5. Rana, D.; Matsuura, T., Surface Modifications for Antifouling Membranes. *Chem. Rev.* **2010,** *110* (4), 2448-2471.

6. Chang, Y.; Ko, C.-Y.; Shih, Y.-J.; Quémener, D.; Deratani, A.; Wei, T.-C.; Wang, D.-M.; Lai, J.-Y., Surface grafting control of PEGylated poly(vinylidene fluoride) antifouling membrane via surface-initiated radical graft copolymerization. *J. Membr. Sci.* **2009,** *345* (1–2), 160-169.

7. Yang, Y.-F.; Li, Y.; Li, Q.-L.; Wan, L.-S.; Xu, Z.-K., Surface hydrophilization of microporous polypropylene membrane by grafting zwitterionic polymer for anti-biofouling. *J. Membr. Sci.* **2010,** *362* (1–2), 255-264.

8. Venault, A.; Chang, Y.; Wang, D.-M.; Lai, J.-Y., Surface anti-biofouling control of PEGylated poly(vinylidene fluoride) membranes via vapor-induced phase separation processing. *J. Membr. Sci.* **2012,** *423–424* (0),

53-64.

9. Liu, C. X.; Zhang, D. R.; He, Y.; Zhao, X. S.; Bai, R., Modification of membrane surface for anti-biofouling performance: Effect of anti-adhesion and anti-bacteria approaches. *J. Membr. Sci.* **2010,** *346* (1), 121-130.

10. Cen, L.; Neoh, K. G.; Ying, L.; Kang, E. T., Surface modification of polymeric films and membranes to achieve antibacterial properties. *Surf. Interface Anal.* **2004,** *36* (8), 716-719.

11. Yu, S.-H.; Mi, F.-L.; Shyu, S.-S.; Tsai, C.-H.; Peng, C.-K.; Lai, J.-Y., Miscibility, mechanical characteristic and platelet adhesion of 6-O-carboxymethylchitosan/polyurethane semi-IPN membranes. *J. Membr. Sci.* **2006,** *276* (1–2), 68-80.

12. Razmjou, A.; Mansouri, J.; Chen, V., The effects of mechanical and chemical modification of TiO2 nanoparticles on the surface chemistry, structure and fouling performance of PES ultrafiltration membranes. *J. Membr. Sci.* **2011,** *378* (1–2), 73-84.

13. Yang, Y.; Zhang, H.; Wang, P.; Zheng, Q.; Li, J., The influence of nano-sized TiO2 fillers on the morphologies and properties of PSF UF membrane. *J. Membr. Sci.* **2007,** *288* (1–2), 231-238.

14. Kim, S. H.; Kwak, S.-Y.; Sohn, B.-H.; Park, T. H., Design of TiO2 nanoparticle self-assembled aromatic polyamide thin-film-composite (TFC) membrane as an approach to solve biofouling problem. *J. Membr. Sci.* **2003,** *211* (1), 157-165.

15. Kwak, S. Y.; Kim, S. H.; Kim, S. S., Hybrid organic/inorganic reverse osmosis (RO) membrane for bactericidal anti-fouling. 1. Preparation and characterization of TiO2 nanoparticle self-assembled aromatic polyamide

thin-film-composite (TFC) membrane. *Environ. Sci. Technol.* **2001,** *35* (11), 2388-2394.

16. Zodrow, K.; Brunet, L.; Mahendra, S.; Li, D.; Zhang, A.; Li, Q.; Alvarez, P. J. J., Polysulfone ultrafiltration membranes impregnated with silver nanoparticles show improved biofouling resistance and virus removal. *Water Res.* **2009,** *43* (3), 715-723.

17. Nisola, G. M.; Park, J. S.; Beltran, A. B.; Chung, W. J., Silver nanoparticles in a polyether-block-polyamide copolymer towards antimicrobial and antifouling membranes. *RSC Adv.* **2012,** *2* (6), 2439-2448.

18. Zhang, M.; Zhang, K.; De Gusseme, B.; Verstraete, W., Biogenic silver nanoparticles (bio-Ag0) decrease biofouling of bio-Ag0/PES nanocomposite membranes. *Water Res.* **2012,** *46* (7), 2077-2087.

19. Taurozzi, J. S.; Arul, H.; Bosak, V. Z.; Burban, A. F.; Voice, T. C.; Bruening, M. L.; Tarabara, V. V., Effect of filler incorporation route on the properties of polysulfone-silver nanocomposite membranes of different porosities. *J. Membr. Sci.* **2008,** *325* (1), 58-68.

20. Kim, Y.; Rana, D.; Matsuura, T.; Chung, W. J., Towards antibiofouling ultrafiltration membranes by blending silver containing surface modifying macromolecules. *Chem. Commun.* **2012,** *48* (5), 693-695.

21. Reich, L.; Stivala, S. S., Autoxidation of poly(alkylene glycols) in solution. *J. Appl. Polym. Sci.* **1969,** *13* (5), 977-988.

22. Ostuni, E.; Chapman, R. G.; Holmlin, R. E.; Takayama, S.; Whitesides, G. M., A survey of structure-property relationships of surfaces that resist the adsorption of protein. *Langmuir* **2001,** *17* (18), 5605-5620.

23. Li, Q.; Mahendra, S.; Lyon, D. Y.; Brunet, L.; Liga, M. V.; Li, D.;

Alvarez, P. J. J., Antimicrobial nanomaterials for water disinfection and microbial control: Potential applications and implications. *Water Res.* **2008,** *42* (18), 4591-4602.

24. Davies, R. L.; Etris, S. F., The development and functions of silver in water purification and disease control. *Catal. Today* **1997,** *36* (1), 107-114.

25. Choi, O.; Deng, K. K.; Kim, N.-J.; Ross Jr, L.; Surampalli, R. Y.; Hu, Z., The inhibitory effects of silver nanoparticles, silver ions, and silver chloride colloids on microbial growth. *Water Res.* **2008,** *42* (12), 3066-3074.

26. Marius, S.; Lucian, H.; Marius, M.; Daniela, P.; Irina, G.; Romeo-Iulian, O.; Simona, D.; Viorel, M., Enhanced antibacterial effect of silver nanoparticles obtained by electrochemical synthesis in poly(amide-hydroxyurethane) media. *J. Mater. Sci. Mater. Med.* **2011,** *22* (4), 789-796.

27. Samberg, M. E.; Orndorff, P. E.; Monteiro-Riviere, N. A., Antibacterial efficacy of silver nanoparticles of different sizes, surface conditions and synthesis methods. *Nanotoxicology* **2011,** *5* (2), 244-253.

28. AshaRani, P. V.; Mun, G. L. K.; Hande, M. P.; Valiyaveettil, S., Cytotoxicity and genotoxicity of silver nanoparticles in human cells. *ACS Nano* **2009,** *3* (2), 279-290.

29. Larese, F. F.; D'Agostin, F.; Crosera, M.; Adami, G.; Renzi, N.; Bovenzi, M.; Maina, G., Human skin penetration of silver nanoparticles through intact and damaged skin. *Toxicology* **2009,** *255* (1-2), 33-37.

30. Yang, Z.; Liu, Z. W.; Allaker, R. P.; Reip, P.; Oxford, J.; Ahmad, Z.; Ren, G., A review of nanoparticle functionality and toxicity on the central nervous system. *Journal of the Royal Society Interface* **2010,** *7* (SUPPL. 4), S411-S422.

31. Mauter, M. S.; Wang, Y.; Okemgbo, K. C.; Osuji, C. O.; Giannelis, E. P.; Elimelech, M., Antifouling ultrafiltration membranes via post-fabrication grafting of biocidal nanomaterials. *ACS Appl. Mater. Interfaces* **2011,** *3* (8), 2861-2868.

32. Lee, G. J.; Shin, S. I.; Kim, Y. C.; Oh, S. G., Preparation of silver nanorods through the control of temperature and pH of reaction medium. *Mater. Chem. Phys.* **2004,** *84* (2-3), 197-204.

33. Schnippering, M.; Carrara, M.; Foelske, A.; Kotz, R.; Fermin, D. J., Electronic properties of Ag nanoparticle arrays. A Kelvin probe and high resolution XPS study. *PCCP* **2007,** *9*, 725-730.

34. Wang, H.; Lee, J.-K.; Moursi, A. M.; Anderson, D.; Winnard, P.; Powell, H.; Lannutti, J., Microstructural disassembly of calcium phosphates. *Journal of Biomedical Materials Research Part A* **2004,** *68A* (1), 61-70.

35. Pearson, R. G., Hard and soft acids and bases. *J. Am. Chem. Soc.* **1963,** *85* (22), 3533-3539.

36. Hiramatsu, H.; Osterloh, F. E., A simple large-scale synthesis of nearly monodisperse gold and silver nanoparticles with adjustable sizes and with exchangeable surfactants. *Chem. Mater.* **2004,** *16* (13), 2509-2511.

CHAPTER IV

REGENERABLE ANTI-FOULING ACTIVE PTFE MEMBRANE WITH THERMO-REVERSIBLE "PEEL-AND-STICK" HYDROPHILIC LAYER

IV-1. Introduction

In order to improve membrane fouling resistance, much efforts have been made to form a hydrophilic layer onto the hydrophobic membrane through various surface modification methods such as coating[1-5] grafting[5-12] and incorporating[13-18] hydrophilic materials. Such a hydrophilic layer on the membrane surface can hinder the adsorption of hydrophobic contaminants onto the membrane and can even render any adsorbed contaminants easily removed by a simple washing process. Nevertheless, water contaminants continually and permanently accumulate on membrane surfaces and in membrane pores, and this brings about a gradual deterioration of membrane performance[14]. Thus, it is necessary to develop a new approach to fundamentally recover the anti-fouling property of a membrane rendered ineffective by permanently accumulated contaminants.

Of particular interest is a dynamic bond-incorporated membrane because it can selectively undergo reversible breaking and reformation of the

modifier to endow the membrane surface with the desired properties. Indeed, such dynamic bonds have been extensively utilized for stimuli-responsive smart materials, such as a self-healing material[19-25], a smart adhesive[26-27] and an actuator[28-30], the reversibility of which can be controlled by light, pH, and temperature. Among the above, Diels-Alder (DA) cycloaddition between furan and maleimide functional groups is a representative dynamic bond to form a covalently thermo-reversible cyclic coupling which can be restored to their original forms by controlling temperature[26,31-34]. Furthermore, DA cycloadditions have been reported to have high and feasible reversible efficiencies[21,35]. Hence, if the thermo-reversible covalent bonding characteristics of DA reaction are applied to the membrane surface, it is expected that a regenerable anti-fouling active membrane would be developed, by changing a degraded hydrophilic layer into a fresh hydrophilic layer.

This study presents a regenerable anti-fouling active membrane by introducing a peelable-and-stickable hydrophilic layer onto the membrane surface. This was achieved with a covalently thermo-reversible dynamic bond, *i.e.*, DA cycloaddition, between the maleimide-modified poly(ethylene glycol) (PEG) and the furan-modified poly(tetrafluoroethylene) (PTFE) membrane surface. The hydrophilic PEG layer was repeatedly peeled off and stuck on the surface of the PTFE membrane by adjusting temperature, and the resulting PEG-coupled PTFE membrane displayed excellent anti-fouling properties. Moreover, the fouling resistance of the PEG-coupled PTFE membrane showed a high degree of recovery after a peel-and-stick process. This approach opens up the possibility of creating a novel platformable separating system for dynamic membranes, multi-functional membranes and smart gas

separation, because desired functionalities can reversibly be assembled and combined on the membrane surface.

IV-2. Experimental Section

IV-2-1. Materials

A porous poly(tetrafluoroethylene) (PTFE) flat membrane with 47 mm diameter and 0.1 μm average pore diameter was purchased from Advantec-MFS, Inc. Poly(ethylene glycol) methyl ether maleimide (M_n 2,000), furfuryl glycidyl ether (96%), hydrazine monohydrate (98%), and LUDOX SM-30 (30 wt% silica suspension, particle diameter about 7 nm) were purchased from Sigma-Aldrich. Toluene (99.8%), tetrahydrofuran (THF, 99.0%), and sodium hydroxide (98%) were obtained from Daejung Chemical & Metals. All chemicals were used as received, without further purification. The aqueous solutions were prepared with deionized (DI) water having a resistivity exceeding 18.0 MΩ cm.

IV-2-2. Preparation of PEG coupled PTFE membrane

In order to provide the furan moiety onto the PTFE membrane surface, the PTFE membrane was treated with UV/hydrazine and then reacted with furfuryl glycidyl ether. The UV/hydrazine treatment is a reactive surface modification method for chemically inert PTFE membranes to introduce amine functional groups [36].

Briefly, the PTFE flat membrane was exposed to hydrazine vapor

under UV light irradiation (λ_{max} = 254 nm, 100 W) in a closed quartz cylinder, for two days. After the reaction, the surface aminated PTFE membrane was carefully removed from the cylinder and dried in a vacuum for six hours to remove unreacted hydrazine vapor. Next, the aminated PTFE membrane was treated with 1 mL of furfuryl glycidyl ether in a 60 °C pre-heated oven overnight. The furan-modified PTFE membrane was obtained after rinsing with acetone and THF several times to remove unreacted chemicals. The resulting furan-modified PTFE membrane was dried at room temperature.

The PEG methyl ether maleimide (PEG-maleimide) was coupled to the furan-modified PTFE membrane by Diels-Alder (DA) reaction. The furan-modified PTFE membrane was placed at the bottom of a jar and then about 1 mL of 5 wt% PEG-maleimide/toluene solution was injected. The closed jar was stored in a pre-heated oven at 60 °C for 18 hours. After the DA reaction, the resulting PEG-coupled PTFE (PEG-PTFE) membrane was rinsed several times with toluene and THF and dried at room temperature.

IV-2-3. Peel-and-stick process of the hydrophilic PEG layer

To regenerate the hydrophilic PEG layer on the membrane surface, the attached PEG layer was peeled off the membrane surface by retro DA (rDA) reaction and the fresh PEG-maleimide was then re-coupled to the membrane surface by DA reaction. As described in the previous section, the PEG-maleimide was coupled to the modified PTFE membrane at 60 °C overnight by DA reaction. To decouple furan-maleimide bonding, the rDA reaction was conducted at 150 °C overnight. Briefly, the PEG-PTFE membrane was put in a 1-neck round flask and about 100 mL of toluene was

added to the flask. The solution was heated to 150 °C with reflux. After the rDA reaction, the PEG peeled membrane, denoted as re-PTFE, was carefully removed from the flask and rinsed several times with toluene and THF. The peel-and-stick of the PEG layer from the furan-modified PTFE was repeated three times. The overall procedure including surface modification and dynamic coupling of the PEG layer is schematically illustrated in Figure IV-1.

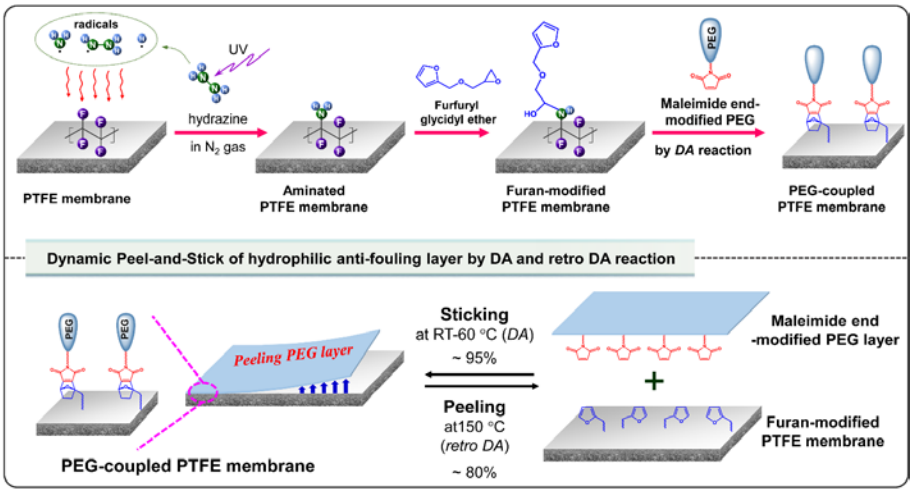

Figure IV-1. Schematic illustration of the preparation procedure for PEG-coupled PTFE membrane and dynamic peel-and-stick of PEG layer on membrane surface

IV-2-4. Membrane characterization

The aminated PTFE membrane, the furan-modified PTFE membrane, preparation of the PEG-PTFE membrane and the repetitive regeneration of the PEG layer by dynamic peel-and-stick process were monitored by attenuated total reflection Fourier-transform infrared (ATR FT-IR, Thermo Scientific Nicolet iS5) spectroscopy with a spectral resolution of 4 cm^{-1} with the range of 650 – 4000 cm^{-1} and X-ray photoelectron spectroscopy (XPS, Kratos AXIS-HSi) using monochromatic Mg K_{α} X-ray source operated at 10 mA. In order to evaluate surface hydrophilicity of the resulting membranes, static pure water contact angle was analyzed at room temperature using BiolinScientific, Attention® THETA LITE. The surface morphologies of the membranes were observed by field-emission scanning electron microscopy (FE-SEM, JEOL 7800F). Pt coating was carried out using Pt sputtering at 10 mA for 100 seconds for the FE-SEM imaging.

To investigate an anti-fouling behavior for the PEG-PTFE membrane, membrane fouling test was conducted using a 500 ppm neutral silica colloidal suspension solution. The fouling test was composed of three cycles for permeation of pure water and 500 ppm silica colloidal suspension, and pure water permeation after regeneration of the hydrophilic PEG layer.

Pure water permeability (PWP) was measured using Amicon® 8010 dead-end stirred cell (Millipore Corp.) connected to a pressure vessel filled with deionized (DI) water at 0.5 bar for 30 minutes. The 500 ppm neutral silica colloidal aqueous suspension was then filtered over the membrane, to generate membrane fouling, for one hour. Next, to remove loosely-attached silica foulants, the membrane was backwashed at 1 bar with DI water for three

minutes. These experiments were repeated three times for evaluation of fouling behavior. After three cycles of fouling, the membranes (*i.e.*, the PEG-PTFE membrane and the neat PTFE membrane), were treated with rDA conditions and a fresh PEG layer was attached to the PEG-PTFE membrane by DA reaction. Finally, the PWP was re-measured for the regenerated membranes. During the entire process, the water fluxes were measured continuously by collecting the permeate on an analytic mass balance (CAS CUW 420H) and calculated using the following equation 1:

$$Flux = Q/(\mathrm{t} \times \mathrm{A}) \quad (1)$$

where Q is the volume of the permeate (L), t is the filtration time (in hours), and A is the effective area of the membrane (m^2).

The degree of membrane fouling was verified by reversible and irreversible fouling tendencies (equations 2-4) for the PEG-PTFE membrane and the neat PTFE membrane:

$$N = F_t/F_i, \quad (2)$$

$$r_{rev}(\%) = (N_w - N_f) \times 100, \quad (3)$$

$$r_{ir}(\%) = (1 - N_w) \times 100, \quad (4)$$

where N is the normalized flux, F_t is the flux value and F_i is the PWP, and r_{rev} and r_{ir} are the percentages of reversible and irreversible foulings, respectively. N_f and N_w are the normalized flux values of the fouled and

backwashed membranes, respectively.

IV-3. Results and Discussion

IV-3-1. PEG-coupled PTFE membrane by Diels-Alder reaction

PTFE and PEG were used as a membrane substance and an anti-fouling active modifier respectively, because PTFE is chemically and thermally stable compared with other polymeric membrane substances and PEG is widely used as a hydrophilic modifier in membrane applications. To reversibly couple the hydrophilic PEG to the chemically inert PTFE membrane, the PTFE membrane was modified by the UV/hydrazine treatment to endow amine group on the membrane surface. Then, furfuryl glycidyl ether was covalently attached with the aminated PTFE membrane surface by a ring opening reaction of epoxy moiety of furfuryl glycidyl ether. FT-IR spectra (Figure IV-2(b)-(d)) exhibited a broad N-H stretching band at around 3600 cm^{-1} and an NH_2 scissoring band at 1635 cm^{-1} after the UV/hydrazine treatment of the neat PTFE membrane. After the ring opening reaction of furfuryl glycidyl ether with the UV/hydrazine treated-PTFE membrane, C=C stretching IR bands corresponding to the furan group were observed at 1607 cm^{-1} and 1558 cm^{-1}. These results revealed that the surface of the PTFE membrane was amine-functionalized and then the aminated PTFE was successfully modified by the furan moieties. In order to attach the hydrophilic PEG layer on the PTFE membrane, maleimide end-modified PEG was chemically coupled to the furan modified-PTFE membrane surface by DA reaction at 60 °C. From the FT-IR spectrum (Figure IV-2(e)), It was clearly

observed the broad O-H stretch from 3600 – 3100 cm^{-1}, C-H stretch at 2945 – 2870 cm^{-1} and the carbonyl stretch of the imide groups at 1702 cm^{-1} corresponding to the maleimide end-modified PEG, indicating the formation of a hydrophilic PEG layer on the surface of the PTFE membrane.

XPS analysis (see Figure IV-3) provided more detailed information about the amine, furan, and PEG functionalization onto the surface of the PTFE membrane. In the XPS spectra of the aminated PTFE membrane, the 286.9 eV of C_{1s} binding energy peak corresponding to C-N species and 400.2 eV of N_{1s} binding energy peak corresponding to N-H species were newly developed, indicating the surface amination of PTFE membrane. After the furan-functionalization of the aminated PTFE membrane, the XPS signals corresponding to the oxygen species of the furan molecule were observed at 286.0 eV (C-O, C_{1s}) and 532.1 eV (O-H, O_{1s}). Particularly, the C_{1s} XPS signal for CH_2 was more developed after the modification of the furfuryl glycidyl ether compared to that of the neat PTFE membrane. This indicated that the furan moieties capable of the DA reaction with PEG-maleimide were well modified at the surface of the PTFE membrane. After the PEG-maleimide was coupled to the furan-modified PTFE membrane by the DA reaction, C_{1s} XPS signals at 288.1 eV, 286.0 eV and 284.5 eV (assigned as CH_2, C-O and C=O of the PEG-maleimide, respectively) were more distinct, and O_{1s} XPS signal at 532.1 eV was also manifested, indicating the successful formation of the PEG layer on the PTFE membrane. In addition, the surface atomic concentrations of carbon increased as the surface modification of the membrane progressed (Table 1); 34.4 atomic% (for neat PTFE), 36.5 atomic% (for aminated PTFE), 48.4 atomic% (for furan-modified PTFE) and 55.3%

atomic% (for PEG-PTFE membrane). In contrast, the surface atomic concentrations of fluorine gradually decreased in the preparation progress of the PEG-PTFE membrane. Thus, the combined results from the FT-IR and XPS clearly showed that the hydrophilic PEG layer was chemically well coupled to the hydrophobic PTFE membrane by the DA reaction between furan-modified PTFE membrane and PEG-maleimide.

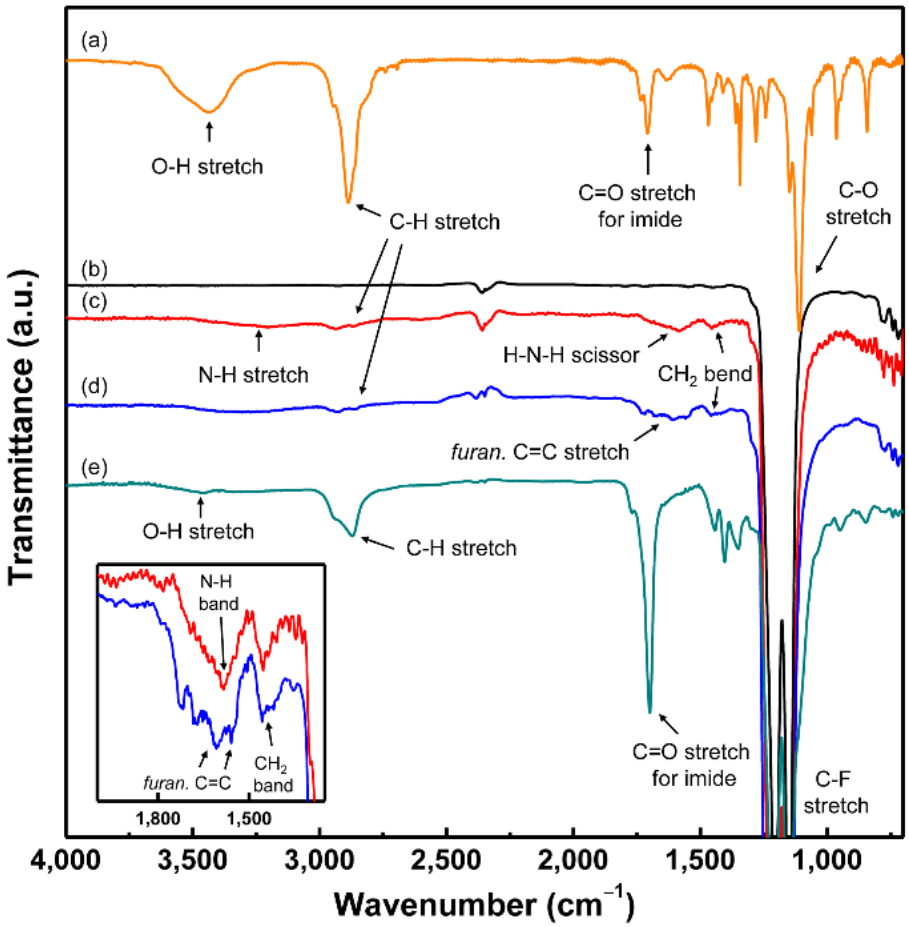

Figure IV-2. FT-IR spectra of (a) PEG-maleimide, (b) neat PTFE membrane, (c) aminated PTFE membrane, (d) furan-modified PTFE membrane, and (e) PEG-PTFE membrane, (b-e) ATR mode

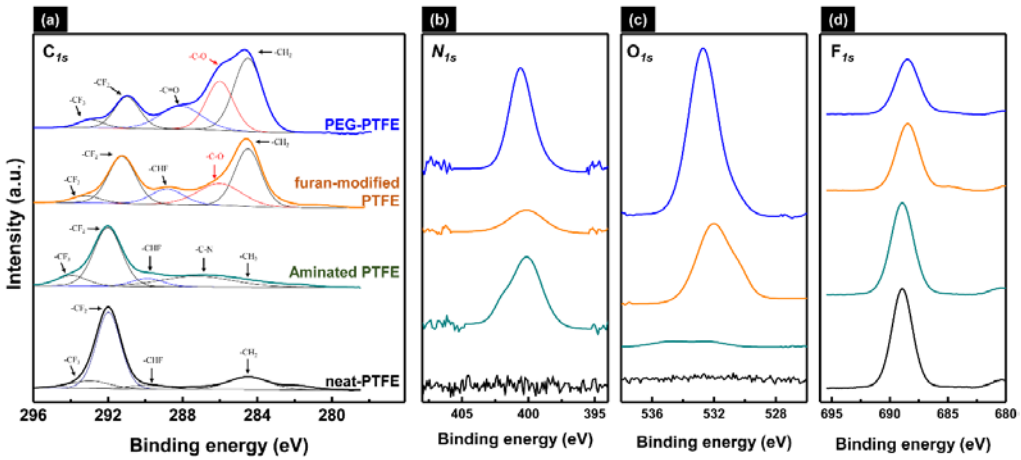

Figure IV-3. XPS spectra of (a) C_{1s}, (b) N_{1s}, (c) O_{1s}, and (d) F_{1s} for neat PTFE membrane, aminated PTFE membrane, furan-modified PTFE membrane and PEG-PTFE membrane

To investigate the morphological change in the membrane surface after sticking the PEG layers onto the PTFE membrane surface, the FE-SEM measurement was carried out. Figure IV-4 shows the FE-SEM images for the top surface morphologies of the neat PTFE, the aminated PTFE, the furan-modified PTFE, and the PEG-PTFE membranes. Except for the PEG-PTFE membrane, the morphologies of all the membranes were similar and showed the morphology typically observed in a stretched membrane. This indicates that the UV/hydrazine treatment and the furan modification did not significantly affect the pore structure of the PTFE membrane. However, after the DA coupling reaction of the furan-modified PTFE membrane with the PEG-maleimide, it was found that the membrane pores were partially occupied and that a dense polymeric layer was generat on the surface of the membrane. This was attributed to the formation of the hydrophilic PEG layer on the PFTE membrane surface, which was in good agreement with FT-IR and XPS results.

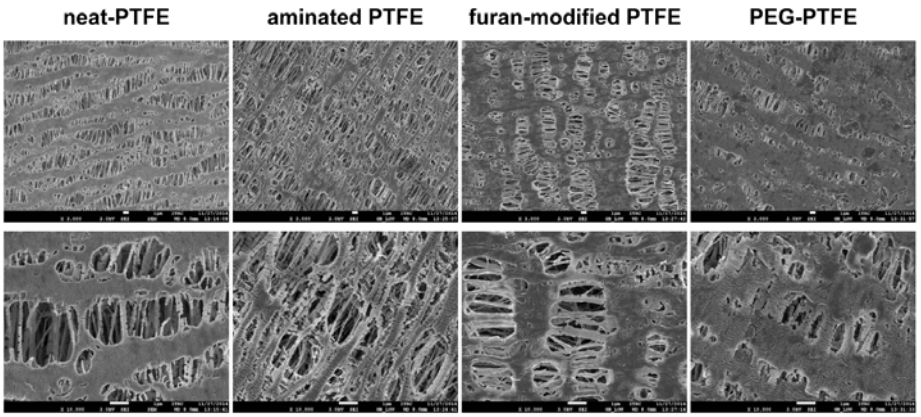

Figure IV-4. . FE-SEM images for top surface morphologies of neat PTFE (1st row), aminated PTFE (2nd row), furan-modified PTFE (3rd row), and PEG-PTFE membranes (4th row). (upper line) lower magnification, 3,000X, (low line) higher magnification 10,000X

IV-3-2. Reversible regeneration of the hydrophilic PEG layer through peel-and-stick process

In order to confirm whether the hydrophilic PEG layer can be regenerated on the membrane surface, repetitive peel-and-stick tests were carried out. A furan-maleimide DA cycloaddition is typically achievable at moderate temperatures from 20 to 80 °C, and the formed furan-maleimide DA cycloaddition is reversibly decoupled through the rDA reaction at temperature above 100 °C. Meanwhile, the PTFE membrane is wetted with a few organic solvents because PTFE has an extremely low surface free energy of around 20 mN m^{-1} at 20 °C[37,38] compared with other polymeric materials. Organic solvents such as acetone, ethanol, chloroform, THF and toluene, which have low liquid surface tension below 30 mN m^{-1} at 20 °C, are able to wet a PTFE membrane. Among these wettable solvents, toluene was thought to be suitable for the rDA reaction because its boiling temperature is 110 °C, while the other wettable solvents have lower boiling points (below 80 °C). Particularly, it is known that the rDA reaction of furan-maleimide bond is more preferred at higher temperature[20,25,34]. Thus, the peeling process of the PEG layer from the PEG-PTFE membrane was performed at 150 °C under a reflux environment to block evaporation of the toluene for effective decoupling of the furan-maleimide bond.

FE-SEM images (see Figure IV-5) show the surface morphological changes via the repetitive peel-and-stick process of the PEG layer on the membrane surface. It was found that the PEG layer of the PEG-PTFE membrane disappeared from the membrane surface after the membrane was treated at 150 °C, suggesting that the PEG layer can be readily peeled from

the membrane surface by adjusting thermal conditions. In addition, as can be seen from the FE-SEM image of the PEG-PTFE (2nd DA), a new PEG layer was re-formed on the membrane surface by DA coupling of fresh PEG-maleimide. In the second and third peel-and-stick processes, similar morphological changes were repeatedly observed on the membrane surface. These features revealed that the surface hydrophilic layer was readily and repeatedly regenerated through a thermally driven peel-and-stick process.

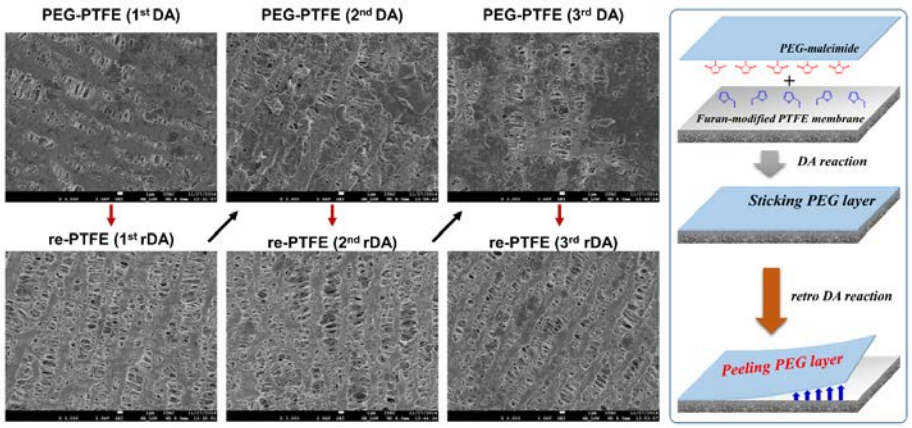

Figure IV-5. (left) FE-SEM images for top surface morphologies of PEG-PTFE membrane (upper line) and re-PTFE membrane (lower line), (right) schematic illustration of thermally driven dynamic peel-and-stick process

Analysis of the surface chemical structure provides more detailed information about the repetitive peel-and-stick process. Figure IV-6(a) shows ATR FT-IR spectra signifying changes of intensity for specific IR bands, such as C-O stretch at 1100 cm^{-1}, carbonyl stretch for imide at 1702 cm^{-1}, and sp^3 C-H stretch at 2945 – 2870 cm^{-1} derived from the PEG-maleimide. After peeling the PEG layer from the membrane surface by rDA reaction, the intensities for these IR bands were mostly reduced. In contrast, the reduced IR bands regained their original intensities through sticking the PEG layer via DA reaction. The reversibility of the peel-and-stick process was over approximately 80% calculated from the ATR FT-IR results. XPS spectra (see Figure IV-6(b)-(c)) also show similar reversibility of the PEG layers. In the XPS spectra for 1st-3rd rDA reactions, the signals at 286 eV assigned as C-O binding energy and 284 eV assigned as CH_2 binding energy were reduced by the peeling of the PEG layer, and the CF_2 signal (290.9 eV) and the C-F signal (687.8 eV) were manifested due to the appearance of the native PTFE surface. In contrast, the C-O and CH_2 binding energy signals originated from PEG-maleimide were recovered by the thermo-assisted sticking of the fresh PEG layer, and the XPS peaks related to CF_2 and C-F binding energies were reduced by shielding the native PTFE membrane surface. Figure IV-7 shows the surface hydrophilicity measured by a static pure water contact angle, as well as the quantitative results for specific IR bands (*i.e.*, C-H stretch and C=O stretch) and XPS atomic concentration (carbon and fluorine). The neat PTFE membrane has very high hydrophobic surfaces (contact angle 147.5 ± 2.95°). Surface hydrophilicity was slightly improved by furan-modification of the PTFE membrane surface (contact angle 119.5 ± 0.92°). After sticking the

hydrophilic PEG layer to the membrane surface, the pure water contact angle was significantly reduced, to 62.4 ± 2.92°, indicating that the hydrophilic PEG layer was successfully coupled with the modified membrane surface. In the re-PTFE (1st rDA) sample, the contact angle recovered to 114.9 ± 5.38°, indicating the peeling of the hydrophilic PEG layer. These tendencies were repeatedly observed during the three-cycle peel-and-stick process of the hydrophilic PEG layers. Therefore, the combined results of surface analyses disclosed that the membrane surface properties can be controlled by a thermally driven dynamic peel-and-stick process.

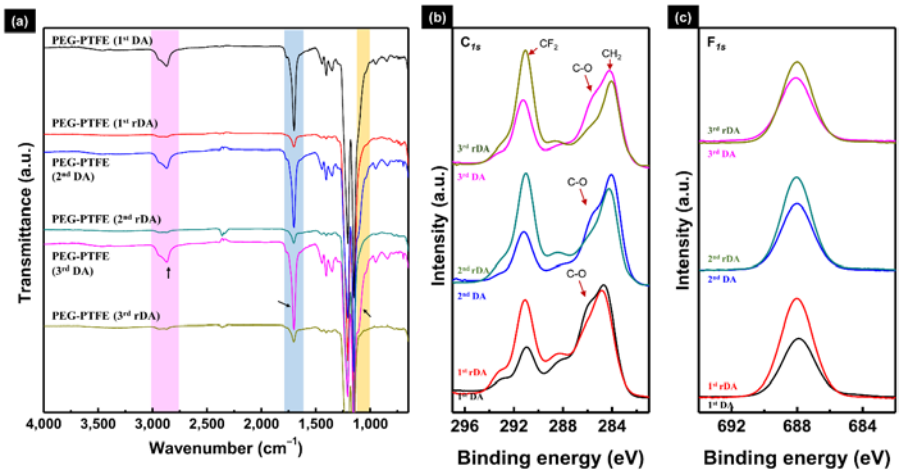

Figure IV-6. (a) ATR FT-IR and (b,c) XPS spectra for PEG-PTFE membrane by sticking PEG layer via Diels-Alder reaction and re-PTFE membrane by peeling of PEG layer via retro Diels-Alder reaction

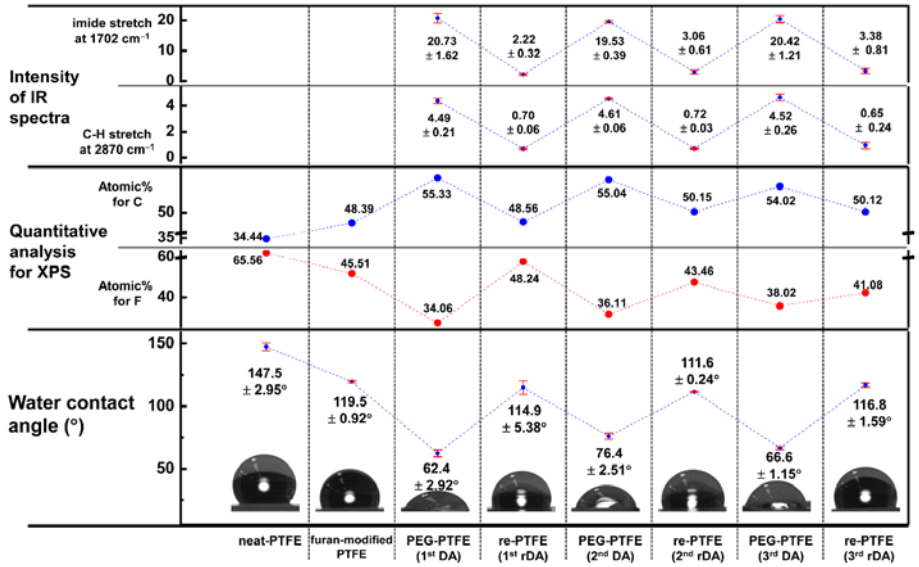

Figure IV-7. Summary of repetitive peel-and-stick of hydrophilic PEG layers on the PTFE membrane surface by intensity of ATR FT-IR spectra for carbonyl imide stretch and sp^3 C-H stretch (upper line), quantitative XPS analysis for carbon and fluorine (middle line) and static pure water contact angle (lower line)

IV-3-3. Evaluation of fouling resistance

In order to investigate the fouling resistance and the recovery of the anti-fouling property of the PEG-PTFE membrane, a filtration test was conducted using 500 ppm silica aqueous colloidal solution at neutral pH condition. The neat PTFE and the PEG-PTFE membranes were first fouled by the permeation of a highly concentrated silica suspension for one hour and the membranes were back-washed in order to eliminate the loosely-bound particles. Then, pure water permeability was recorded. After these processes were repeated three times, the PEG layer in the PEG-PTFE membrane was regenerated by a thermally driven peel-and-stick process and the pure water permeability of the regenerated membrane was measured. As a counterpart of the PEG-PTFE membrane, the neat PTFE membrane was treated in the same manner used for the water permeability measurement of the PEG-PTFE membrane.

As can be seen in Figure IV-8(a), normalized fluxes for the neat PTFE and the PEG-PTFE membranes dropped considerably after the permeation of the highly concentrated silica solution, indicating the occurrence of membrane fouling. The pure water fluxes were partially recovered by the back-washing process, and the recovered flux of the PEG-PTFE membrane was higher than that for the neat PTFE membrane. This indicated the superior anti-fouling property of the PEG-PTFE membrane due to the surface PEG layer. These tendencies were also observed in the second and the third filtration cycles. Nevertheless, the water permeability of both the neat PTFE and the PEG-PTFE membranes gradually decreased as the fouling and the back-washing was repeated. After three cycle filtration tests, the neat

PTFE and the PEG-PTFE membranes lost about 83.5% and 65.2% of their permeation properties, respectively (see Figure IV-8(b)). Thus, regeneration of the PEG layer was carried out by a thermally driven peel-and-stick process to recover membrane performance. As shown in Figure IV-8, the water permeability of the PEG-PTFE membrane recovered to 73.6% of its original performance after the peel-and-stick process. This was attributed to the fact that the permanently fouling silica was eliminated from the membrane together with the PEG layer, and that the fresh PEG layer was re-formed on the membrane surface. On the other hand, the neat PTFE membrane is recovery of its original performance was weak (about 24.1%) owing to the absence of an eliminable layer with foulants and regenerable layer by DA and rDA reactions. These results obviously show that the anti-fouling layer on the membrane surface can be regenerated and that membrane performance can be successfully recovered by the peel-and-stick process.

A regenerable surface functionality will prolong the lifetime of a membrane without need of the disassembly of the membrane module and replacement of the membrane, through the reversible introduction of an antifouling active layer on the membrane surface. Furthermore, this can realize a novel functional separating system via a combination of desired functionalities onto the membrane surface.

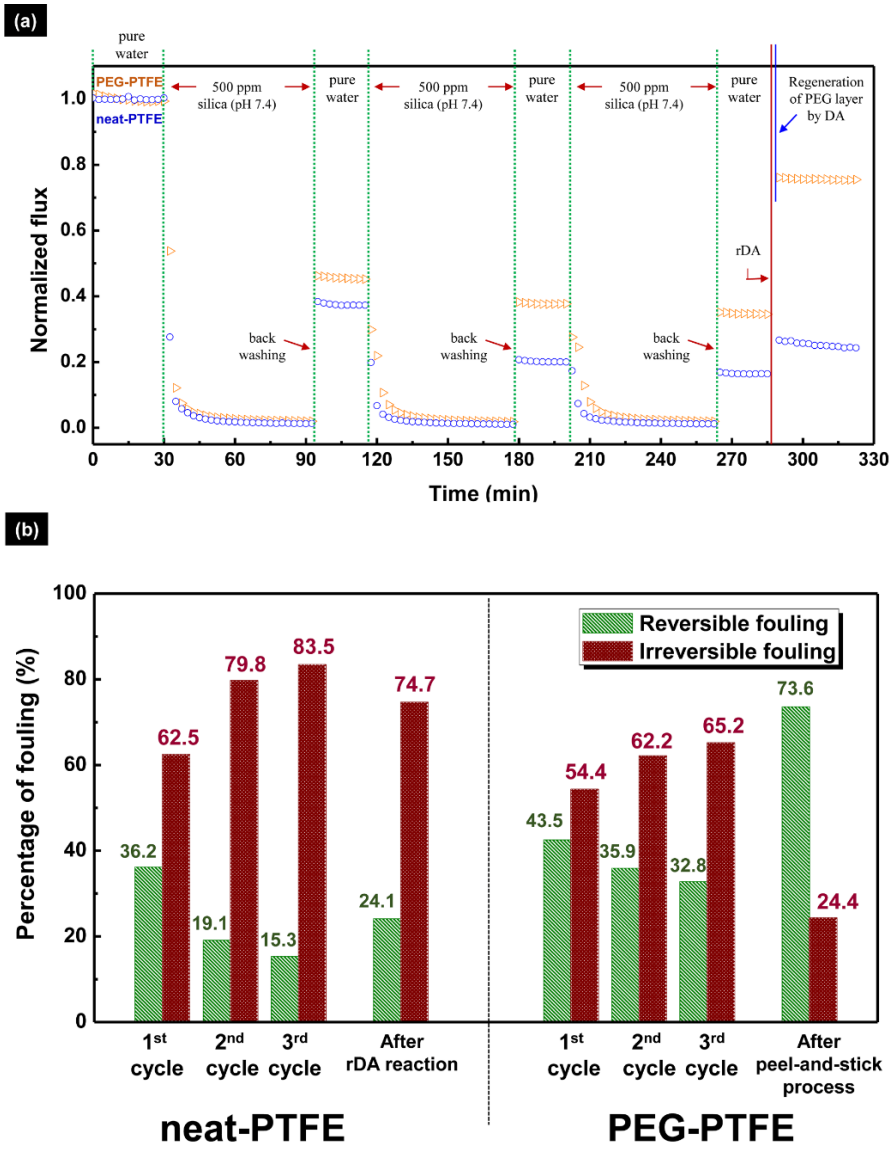

Figure IV-8. (a) Filtration tests of neat PTFE and PEG-PTFE membranes using 500 ppm silica colloidal aqueous suspension, (b) calculated reversible and irreversible fouling percentages for neat PTFE and PEG-PTFE membranes

IV-4. Conclusions

In this chapter, a regenerable anti-fouling membrane platform was developed via dynamic peel-and-stick of a hydrophilic PEG layer onto a PTFE membrane surface by thermo-responsive reversible Diels-Alder covalent bonding. The combined results of ATR FT-IR, XPS, and FE-SEM analyses showed that the maleimide end-modified PEG was successfully coupled with the furan-modified PTFE membrane surface by DA reaction between the furan and maleimide groups. As expected, the hydrophilic PEG layer was readily and repeatedly reformed on the surface of the membrane through the peel-and-stick process, which was verified by surface chemical and morphological analyses. In addition, the evaluation of fouling resistance showed that the hydrophilic PEG layers effectively suppressed membrane fouling by repeated permeation of high concentration colloidal silica suspension. In particular, the anti-fouling property was remarkably recovered after regeneration of the anti-fouling layer, *i.e.*, PEG, via the peel-and-stick process without membrane replacement. This approach opens up a new paradigm membrane platform by providing reversible covalent bonding between the functional material and the membrane surface.

References and Notes

1. Lei, J.; Ulbricht, M., Macroinitiator-mediated photoreactive coating of membrane surfaces with antifouling hydrogel layers. *J. Membr. Sci.* **2014,** *455*, 207-218.

2. Ji, Y. L.; An, Q. F.; Zhao, Q.; Sun, W. D.; Lee, K. R.; Chen, H. L.; Gao, C. J., Novel composite nanofiltration membranes containing zwitterions with high permeate flux and improved anti-fouling performance. *J. Membr. Sci.* **2012,** *390-391*, 243-253.

3. Wang, X.; Fang, D.; Yoon, K.; Hsiao, B. S.; Chu, B., High performance ultrafiltration composite membranes based on poly(vinyl alcohol) hydrogel coating on crosslinked nanofibrous poly(vinyl alcohol) scaffold. *J. Membr. Sci.* **2006,** *278* (1-2), 261-268.

4. Ba, C.; Ladner, D. A.; Economy, J., Using polyelectrolyte coatings to improve fouling resistance of a positively charged nanofiltration membrane. *J. Membr. Sci.* **2010,** *347* (1-2), 250-259.

5. Li, F.; Meng, J.; Ye, J.; Yang, B.; Tian, Q.; Deng, C., Surface modification of PES ultrafiltration membrane by polydopamine coating and poly(ethylene glycol) grafting: Morphology, stability, and anti-fouling. *Desalination* **2014,** *344*, 422-430.

6. Wang, P.; Tan, K. L.; Kang, E. T.; Neoh, K. G., Synthesis, characterization and anti-fouling properties of poly(ethylene glycol) grafted poly(vinylidene fluoride) copolymer membranes. *J. Mater. Chem.* **2001,** *11* (3), 783-789.

7. Nikkola, J.; Sievänen, J.; Raulio, M.; Wei, J.; Vuorinen, J.; Tang, C. Y., Surface modification of thin film composite polyamide membrane using

atomic layer deposition method. *J. Membr. Sci.* **2014,** *450*, 174-180.

8. Xu, L. Q.; Chen, J. C.; Wang, R.; Neoh, K. G.; Kang, E. T.; Fu, G. D., A poly(vinylidene fluoride)-graft-poly(dopamine acrylamide) copolymer for surface functionalizable membranes. *RSC Adv.* **2013,** *3* (47), 25204-25214.

9. Sui, Y.; Wang, Z.; Gao, X.; Gao, C., Antifouling PVDF ultrafiltration membranes incorporating PVDF-g-PHEMA additive via atom transfer radical graft polymerizations. *J. Membr. Sci.* **2012,** *413-414*, 38-47.

10. Yang, Q.; Xu, Z. K.; Dai, Z. W.; Wang, J. L.; Ulbricht, M., Surface modification of polypropylene microporous membranes with a novel glycopolymer. *Chem. Mater.* **2005,** *17* (11), 3050-3058.

11. Wang, P.; Tan, K. L.; Kang, E. T.; Neoh, K. G., Plasma-induced immobilization of poly(ethylene glycol) onto poly(vinylidene fluoride) microporous membrane. *J. Membr. Sci.* **2001,** *195* (1), 103-114.

12. Park, S. Y.; Chung, J. W.; Chae, Y. K.; Kwak, S. Y., Amphiphilic thiol functional linker mediated sustainable anti-biofouling ultrafiltration nanocomposite comprising a silver nanoparticles and poly(vinylidene fluoride) membrane. *ACS Appl. Mater. Interfaces* **2013,** *5* (21), 10705-10714.

13. Zodrow, K.; Brunet, L.; Mahendra, S.; Li, D.; Zhang, A.; Li, Q.; Alvarez, P. J. J., Polysulfone ultrafiltration membranes impregnated with silver nanoparticles show improved biofouling resistance and virus removal. *Water Res.* **2009,** *43* (3), 715-723.

14. Rana, D.; Matsuura, T., Surface Modifications for Antifouling Membranes. *Chem. Rev.* **2010,** *110* (4), 2448-2471.

15. Asatekin, A.; Kang, S.; Elimelech, M.; Mayes, A. M., Anti-fouling ultrafiltration membranes containing polyacrylonitrile-graft-poly(ethylene

oxide) comb copolymer additives. *J. Membr. Sci.* **2007,** *298* (1-2), 136-146.

16. Ahmad, A. L.; Abdulkarim, A. A.; Ooi, B. S.; Ismail, S., Recent development in additives modifications of polyethersulfone membrane for flux enhancement. *Chem. Eng. J.* **2013,** *223*, 246-267.

17. Kanagaraj, P.; Neelakandan, S.; Nagendran, A., Poly(ether imide) membranes modified with charged surface-modifying macromolecule - Its performance characteristics as ultrafiltration membranes. *J. Appl. Polym. Sci.* **2014,** *131* (11).

18. Zhao, Y. H.; Zhu, B. K.; Kong, L.; Xu, Y. Y., Improving hydrophilicity and protein resistance of poly(vinylidene fluoride) membranes by blending with amphiphilic hyperbranched-star polymer. *Langmuir* **2007,** *23* (10), 5779-5786.

19. Syrett, J. A.; Becer, C. R.; Haddleton, D. M., Self-healing and self-mendable polymers. *Polym. Chem.* **2010,** *1* (7), 978-987.

20. Zhang, Y.; Broekhuis, A. A.; Picchioni, F., Thermally self-healing polymeric materials: The next step to recycling thermoset polymers? *Macromolecules* **2009,** *42* (6), 1906-1912.

21. Peterson, A. M.; Jensen, R. E.; Palmese, G. R., Room-temperature healing of a thermosetting polymer using the diels-alder reaction. *ACS Appl. Mater. Interfaces* **2010,** *2* (4), 1141-1149.

22. Scheltjens, G.; Diaz, M. M.; Brancart, J.; Van Assche, G.; Van Mele, B., A self-healing polymer network based on reversible covalent bonding. *React. Funct. Polym.* **2013,** *73* (2), 413-420.

23. Watanabe, M.; Yoshie, N., Synthesis and properties of readily recyclable polymers from bisfuranic terminated poly(ethylene adipate) and

multi-maleimide linkers. *Polymer* **2006,** *47* (14), 4946-4952.

24. Chen, X.; Dam, M. A.; Ono, K.; Mal, A.; Shen, H.; Nutt, S. R.; Sheran, K.; Wudl, F., A thermally re-mendable cross-linked polymeric material. *Science* **2002,** *295* (5560), 1698-1702.

25. Liu, Y. L.; Hsieh, C. Y.; Chen, Y. W., Thermally reversible cross-linked polyamides and thermo-responsive gels by means of Diels-Alder reaction. *Polymer* **2006,** *47* (8), 2581-2586.

26. Tasdelen, M. A., Diels-Alder "click" reactions: Recent applications in polymer and material science. *Polym. Chem.* **2011,** *2* (10), 2133-2145.

27. Hu, J.; Liu, S., Engineering Responsive Polymer Building Blocks with Host–Guest Molecular Recognition for Functional Applications. *Acc. Chem. Res.* **2014,** *47* (7), 2084-2095.

28. Rajagopalan, M.; Jeon, J.-H.; Oh, I.-K., Electric-stimuli-responsive bending actuator based on sulfonated polyetherimide. *Sensors Actuators B: Chem.* **2010,** *151* (1), 198-204.

29. Asoh, T. A.; Matsusaki, M.; Kaneko, T.; Akashi, M., Fabrication of temperature-responsive bending hydrogels with a nanostructured gradient. *Adv. Mater.* **2008,** *20* (11), 2080-2083.

30. Ahn, S. K.; Kasi, R. M.; Kim, S. C.; Sharma, N.; Zhou, Y., Stimuli-responsive polymer gels. *Soft Matter* **2008,** *4* (6), 1151-1157.

31. Ripoll, J. L.; Rouessac, A.; Rouessac, F., Applications recentes de la reaction de retro-diels-alder en synthese organique. *Tetrahedron* **1978,** *34* (1), 19-40.

32. Wei, H. L.; Yang, Z.; Chen, Y.; Chu, H. J.; Zhu, J.; Li, Z. C., Characterisation of N-vinyl-2-pyrrolidone-based hydrogels prepared by a

Diels-Alder click reaction in water. *Eur. Polym. J.* **2010,** *46* (5), 1032-1039.

33. Domingo, L. R.; Sáez, J. A., Understanding the mechanism of polar Diels-Alder reactions. *Org. Biomol. Chem.* **2009,** *7* (17), 3576-3583.

34. Wei, H. L.; Yang, Z.; Zheng, L. M.; Shen, Y. M., Thermosensitive hydrogels synthesized by fast Diels-Alder reaction in water. *Polymer* **2009,** *50* (13), 2836-2840.

35. Inglis, A. J.; Nebhani, L.; Altintas, O.; Schmidt, F. G.; Barner-Kowollik, C., Rapid bonding/debonding on demand: Reversibly cross-linked functional polymers via diels-alder chemistry. *Macromolecules* **2010,** *43* (13), 5515-5520.

36. Yoo, H.; Kwak, S. Y., Surface functionalization of PTFE membranes with hyperbranched poly(amidoamine) for the removal of Cu2+ ions from aqueous solution. *J. Membr. Sci.* **2013,** *448*, 125-134.

37. Chaudhuri, R. G.; Paria, S., Dynamic contact angles on PTFE surface by aqueous surfactant solution in the absence and presence of electrolytes. *J. Colloid Interface Sci.* **2009,** *337* (2), 555-562.

38. Szymczyk, K.; Zdziennicka, A.; Jańczuk, B.; Wójcik, W., The wettability of polytetrafluoroethylene and polymethyl methacrylate by aqueous solution of two cationic surfactants mixture. *J. Colloid Interface Sci.* **2006,** *293* (1), 172-180.

CHAPTER V

CONVERTIBLE POLY(TETRAFLUORO-ETHYLENE) (PTFE) MEMBRANES BY REVERSIBLE ALTERATION OF SURFACE FUNCTIONALITIES USING THERMALLY DRIVEN "PEEL-AND-STICK" PROCESS

V-1. Introduction

Traditional functional membranes were typically developed by irreversible introduction of surface modifying materials to the membrane[1-12]. The introduced functionalities can provide desired properties to the membrane such as anti-fouling, high-rejection, high-permeability, durability and enhanced ion selectivity. However, these functionalities were gradually vanished by irreversible accumulation of water contaminants on the membrane surfaces into the membrane pores[11]. This brings about a deterioration of membrane performance. In order to solve these limitations, in the previous chapter, an exchangeable functional layer was introduced onto the membrane surface by thermally driven peel-and-stick process[13].

Through the thermo responsive reversible bonding, not only regeneration of the identical functionality but the new functionality can be also introduced to the membrane surface by elimination of an existing

functional layer. Among thermo responsive bondings, Diels-Alder (DA) reaction between furan and maleimide groups can be formed covalent bonding and restored to their original forms by adjusting thermal condition[14-17]. The membrane surface property is able to replace with other functionalities by coupling the new functional material with maleimide moiety onto the furan re-activated membrane surface via thermally driven peel-and-stick process which was established in the previous chapter. Thus, if the peel-and-stick process is applied to a membrane functionalization method, it is expected that a convertible membrane platform would be developed by changing the existing functional layer into a desired functional layer.

This study presents a convertible membrane by alteration of surface functionality by a thermo responsive peel-and-stick process. In order to convert membrane property, specific functional materials which were reversibly introduced onto the PTFE membrane surface were eliminated by the peeling process and desired properties were then re-coupled with the PTFE membrane surface by the sticking process. In this chapter, three types of maleimide modified functional materials *i.e.,* silica nanoparticles, silver nanoparticles, poly(ethylene) glycol, were reversibly assembled onto the furan modified PTFE membrane surface. These functional materials were repeatedly peeled off and stuck on the membrane surface by controlling temperature. In addition, the surface introduced functionalities were converted into desired other functionalities by the thermally driven peel-and-stick process. This approach opens up new generation membrane platform by creating convertible surface functional layers. This approach could create

various potential membrane applications such as adjustable anti-fouling membranes and multi-functional membranes.

V-2. Experimental Section

V-2-1. Materials

A porous poly(tetrafluoroethylene) (PTFE) flat membrane with 47 mm diameter and 0.1 μm average pore diameter was purchased from Advantec-MFS, Inc. Silica nanoparticles (fumed, average diameter 0.007 μm), silver nitrate (99.0%), sodium borohydride ($NaBH_4$, 98.5%), maleic anhydride (99.0%), 4-aminobenzoic acid (99.0%), sodium acetate (99.0%), Poly(ethylene glycol) methyl ether maleimide (M_n 2,000), furfuryl glycidyl ether (96%), hydrazine monohydrate (98%), triblock Pluronic copolymer F127 (EO_{97}-PO_{67}-EO_{97}, M_w 126,000), *N*,*N*'-dicyclohexylcarbodiimide (DCC, 99%), 4-(dimethylamino) pyridine (DMAP, 99%) were purchased from Sigma-Aldrich. Toluene (99.8%), tetrahydrofuran (THF, 99.0%), sodium hydroxide (98%), thionyl chloride (98%) were obtained from Daejung Chemical & Metals. All chemicals were used as received, without further purification. The aqueous solutions were prepared with deionized (DI) water having a resistivity exceeding 18.0 MΩ cm.

V-2-2. Synthesis of maleimide derivatives

In order to introduce maleimide moiety to inorganic (silica) and metal (silver) nanoparticles, N-(4-carboxy phenyl) maleimide (*p*-CPMI) was

prepared by reaction between maleic anhydride and 4-aminobenzoic acid[18]. The maleic anhydride (9.8 g, 0.1 mol) and the 4-aminobenzoic acid (13.7 g, 0.1 mol) were dissolved in 100 mL DMF solvent at room temperature. The reaction was kept for 5 hours with vigorous stirring. The intermediate product, N-(4-carboxyphenyl) maleiamic acid (*p*-CPMA), was obtained by precipitation in large amount cold DI water and dried at vacuum oven for overnight. The *p*-CPMI was synthesized by intramolecular condensation reaction of *p*-CPMA. The *p*-CPMA (2.35 g, 0.01 mol) was dissolved into 100 mL of acetic anhydride. Equal molecular weight of sodium acetate (0.82 g, 0.01 mol) was then added to the *p*-CPMA/acetic anhydride solution. The mixture was refluxed for 2 hours with vigorous stirring. In order to obtain crude *p*-CPMI, the reacted solution was poured into large amount cold DI water and then vacuum drying. Next, the crude *p*-CPMI product was dissolved in methanol/water (6:1 v/v%) solution and recrystallized to obtain high purified *p*-CPMI product. The *p*-CPMA and the *p*-CPMI were analyzed by Fourier-transform infrared spectroscopy (FT-IR; Thermo Scientific Nicolet iS5 FT-IR spectrometer) with a spectral resolution of 4 cm^{-1} over the range 4000–400 cm^{-1} and ^{1}H nuclear magnetic resonance (^{1}H NMR, Bruker Avance 600) spectroscopy using DMSO-d_6 as a solvent.

V-2-3 Preparation of maleimide modified silica nanoparticles

Surface maleimide functionalized silica nanoparticles (SiO_2 NPs) were prepared by reaction of aminated SiO_2 NPs with the *p*-CPMI. First, the aminated SiO_2 NPs were prepared by surface modification of SiO_2 NPs with (3-Aminopropyl)triethoxysilane (APTES)[19]. The SiO_2 NPs (1 g) were

dispersed into 70 mL of 1% APTES/toluene solution, and then the mixture was refluxed at 110 °C for 24 hours with stirring. The aminated SiO_2 NPs were obtained by centrifugation and rinsed several times with toluene. The final products were dried in vacuum at 60 °C for overnight. Second, the dried aminated SiO_2 NPs (1 g) and 4-(dimethylamino)pyridine (1 g, DMAP) were added to 20 mL anhydrous THF. The *p*-CPMI solution which was prepared by dissolving 0.45 g of the *p*-CPMI into 50 mL of anhydrous THF was injected the above solution with vigorous stirring at 0 °C. Next, *N*,*N*'-dicyclohexylcarbodiimide (0.41 g, DCC) was added into the reaction solution and then the reaction was kept at 0 °C for overnight. The crude products were obtained by centrifugation, and washed several times with ethanol and acetone to remove urea precipitates. The final product was dried in vacuum oven at 60 °C for overnight. The aminated SiO_2 NPs, and maleimide modified SiO_2 NPs were analyzed by FT-IR spectroscopy with a spectral resolution of 4 cm^{-1} over the range 4000–400 cm^{-1}.

V-2-4 Preparation of maleimide modified silver nanoparticles

Ag NPs with surface maleimide moieties were prepared by stabilization of Ag NPs with maleimide modified triblock Pluronic copolymer. First, the maleimide-modified triblock Pluronic copolymer was synthesized by esterification of end-hydroxyl group in F127 with 4-(chlorocarbonyl)phenyl maleimide (*p*-CPMIC). The *p*-CPMIC was converted from *p*-CPMI by reaction with thionyl chloride. Second, 10 mM $AgNO_3$ aqueous solution was injected to 8 wt% of the maleimide modified F127 (F127-maleimide) and then the mixture was agitated using a vortex mixer. 0.1

mL of 100 mM $NaBH_4$ aqueous solution was quickly injected into the above mixture following by vigorous shaking[20-21]. The solution was stored in a refrigerator during nucleation and growth of Ag NPs. The modification process for maleimide modified F127 was monitoring by FT-IR (Thermo Scientific Nicolet iS5 FT-IR spectrometer) with a spectral resolution of 4 cm^{-1} over the range 4000–400 cm^{-1} and ^1H nuclear magnetic resonance (^1H NMR, Bruker Avance 600) spectroscopy using DMSO as a solvent. The Ag NPs morphology was obtained by transmittance electron microscopy (TEM) analysis by Carl Zeiss LIBRA 120 at 120 kV acceleration voltage.

V-2-5 Preparation of silica, silver nanoparticles coupled PTFE membranes

In order to couple SiO_2 and Ag NPs to membrane surface, the maleimide modified SiO_2 and Ag NPs were bound to the furan-modified PTFE membrane via thermo-responsive peel-and-stick process. The furan modification of PTFE membrane was described in the previous chapter (see IV-2-2). The furan-modified PTFE membranes were placed at the bottom of jars and then 10 mL of 0.5 wt% maleimide modified SiO_2 NPs suspended toluene solution for preparation of SiO_2 NPs coupled PTFE membrane (denoted as SiO_2-PTFE), or 10 mL of Ag NPs colloidal solution for preparation of Ag NPs coupled PTFE membrane (denoted as Ag-PTFE). The closed jars were gentle agitated in the pre-heated oven at 50 °C for 1 day. After coupling reaction, the membranes were rinsed several times with toluene and THF and dried at room temperature.

V-2-6 Evaluation of regeneration and conversion of surface functionalities by thermo-responsive peel-and-stick process

To regenerate the surface functional layer on the membrane, the attached SiO_2 or Ag NPs were peeled off membrane surface by retro Diels-Alder (rDA) reaction and the new SiO_2 or Ag NPs were re-coupled to the membrane surface by DA reaction. The regeneration process had already described in the previous chapter (IV-2-3). Peeling off the surface layer was conducted at 150 °C for overnight. Re-sticking process was conducted at mild condition which is the same method described in the previous section. Furthermore, the conversion of surface functionalities was carried out by the peel-and-stick process. After peeling surface layer, another functionality was coupled by DA reaction to alter surface properties. Briefly, the SiO_2-PTFE was converted into PEG coupled PTFE membrane (PEG-PTFE) and Ag-PTFE, respectively. The Ag-PTFE was converted into PEG-PTFE and SiO_2-PTFE, respectively. The sticking of new PEG layer onto the peeled membrane surface was the same process in the previous chapter (IV-2-3). The sticking process of Ag NPs or SiO_2 NPs was the described in the previous section (V-2-5). These processes were schematically illustrated in Fig V-1.

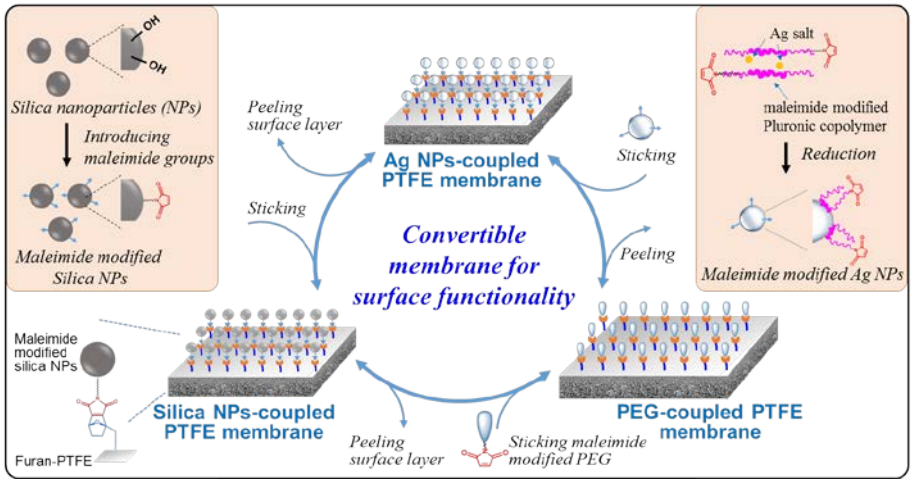

Figure V-1. Schematic illustration for conversion of surface functionalities via thermo responsive peel-and-stick process

V-2-7 Membrane characterization

The preparation of the SiO_2-PTFE, the Ag-PTFE, the repetitive regeneration of the surface layer, and the conversion of surface layer through thermo responsive peel-and-stick process were monitored by attenuated total reflection (ATR) FT-IR (Thermo Scientific Nicolet iS5) spectroscopy with a spectral resolution of 4 cm^{-1} with the range of 650 – 4000 cm^{-1} and X-ray photoelectron spectroscopy (XPS, Kratos AXIS-HSi) using monochromatic Mg K_α X-ray source operated at 10 mA. In order to evaluate surface hydrophilicity of the resulting membranes, static pure water contact angle was analyzed at room temperature using BiolinScientific, Attention® THETA LITE. The surface morphologies of the membranes were observed by field-emission scanning electron microscopy (FE-SEM, JEOL 7800F) with energy dispersive x-ray spectroscopy (EDXS) for analyzing morphology and chemical composition of membrane surface. Pt coating was carried out using Pt sputtering at 10 mA for 100 seconds for the FE-SEM/EDXS analyzing.

V-3. Results and Discussion

V-3-1 Maleimide modified SiO_2 and Ag nanoparticles

To reversibly couple SiO_2 or Ag NPs onto membrane surface via DA reaction, maleimide functional groups were introduced at the surface of SiO_2 or Ag NPs using maleimide derivatives. The maleimide derivative composed of a maleimide functional group and a carboxylic acid was synthesized from maleic anhydride and 4-aminobenzoic acid. The reaction between maleic anhydride and 4-aminobenzoic acid formed an intermediate product (*p*-CPMA). The *p*-CPMA was converted into *p*-CPMI by an intramolecular condensation reaction. Figure V-2 shows FT-IR spectra for the preparation of *p*-CPMA and *p*-CPMI. NH_2 stretches (3460 cm^{-1}, 3365 cm^{-1}) in the 4-aminobenzoic acid were converted into NH stretch (3316 cm^{-1}) in the IR spectra of *p*-CPMA by formation of amide bonding. In the IR spectra of *p*-CPMI, this NH IR band was disappeared by an intramolecular condensation reaction and C=O stretch for imide group was found at 1710 cm^{-1} in the IR spectra of *p*-CPMI, indicating successful synthesis of the *p*-CPMI. ^{1}H NMR analysis shows more detailed results regarding the reaction progress for the maleimide derivatives. As shown in Figure V-3, the ^{1}H NMR spectra of *p*-CPMA showed new NMR peaks at 10.6 ppm, 6.48 ppm and 6.36 ppm corresponding to the -CONH- and -CO-CH=CH-CO- indicating the successful preparation of the *p*-CPMA. After the intramolecular condensation reaction, ^{1}H NMR peak at 10.6 ppm corresponding to –CONH- was completed disappeared and -CO-CH=CH-CO- NMR peaks were merged into a single NMR peak (7.20 ppm) by recovering symmetric ring structure. These

results disclosed that the maleimide derivative (*p*-CPMI) composed of maleimide and carboxylic acid groups was successfully synthesized.

The maleimide modified SiO_2 NPs were prepared by amidation of aminated SiO_2 NPs with *p*-CPMI. The fumed SiO_2 NPs were reacted with APTES to form the aminated SiO_2 NPs. To introduce a maleimide moiety, the aminated SiO_2 NPs reacted with p-CPMI using a DCC/DMAP catalyst. As shown in Figure V-4, sp^3 C-H stretch and NH_2 bend were appeared in the FT-IR spectra for the aminated SiO_2 NPs. After reaction with *p*-CPMI, C=O stretch for imide at 1715 cm^{-1} was observed, indicating successfully modification of SiO_2 NPs with a maleimide moiety.

The maleimide modified Ag NPs were prepared by stabilization of Ag NPs with maleimide modified F127. The maleimide modified F127 was prepared by conversion of a hydroxyl end group into a maleimide group through esterification. From FT-IR analysis (see Figure V-5), carbonyl imide stretch at 1721 cm^{-1} was observed in the FT-IR spectra of F127-maleimide, indicating conversion of the end hydroxyl group into the maleimide group. ^1H NMR spectra (see Figure V-6) provided more detailed information for this modification. After introducing maleimide moiety, new ^1H NMR peaks were appeared at 7.20, 7.54, 8.07 ppm corresponding to –CO-CH=CH-CO- in the maleimide structure, hydrogen atoms in the benzene ring, respectively. Degree of substitution for F127-maleimide was calculated as 0.5 through comparing integral ratio between 4.55 ppm and 4.41 ppm. Ag NPs were synthesized and stabilized with the F127-maleimide. As shown in Figure V-7, TEM analysis showed that spherical shape particles were observed with their size around 10 nm.

Maleimide modified inorganic and metal nanomaterials were effectively fabricated using the maleimide derivatives. Chemical structure and morphological analyses indicated that maleimide moieties were successfully introduced onto the surface of SiO_2 and Ag NPs.

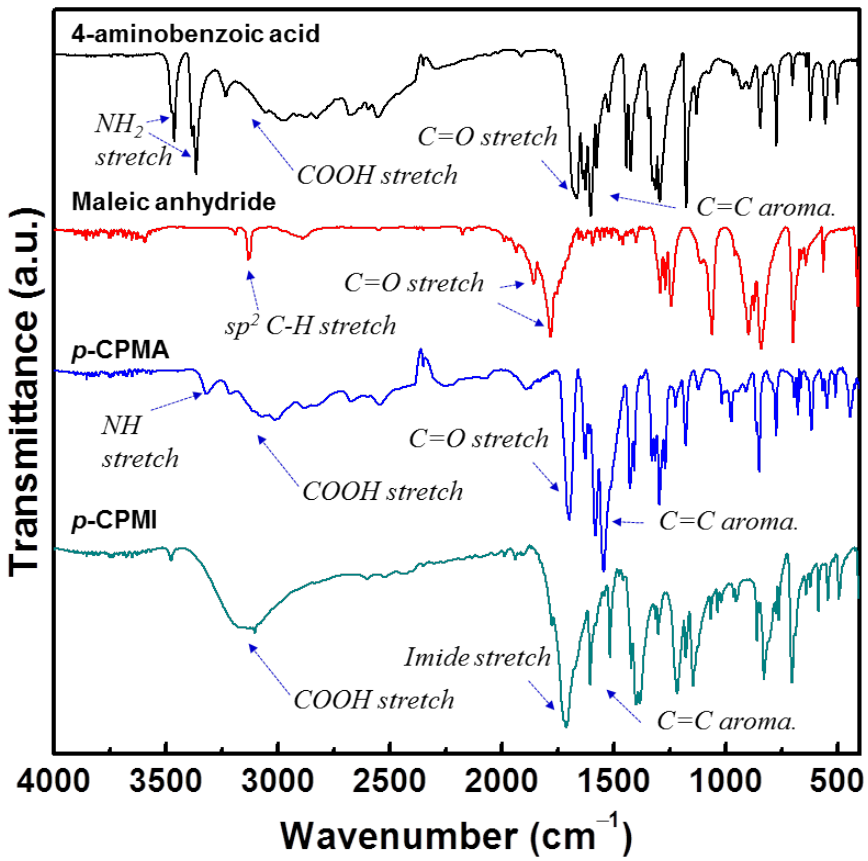

Figure V-2. FT-IR spectra for 4-amino benzoic acid (1st line), maleic anhydride (2nd line), p-CPMA (3rd line) and p-CPMI (4th line)

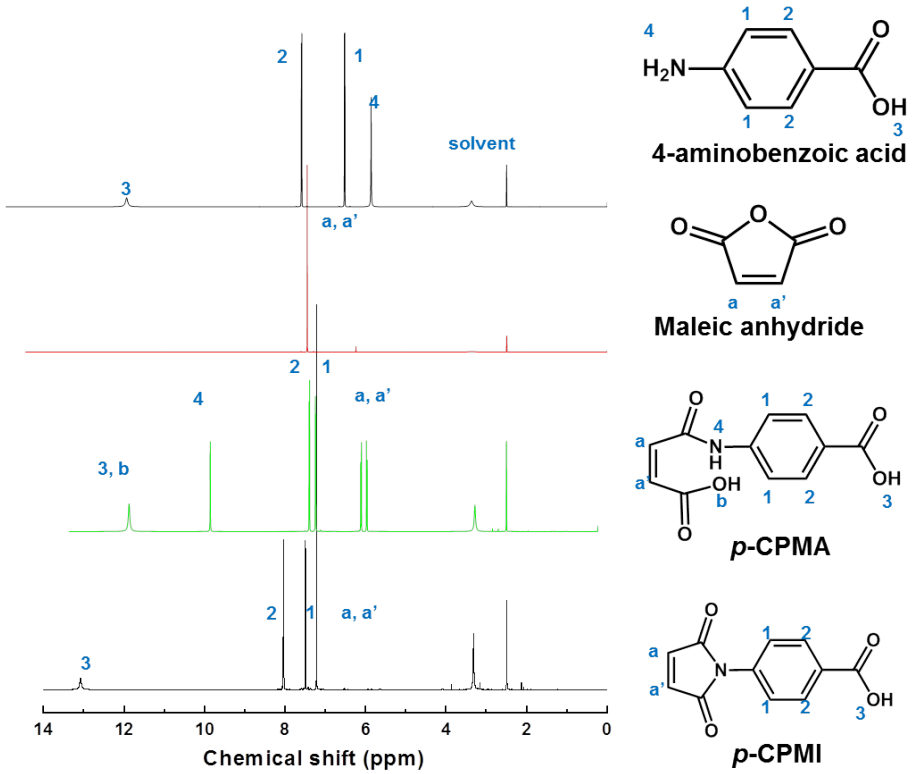

Figure V-3. ^{1}H NMR spectra for 4-amino benzoic acid (1st line), maleic anhydride (2nd line), p-CPMA (3rd line) and p-CPMI (4th line)

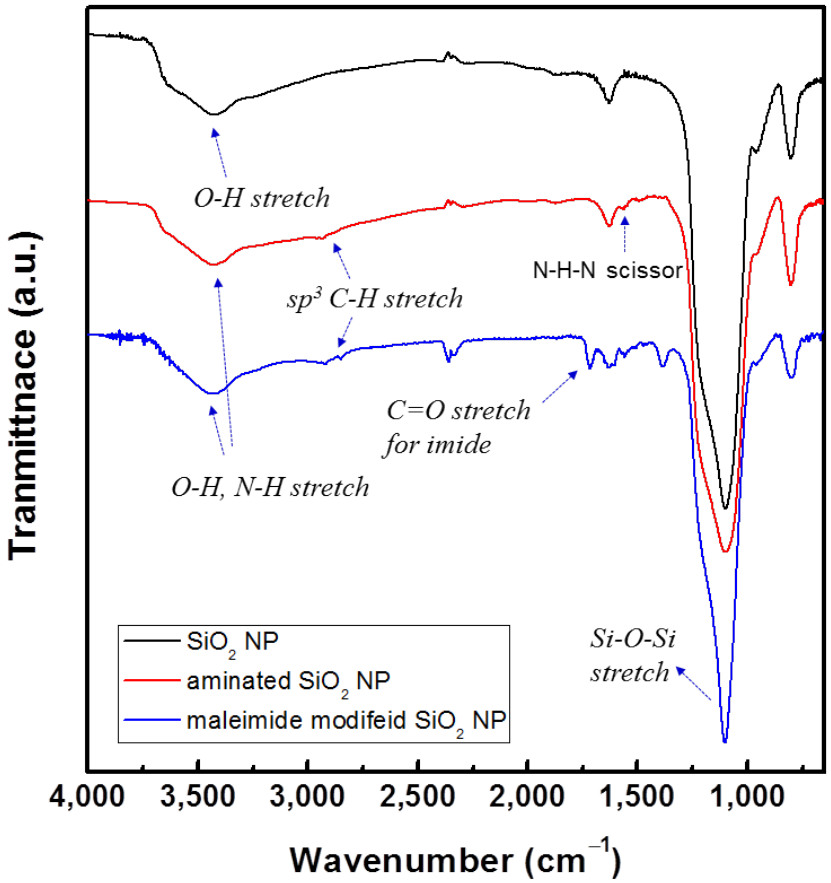

Figure V-4. FT-IR spectra for SiO_2 NP (top line), aminated SiO_2 NP (middle line) and maleimide modified SiO_2 NP (bottom line)

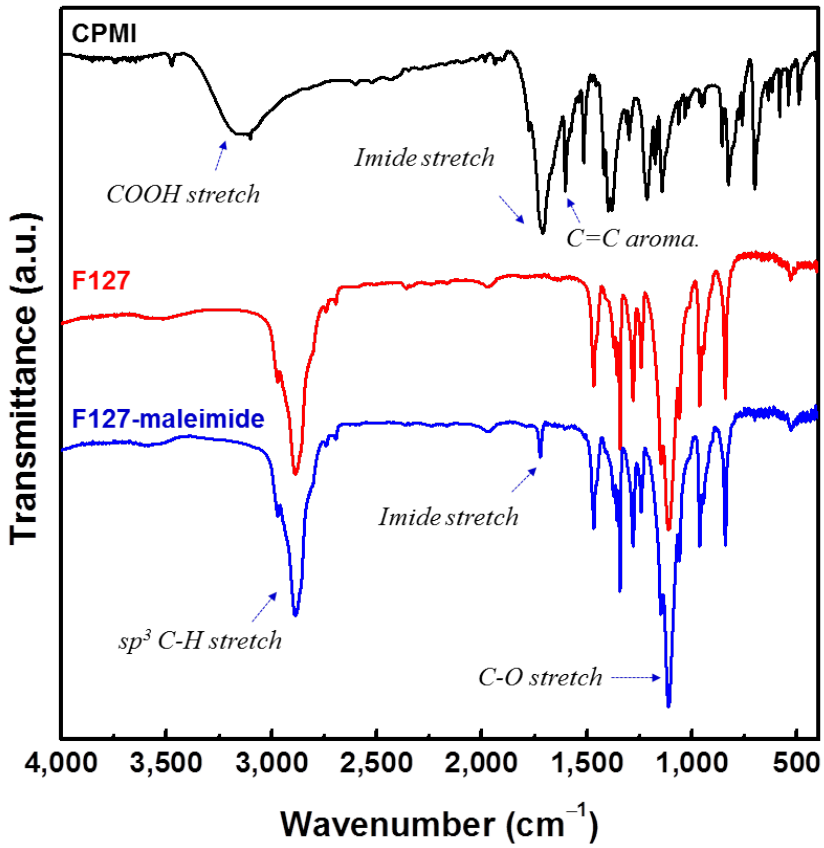

Figure V-5. FT-IR spectra for *p*-CPMI (top line), triblock Pluronic copolymer F127 (middle line) and maleimide modified F127 (bottom line)

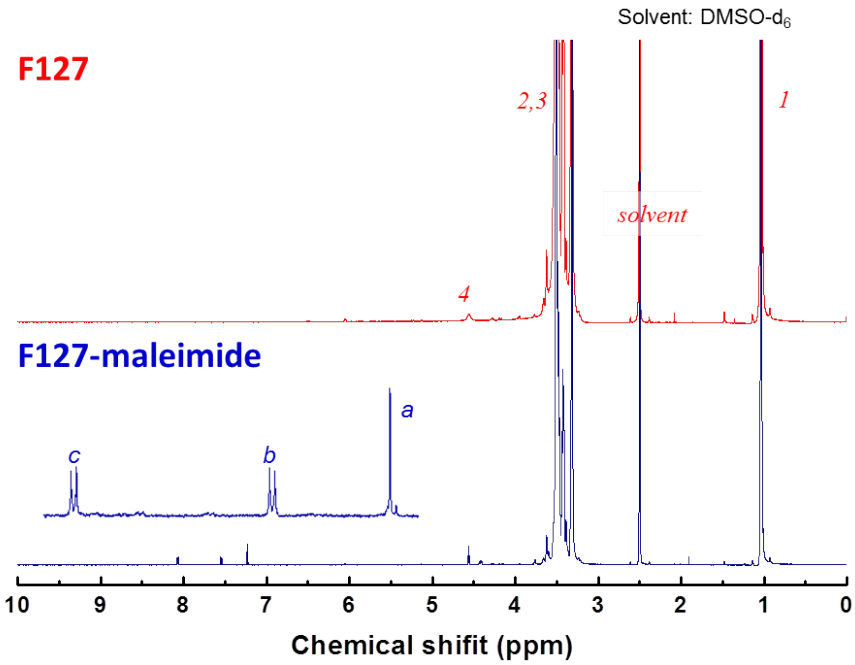

Figure V-6. ^{1}H NMR spectra for F127 (top line) and maleimide modified F127 (bottom line)

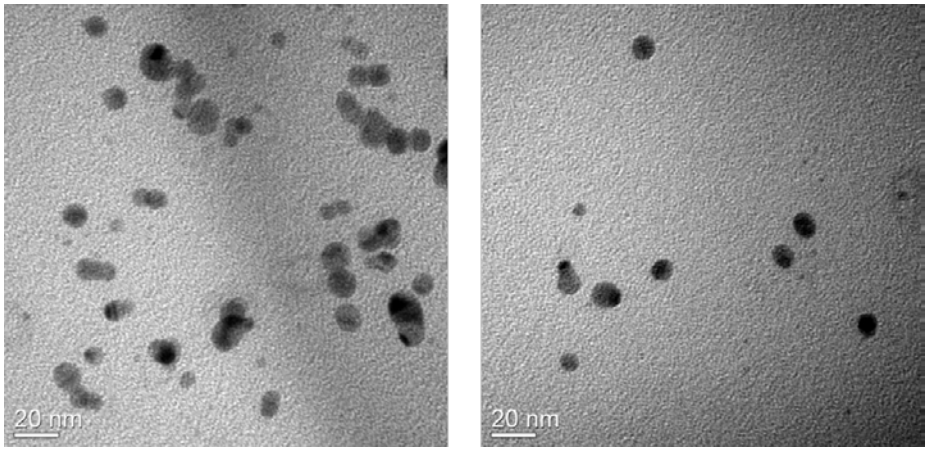

Figure V-7. TEM images for Ag NPs stabilized with maleimide modified F127

V-3-2 SiO_2 and Ag nanoparticles coupled PTFE membrane

The maleimide modified SiO_2 and Ag NPs were coupled with the furan modified PTFE membrane surface via DA reaction at 50 °C. The fabrication of furan modified PTFE membrane was described in the previous chapter (IV-3-1). Figure V-8 shows ATR FT-IR results for the SiO_2- PTFE. In the IR spectrum of SiO_2-PTFE, O-H stretch at 3600 – 3100 cm^{-1} and Si-O-Si stretch at 1095 cm^{-1} were appeared by coupling SiO_2 NPs. As coupling SiO_2 NPs, spherical shape particles were observed at the surface of SiO_2-PTFE (see Figure V-9(d)). As shown in Figure V-9(e-f), EDXS and XPS analyses detected a Si element at the membrane surface. Pure water contact angle was significantly reduced by assembly of hydrophilic SiO_2 NPs. These combined results disclosed that the SiO_2 NPs were attached at the membrane surface via thermo responsive DA reaction.

Figure V-10 shows the coupling of Ag NPs onto the furan modified PTFE membrane. sp^3 C-H stretch at 2879 cm^{-1}, C-O stretch at 1113 cm^{-1} IR bands were observed in IR spectrum of the Ag-PTFE. Partially occupied surface layer was observed on the membrane surface and pure water contact angle was also reduced by assembly of F127 stabilized Ag NPs. In addition, XPS analysis (see Figure V-10(c)) detected an Ag element, indicating that the Ag NPs stabilized with F127-maleimide was chemically bound onto the membrane surface.

To investigate biocidal effect for the Ag-PTFE, *E. coli.* (CCARM 1001) were fixed onto the surface of both neat PTFE and Ag-PTFE membranes by filtration method and they were observed by FE-SEM imaging after incubating the *E. coli.* adhered membranes at 37 °C for hours. Figure V-

11 shows FE-SEM images of the bacteria-adhered membrane surface. Debris from dead *E. coli* could be observed on the surface of Ag-PTFE, whereas intact live *E. coli* were observed on the neat PTFE membrane surface indicating that the assembled Ag NPs effectively killed the bacteria on the membrane surface. It is expected that the antibacterial effects of the Ag-PTFE may reduce biofouling of the membrane.

As expected, the maleimide modified inorganic and metal nanomaterials were assembled onto the furan-modified membrane surface by DA coupling reaction. The surface chemical structural and morphological assessments disclosed the assembly of desired properties onto membrane surface.

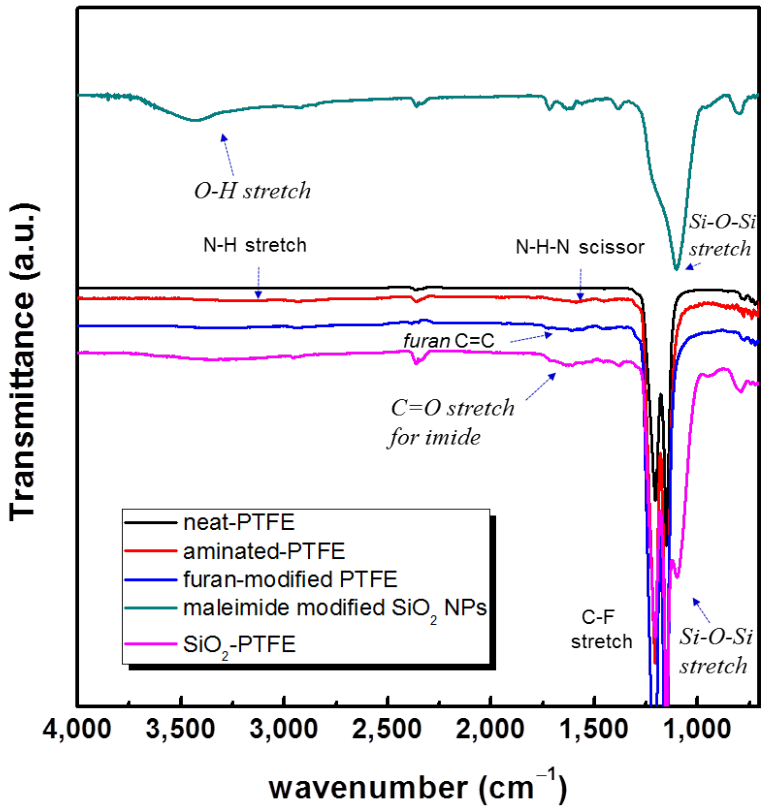

Figure V-8. FT-IR spectra of maleimide modified SiO_2 NPs (1st line), neat PTFE (2nd line), aminated PTFE (3rd line), furan-modified PTFE (4th line) and SiO_2-PTFE (5th line)

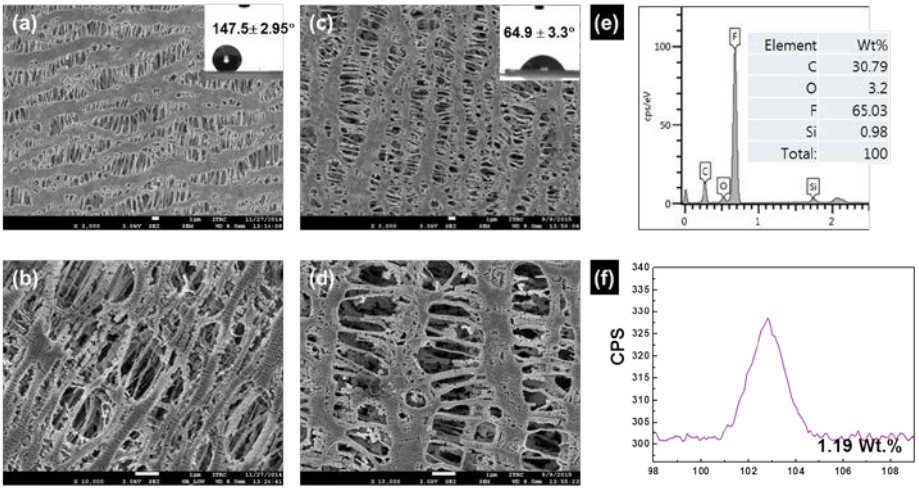

Figure V-9. FE-SEM image of (a,b) neat PTFE and (c,d) SiO_2-PTFE, inset images in (a) and (c): pure water contact angle, (e) EDXS result and (f) XPS spectrum of S 2p for SiO_2-PTFE

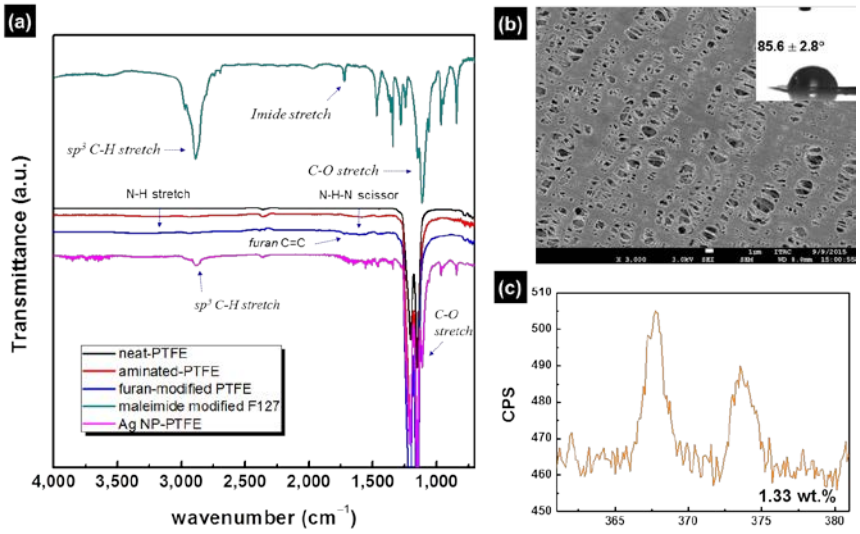

Figure V-10. (a) FT-IR spectra of maleimide-modified F127 (1st line), neat PTFE (2nd line), aminated PTFE (3rd line), furan-modified PTFE (4th line) and Ag-PTFE (5th line), (b) FE-SEM image (inset: pure water contact angle) of Ag-PTFE, (c) XPS spectra of Ag 3d of Ag-PTFE

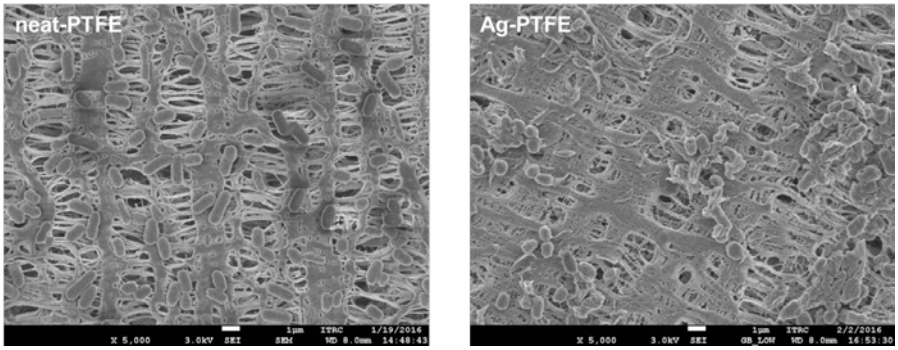

Figure V-11. FE-SEM images of the surface adhered *E. coli* on (left) the neat PTFE and (right) Ag-PTFE membranes

V-3-3 Regeneration and conversion of surface functionalities by thermo responsive peel-and-stick process

In order to confirm regeneration of surface functionalities, the SiO_2 NPs and Ag NPs were reversibly peeled and stuck on the membrane surface by adjusting thermal conditions.

In case of the SiO_2-PTFE, after peeling the SiO_2 NPs from the membrane surface, SiO_2 NPs related IR bands such as Si-O-Si stretch(1093 cm^{-1}), O-H stretch (3600 – 3100 cm^{-1}) were almost disappeared (see Figure V-12). These IR bands were regained after sticking fresh SiO_2 NPs onto the membrane surface by DA reaction. In the 2nd and 3rd cycle of peel-and-stick test for maleimide modified SiO_2 NPs, the SiO_2 related IR bands were repeatedly reduced and regained. Other analyses showed more detailed information about regeneration of surface functionality. Figure V-13 showes FE-SEM images and pure water contact angles for coupling and decoupling SiO_2 NPs onto the membrane surface. After peeling the SiO_2 NPs, the particles were disappeared at the membrane surface. In contrast, these spherical shape particles were observed again by sticking SiO_2 NPs. Pure water contact angles were also reversibly altered via repeatedly peel-and-stick process. The hydrophobicity of PTFE membrane was recovered by elimination of hydrophilic SiO_2 NPs. Then, contact angles were reduced by attaching SiO_2 NPs through DA reaction. Quantitative results for the peeling and sticking SiO_2 NPs were confirmed by EDXS (Figure V-14) and XPS (Figure V-15) analyses. The quantitative amount for a Si element was around 1 wt% by sticking SiO_2 NPs. As decoupling of SiO_2 NPs, the Si element was mostly reduced at the membrane surface.

The regeneration process for Ag-PTFE was also showed similar tendency of the SiO_2-PTFE. As shown in Figure V-16, C-O stretch (1113 cm^{-1}) and sp^3 C-H stretch (2879 cm^{-1}) which were derived from the F127-maleimide were repetitive reduced and regained by 3 cycles of peel-and-stick process. As sticking hydrophilic F127 stabilized Ag NPS, partially occupied layer was observed on the membrane surface (see Figure V-17). This layer was peeled off from the membrane surface after rDA reaction. Membrane surface hydrophilicity was enhanced by sticking F127-maleimide stabilized Ag NPs. The contact angles (see Figure V-17 inset) were recorded from 85.6° to 94.2° after coupling Ag NPs. In contrast, it was recovered after elimination of Ag NPs surface layer. The contact angles were from 134.0° to 147.9°. As shown in Figure V-18, the XPS signals assigned as Ag 3d orbital binding energy were observed. The quantity of Ag element was analyzed to 1.33 wt% for 1st cycle sticking Ag NPs. After peeling Ag NPs, the Ag XPS peaks were mostly reduced. The quantity of Ag element was also dramatically reduced due to absence of Ag NPs. As expected, the Ag elements were developed again after the second and third cycles for sticking process and the Ag NPs layer were readily removed by thermally driven peeling process. These combined results of surface analyses indicated that the surface assembled inorganic and metal nanomaterials can be reversibly functionalized by a thermally driven peel-and-stick process.

Membrane surface functionality is able to convert by the peel-and-stick process. Another functional material was coupled with the peeled membrane surface using DA reaction. Figure V-19(a) and V-20(a) show schematic illustration for conversion process from SiO_2-PTFE and Ag-PTFE,

respectively. Figure V-19 shows the conversion process from the SiO_2-PTFE. The SiO_2 NPs was peeled from the membrane surface and the PEG-maleimide or maleimide modified Ag NPs were then re-coupled with the peeled membrane surface by DA reaction. After peeling process, Si-O-Si stretch at 1093 cm^{-1} was disappeared at the membrane surface. As sticking the PEG-maleimide, the new IR bands assigned as O-H stretch, sp^3 C-H stretch 2870 cm^{-1} and imide C=O stretch at 1701 cm^{-1} were newly developed in the IR spectra for PEG-PTFE. Surface morphology was also changed by assembly of a dense PEG layer. Ag NPs was also successfully introduced onto the membrane surface via the conversion process. After sticking the maleimide modified Ag NPs, new IR bands such as O-H stretch, sp^3 C-H stretch at 2876 cm^{-1}, C-O stretch at 1106 cm^{-1} derived from the F127 stabilizer were observed in the Ag-PTFE. From FE-SEM imaging, polymeric layer was observed by conversion of the SiO_2 NPs into the F127 stabilized Ag NPs layer. In addition, 1.02 wt% of Ag element was detected by XPS analysis, indicating the Ag NPs layer successfully converted from SiO_2 NPs.

Figure V-20 shows the conversion process from the Ag-PTFE. To convert surface functionality, Ag NPs layer in the Ag-PTFE was removed by peeling process and then organic polymer layer (PEG) or inorganic layer (SiO_2 NPs) were re-coupled with the peeled membrane surface. In the ATR FT-IR spectra of peeled membrane, IR bands associated with Ag NPs were disappeared by peeling process. After re-coupling the PEG-maleimide or the maleimide modified SiO_2 NPs, the major IR bands for PEG-maleimide or SiO_2 NPs were appeared by conversion process. Surface morphologies were also altered by sticking different functionalities. Dense polymeric layer was

observed by sticking the PEG-maleimide. Aggregated particles appeared after sticking the SiO_2 NPs. XPS analysis confirmed presence of 0.84 wt% of Si concentration at the membrane surface. The Ag element did not detect by XPS analysis, disclosing the SiO_2 NPs layer successfully converted from Ag NPs. These combined results were indicated that new functionality was introduced to membrane instead of existing functionality through the thermally driven peel-and-stick process.

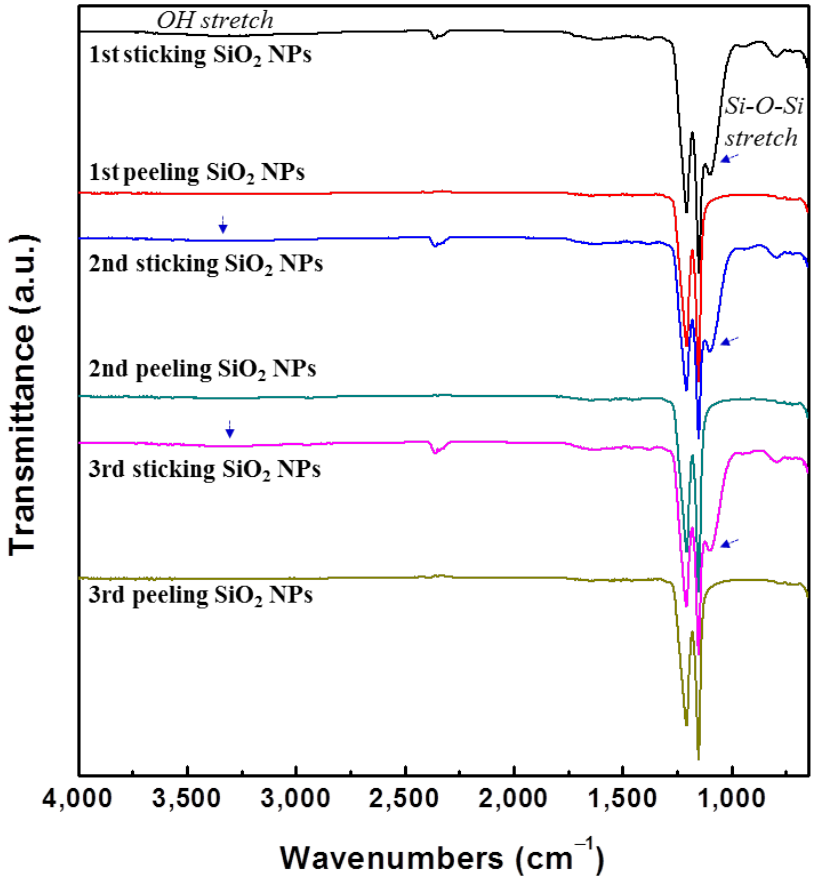

Figure V-12. ATR FT-IR spectra for SiO_2-PTFE by sticking SiO_2 NPs layer via Diels-Alder reaction and re-PTFE membrane by peeling of SiO_2 NPs layer via retro Diels-Alder reaction

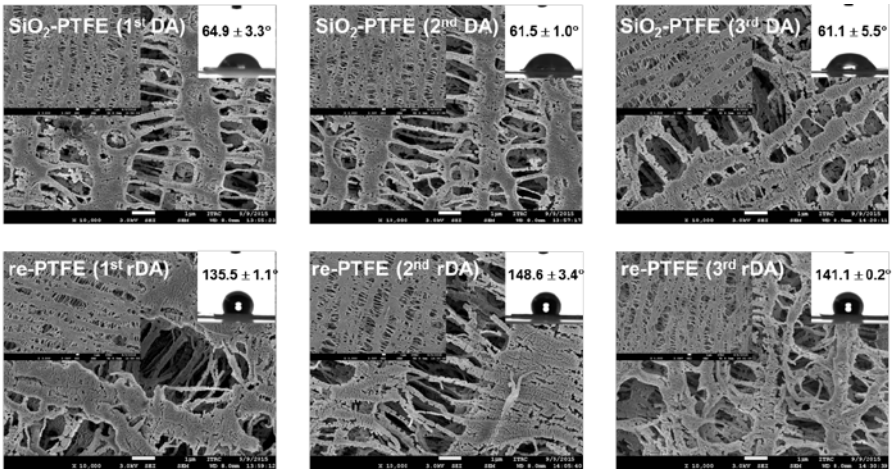

Figure V-13. FE-SEM images for top surface morphologies of SiO_2-PTFE membrane (top line) and re-PTFE membrane (bottom line), (Inset image) pure water contact angle

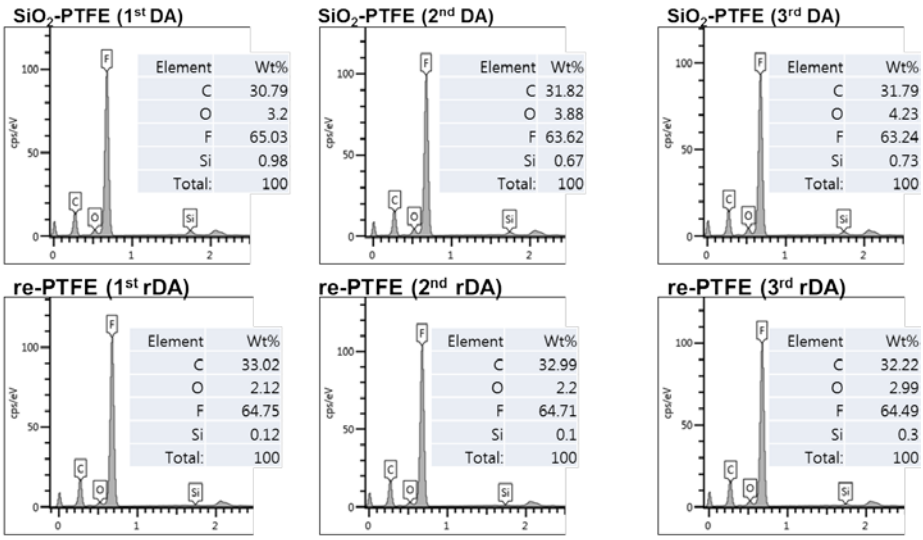

Figure V-14. EDXS results for SiO_2-PTFE membrane (top line) and re-PTFE membrane (bottom line), (inset table) chemical composition of membrane surface

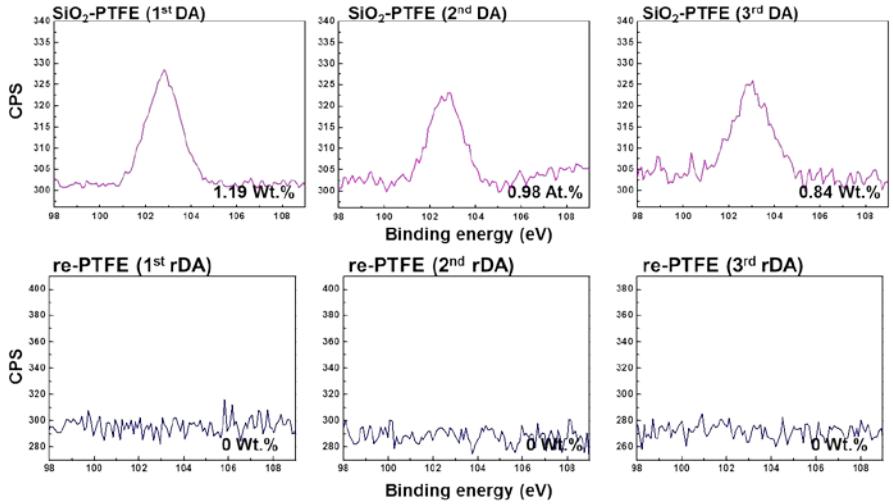

Figure V-15. XPS spectra of S 2p for SiO_2-PTFE membrane (top line) and re-PTFE membrane (bottom line)

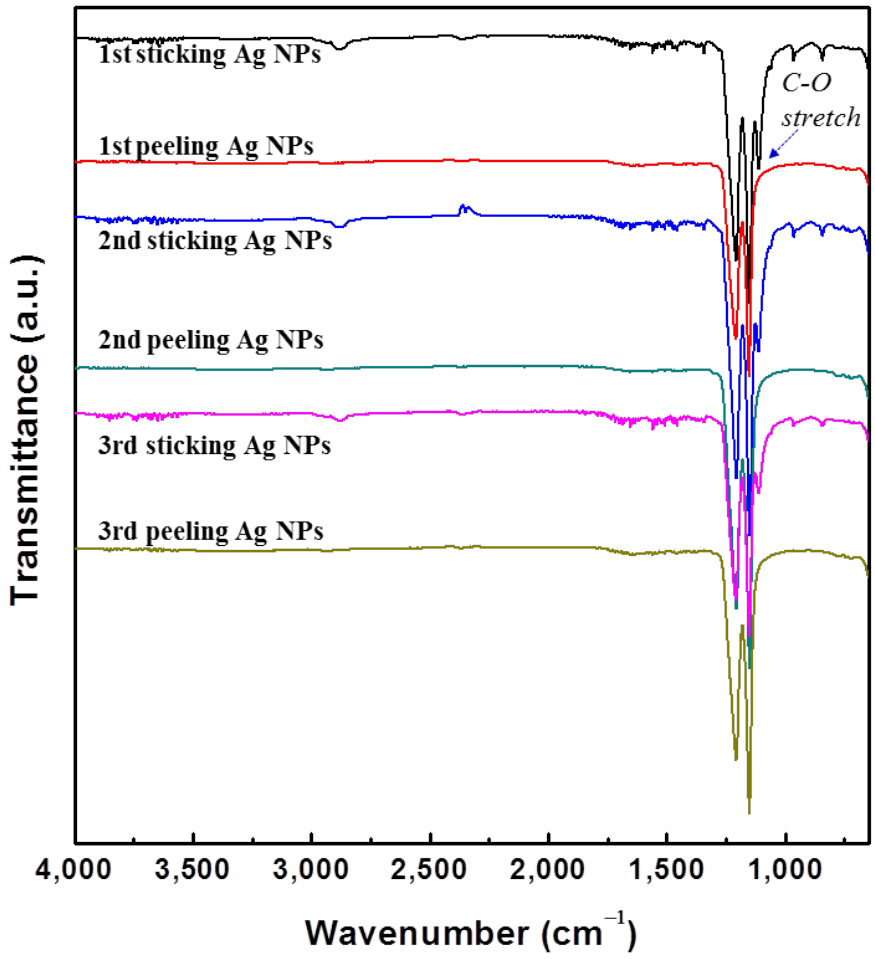

Figure V-16. ATR FT-IR spectra for Ag-PTFE by sticking Ag NPs layer via Diels-Alder reaction and re-PTFE membrane by peeling of Ag NPs layer via retro Diels-Alder reaction

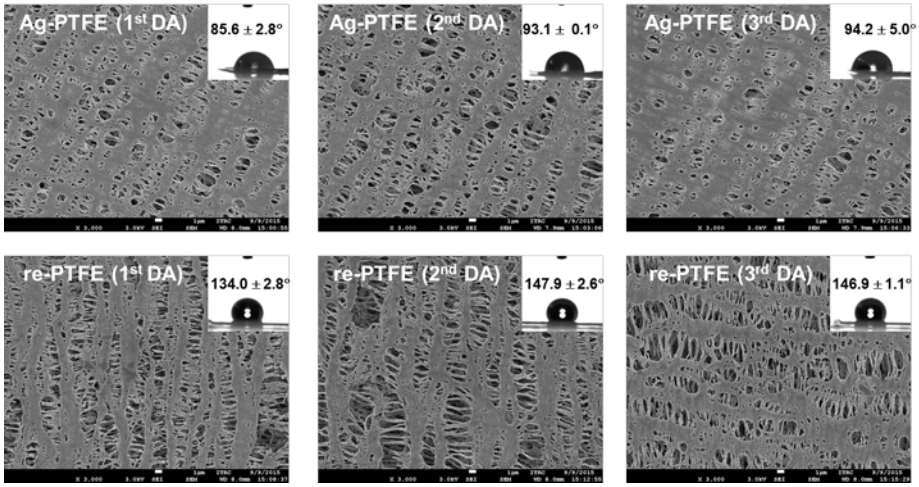

Figure V-17. FE-SEM images for top surface morphologies of Ag-PTFE membrane (top line) and re-PTFE membrane (bottom line), (Inset image) pure water contact angle

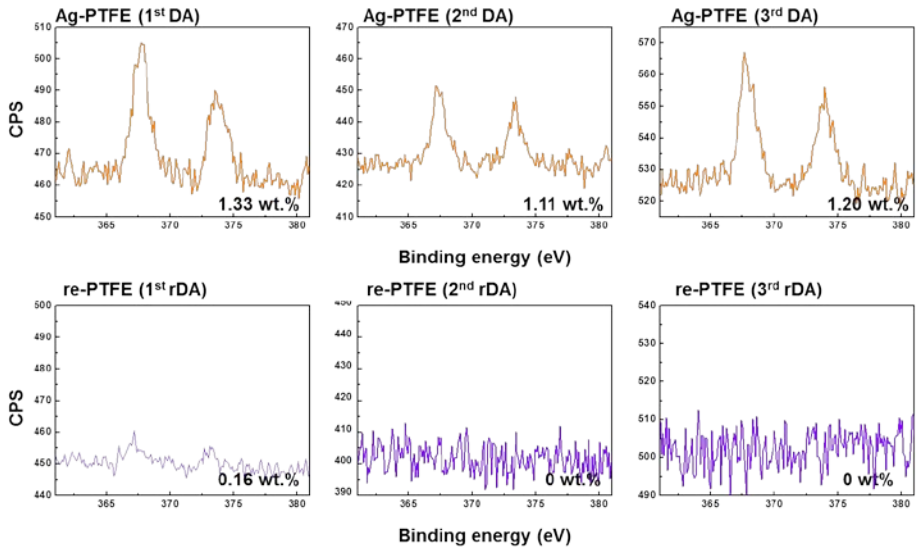

Figure V-18. XPS spectra of Ag 3d for Ag-PTFE membrane (top line) and re-PTFE membrane (bottom line)

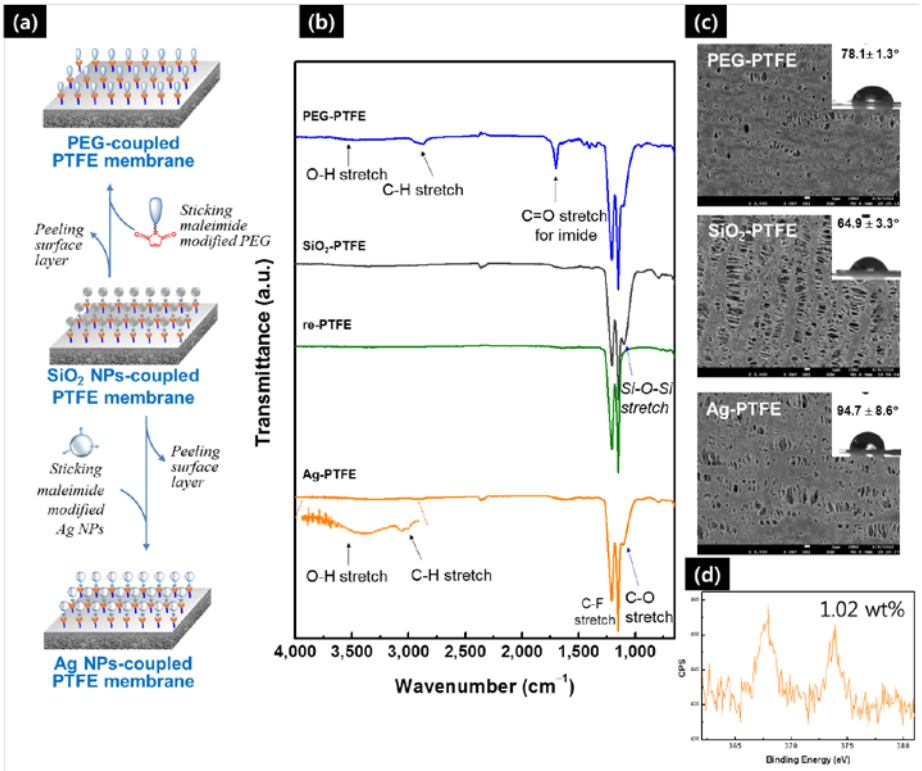

Figure V-19. (a) Schematic illustration of conversion process from SiO_2-PTFE, (b) ATR FT-IR spectra for PEG-PTFE converted from SiO_2-PTFE (1st line), SiO_2-PTFE (2nd line), re-PTFE prepared by peeling SiO_2 NPs layer form SiO2-PTFE (3rd line) and Ag-PTFE converted from SiO_2-PTFE (4th line), (c) FE-SEM images of PEG-PTFE converted from SiO_2-PTFE (top), SiO_2-PTFE (middle), Ag-PTFE converted from SiO_2-PTFE (bottom), (d) XPS spectra for Ag 3d of Ag-PTFE converted from SiO_2-PTFE

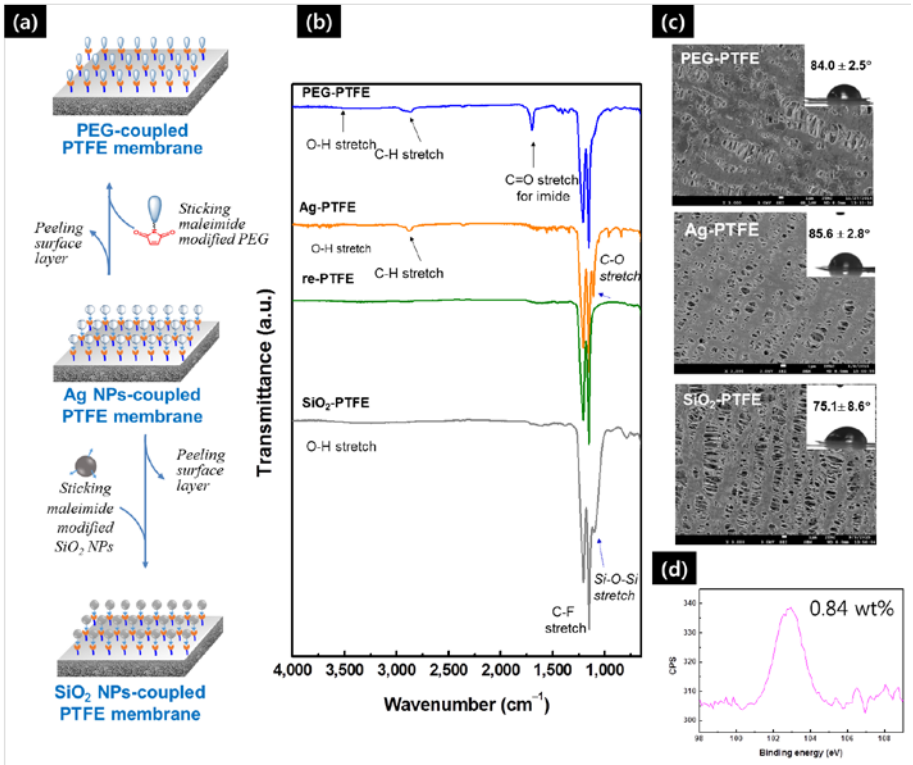

Figure V-20. (a) Schematic illustration of conversion process from Ag-PTFE, (b) ATR FT-IR spectra for PEG-PTFE converted from Ag-PTFE (1st line), Ag-PTFE (2nd line), re-PTFE prepared by peeling Ag NPs layer form Ag-PTFE (3rd line) and SiO_2-PTFE converted from Ag-PTFE (4th line), (c) FE-SEM images of PEG-PTFE converted from Ag-PTFE (top), Ag-PTFE (middle), SiO_2-PTFE converted from Ag-PTFE (bottom), (d) XPS spectra for Si 2p of SiO_2-PTFE converted from Ag-PTFE

V-3. Conclusions

In this chapter, a convertible membrane platform was verified by changing membrane surface introduced materials using thermally driven peel-and-stick process. SiO_2 and Ag NPs were selected as membrane surface modifying materials to prepare inorganic and metallic nanomaterials surface functionalized membrane, respectively. The combined results of FT-IR and ^1H NMR analyses showed that the maleimide derivatives were successfully synthesized. They were effectively functionalized at the surface of SiO_2 and Ag NPs for introducing maleimide moiety. The various surface analyses results indicated that the SiO_2 and Ag NPs were successfully coupled with the furan-modified PTFE membrane by DA reaction. As expected, the inorganic and metallic layers were repeatedly regenerated on the surface of the membrane through the peel-and-stick process, which was verified by ATR FT-IR, XPS, FE-SEM/EDXS results. In particular, surface chemical and morphological analyses were disclosed that the surface introduced functionalities were converted into desired other functionalities by the peel-and-stick process. This approach shows a new generation membrane platform by changing surface properties through adjusting thermal condition. This has various potential applications in advanced dynamic functionalized membrane processes through reversible control of surface functionality.

References and Notes

1. Lei, J.; Ulbricht, M., Macroinitiator-mediated photoreactive coating of membrane surfaces with antifouling hydrogel layers. *J. Membr. Sci.* **2014,** *455*, 207-218.

2. Ji, Y. L.; An, Q. F.; Zhao, Q.; Sun, W. D.; Lee, K. R.; Chen, H. L.; Gao, C. J., Novel composite nanofiltration membranes containing zwitterions with high permeate flux and improved anti-fouling performance. *J. Membr. Sci.* **2012,** *390-391*, 243-253.

3. Ba, C.; Ladner, D. A.; Economy, J., Using polyelectrolyte coatings to improve fouling resistance of a positively charged nanofiltration membrane. *J. Membr. Sci.* **2010,** *347* (1-2), 250-259.

4. Li, F.; Meng, J.; Ye, J.; Yang, B.; Tian, Q.; Deng, C., Surface modification of PES ultrafiltration membrane by polydopamine coating and poly(ethylene glycol) grafting: Morphology, stability, and anti-fouling. *Desalination* **2014,** *344*, 422-430.

5. Wang, P.; Tan, K. L.; Kang, E. T.; Neoh, K. G., Synthesis, characterization and anti-fouling properties of poly(ethylene glycol) grafted poly(vinylidene fluoride) copolymer membranes. *J. Mater. Chem.* **2001,** *11* (3), 783-789.

6 Xu, L. Q.; Chen, J. C.; Wang, R.; Neoh, K. G.; Kang, E. T.; Fu, G. D., A poly(vinylidene fluoride)-graft-poly(dopamine acrylamide) copolymer for surface functionalizable membranes. *RSC Adv.* **2013,** *3* (47), 25204-25214.

7. Sui, Y.; Wang, Z.; Gao, X.; Gao, C., Antifouling PVDF ultrafiltration membranes incorporating PVDF-g-PHEMA additive via atom transfer radical graft polymerizations. *J. Membr. Sci.* **2012,** *413-414*, 38-47.

8. Yang, Q.; Xu, Z. K.; Dai, Z. W.; Wang, J. L.; Ulbricht, M., Surface modification of polypropylene microporous membranes with a novel glycopolymer. *Chem. Mater.* **2005,** *17* (11), 3050-3058.

9. Wang, P.; Tan, K. L.; Kang, E. T.; Neoh, K. G., Plasma-induced immobilization of poly(ethylene glycol) onto poly(vinylidene fluoride) microporous membrane. *J. Membr. Sci.* **2001,** *195* (1), 103-114.

10. Zodrow, K.; Brunet, L.; Mahendra, S.; Li, D.; Zhang, A.; Li, Q.; Alvarez, P. J. J., Polysulfone ultrafiltration membranes impregnated with silver nanoparticles show improved biofouling resistance and virus removal. *Water Res.* **2009,** *43* (3), 715-723.

11. Rana, D.; Matsuura, T., Surface Modifications for Antifouling Membranes. *Chem. Rev.* **2010,** *110* (4), 2448-2471.

12. Ahmad, A. L.; Abdulkarim, A. A.; Ooi, B. S.; Ismail, S., Recent development in additives modifications of polyethersulfone membrane for flux enhancement. *Chem. Eng. J.* **2013,** *223*, 246-267.

13. Park, S. Y.; Chung, J. W.; Kwak, S.-Y., Regenerable anti-fouling active PTFE membrane with thermo-reversible “peel-and-stick” hydrophilic layer. *J. Membr. Sci.* **2015**, 491, 1-9.

14. Tasdelen, M. A., Diels-Alder "click" reactions: Recent applications in polymer and material science. *Polym. Chem.* **2011,** *2* (10), 2133-2145.

15. Wei, H. L.; Yang, Z.; Chen, Y.; Chu, H. J.; Zhu, J.; Li, Z. C., Characterisation of N-vinyl-2-pyrrolidone-based hydrogels prepared by a Diels-Alder click reaction in water. *Eur. Polym. J.* **2010,** *46* (5), 1032-1039.

16. Domingo, L. R.; Sáez, J. A., Understanding the mechanism of polar Diels-Alder reactions. *Org. Biomol. Chem.* **2009,** *7* (17), 3576-3583.

17. Wei, H. L.; Yang, Z.; Zheng, L. M.; Shen, Y. M., Thermosensitive hydrogels synthesized by fast Diels-Alder reaction in water. *Polymer* **2009,** *50* (13), 2836-2840.

18. Wei, H.-L.; Yang, Z.; Zheng, L.-M.; Shen, Y.-M., Thermosensitive hydrogels synthesized by fast Diels–Alder reaction in water. *Polymer* **2009,** *50* (13), 2836-2840.

19. Boday, D. J.; Stover, R. J.; Muriithi, B.; Keller, M. W.; Wertz, J. T.; DeFriend Obrey, K. A.; Loy, D. A., Strong, Low-Density Nanocomposites by Chemical Vapor Deposition and Polymerization of Cyanoacrylates on Aminated Silica Aerogels. *ACS Appl. Mater. Interfaces* **2009,** *1* (7), 1364-1369.

20. Soni, S. S.; Vekariya, R. L.; Aswal, V. K., Ionic liquid induced sphere-to-ribbon transition in the block copolymer mediated synthesis of silver nanoparticles. *RSC Adv.* **2013,** *3* (22), 8398-8406.

21. Angelescu, D. G.; Vasilescu, M.; Anastasescu, M.; Baratoiu, R.; Donescu, D.; Teodorescu, V. S., Synthesis and association of Ag(0) nanoparticles in aqueous Pluronic F127 triblock copolymer solutions. *Colloids Surf. Physicochem. Eng. Aspects* **2012,** *394*, 57-66.

국 문 초 록

수 처리 분리막 공정은 막을 투과시키는 단순한 과정을 통해 우수한 품질의 정화된 물을 경제적으로 얻을 수 있는 방법이다. 수 처리 분리막 공정은 분리막의 기공 크기와 구동압력에 따라 역삼투여과, 나노여과, 한외여과, 정밀여과 공정으로 크게 분류된다. 이중에서도 한외/정밀여과공정은 비교적 적은 에너지를 소모하면서 적절한 정화품질과 함께 생산성이 높아 산업, 공공분야에서 널리 이용되고 있다. 하지만, 분리막 공정을 적용하는데 있어 다양한 수중 오염물질(유기, 무기, 미생물 등)들이 분리막의 표면 또는 기공이 쌓이거나 막아 분리막 성능 및 수명을 감소시키는 분리막 파울링 현상이 발생된다. 분리막 파울링은 분리막의 성능을 저하시킬 뿐만 아니라 분리막의 세정 및 교체주기 증가 등 분리막 운영비용을 크게 증가시키게 된다. 이러한 분리막 파울링 현상을 억제하고자 다양한 형태의 기능성 재료들을 분리막에 도입시켜 내 파울링 기능성 분리막을 개발하는 연구가 활발하게 시도되고 있다. 그럼에도 불구하고, 이들 내 파울링 분리막의 상당수가 분리막 표면과 기능성 표층의 약한 상호작용으로 인한 내 파울링 기능성의 유실 또는 비가역적인 분리막 파울링에 의해 분리막의 성능이 점진적으로 저하되는 문제들이 발생한다. 따라서 본 연구에서는 강한 상호작용을 통해 내 파울링기능성 재료를 분리막에 도입시켜 지속성이 높은 내 파울링

분리막을 제조한다. 더 나아가 온도에 응답하여 가역적으로 결합 할 수 있는 기능성 층을 분리막 표면에 도입시켜 재생기능성 또는 기능성을 전환 시킬 수 있는 특성을 분리막에 도입시키고자 한다.

첫째, 내 스케일 기능성 분리막을 개발하기 위해 높은 양전하 밀도를 지닌 가지구조-폴리에틸렌이민 (branched-poly(ethylene imine) b-PEI)를 폴리비닐리덴플루오라이드 (poly(vinylidene fluoride) PVDF) 분리막에 도입시켰다. b-PEI 를 PVDF 분리막에 단단히 고정시키기 위해 b-PEI 말단을 양친성 고분자인 Brij S10 에 연결시켰고 이를 분리막 제조과정에 투입하여 친수성-소수성 자기집합 원리를 이용하여 분리막 표면에 고정시켰다. ATR FT-IR, FE-SEM, Zeta-potential, 표면기공분석 등으로 통해 양전하 b-PEI 가 표면 도입된 PVDF 분리막의 제조를 검증하였다. 순수 투과도 평가와 고농도 칼슘 이온과 실리카 입자 분산 용액을 이용해서 내 스케일링 기능성이 성공적으로 발현된 것을 확인하였다.

둘째, 고 내구성을 지닌 내 바이오파울링 기능성 분리막을 개발하기 위해 티올기를 지닌 링커를 이용하여 항균 기능을 지닌 은 나노입자를 PVDF 분리막 표면에 공유결합으로 도입시켰다. ATR FT-IR, FE-SEM, EDXS, XPS 분석을 통해 은 나노입자가 PVDF 분리막 표면에 성공적으로 도입되었음을 확인하였고, 연속적인 수 투과평가를 통해서 은 나노입자가 분리막 표면에서 유출 없이 단단히 결합되고 있음을 증명하였다. 대장균을 이용한

바이오파울링 저감평가를 통해 분리막 표면에 도입된 은 나노입자가 높은 효율로 파울링을 억제하는 것을 확인하여 고 내구성을 지닌 내 바이오파울링 분리막을 성공적으로 개발하였음을 확인하였다.

셋째, 비가적인 분리막 오염에 의해 내 파울링 기능의 한계를 극복하기 위해 내 파울링 기능성이 재생시킬 수 있는 분리막을 개발 하였다. 이를 위해 온도에 의해 조절 가능한 퓨란(furan)과 말레이미드(maleimide)의 Diels-Alder 반응을 이용하여 친수성 고분자 재료인 폴리에틸렌글리콜(poly(ethylene glycol), PEG)를 폴리테트라플루오로에틸렌(poly(tetrafluoro ethylene)), PTFE) 분리막에 도입하였다. ATR FT-IR, XPS, FE-SEM 분석을 통해 말레이미드로 말단 개질된 PEG 가 퓨란으로 표면 개질된 PTFE 분리막에 성공적으로 결합되었음을 확인하였고 온도조절을 통해 반복적으로 PEG 층이 재생 가능한 것을 증명하였다. 실리카 입자가 고 농도로 분산된 가상오염수 투과평가를 통해 PEG 가 결합된 PTFE 분리막은 효과적인 내파울링 기능성을 발현하였고 특히, 비가역적인 파울링을 분리막 재생을 통해 높은 효율로 제거 할 수 있음을 확인하였다.

넷째, 온도에 의해 조절 가능한 동적 결합을 통해 분리막 기능성의 전환가능성을 검증하였다. 이를 위해 실리카 나노입자와 은 나노입자를 각각 분리막 표면 개질용 무기, 금속재료 선정하였고 분리막 표면과 가역적인 결합을 위해 이들 표면에 말레이미드

작용기를 도입하였다. FT-IR, ^{1}H NMR 분석을 통해 말레이미드 유도체가 성공적으로 합성되었음을 증명하였고 말레이미드 유도체를 이용하여 말레이미드로 표면 개질된 실리카 나노입자와 은 나노입자가 제조되었음을 확인하였다. ATR FT-IR, XPS, FE-SEM 분석을 통해 말레이미드로 개질된 실리카 나노입자와 은 나노입자가 성공적으로 퓨란으로 개질된 PTFE 분리막 표면에 Diels-Alder 결합되고 온도 조절변수에 의해서 반복적으로 해당 기능성을 재생 시키는 것을 확인하였다. 최종적으로 유기재료인 PEG, 무기재료인 실리카 나노입자, 금속 재료인 은 나노입자들이 본 연구에서 제시한 온도에 의해 조절 가능한 결합을 통해 서로 분리막 표면에서 전환될 수 있음을 확인하였다.

본 연구에서는 다양한 내 파울링 기능성 (양전하, 항균성, 친수성)재료들을 수 처리 분리막 표면에 강한 상호작용을 통해 도입시켜 지속적으로 사용 가능한 내 파울링 기능성 수처리 분리막을 개발하였다. 특히, 가역적인 결합을 통해 제조된 내 파울링 기능성 분리막은 기존 분리막의 한계로 여겨지는 비가역적인 분리막 오염을 극복할 수 있고 표면 기능성의 변환시킬 수 있어 새로운 패러다임의 분리막 제조 방법으로 활용 될 수 있을 것으로 기대된다.

주요어: 수 처리 분리막, 한외/정밀여과, 내 파울링, 내 스케일링, 재생, 기능성 변환, 공유결합, 온도에 감응하는 동적 결합, Diels-Alder 반응
학번: 2007-22951

Paper Lists

1. **S. Y. Park**, J. W. Chung, R. D. Priestley, and S.-Y. Kwak, *Cellulose* **2012**, *19*, 2151.

2. **S. Y. Park**, J. W. Chung, Y. K. Chae, and S.-Y. Kwak, *ACS Appl. Mater. Interfaces* **2013**, *5*, 10705.

3. **S. Y. Park**, S. H. Choi, J. W. Chung, and S.-Y. Kwak, *J. Membr. Sci.* **2015**, *480*, 122.

4. **S. Y. Park**, J. W. Chung, and S.-Y. Kwak, *J. Membr. Sci.* **2015**, *491*, 1.

5. **S. Y. Park**, H. W. Ahn, J. W. Chung, and S.-Y. Kwak, *Desalination* **2016**, *397*,22

Patent Lists

1. 곽승엽, 박성용, '화학결합을 이용하여 금속 나노입자가 도입된 항균성 섬유의 제조방법 및 이로부터 형성된 항균성 섬유'

대한민국 특허등록 10-1046694 (출원일 2009. 5. 6)

2. 곽승엽, 박성용, '내바이오파울링성 수처리 분리막 및 그 제조방법'

대한민국 특허등록 10-1448551 (출원일 2013. 2. 20)

3. 곽승엽, 박성용, '재생 가능한 수처리 분리막 및 이의 제조방법'

대한민국 특허출원 10-2015-0108347 (출원일 2015. 8. 13)

4. 곽승엽, 박성용, 김예지, '양전하, 음전하 또는 중성입자로 표면개질된 내오염성 수처리 분리막 및 그 제조방법'

대한민국 특허출원 10-2015-0114841 (출원일 2015. 7. 30)

Symposium Lists

1. 2008년, ICIT 2008, "Preparation of Antimicrobial Textile with Covalent Attachment of Silver and Palladium Nanoparticles"

2. 2009년 춘계 고분자학회, "Evaluation of Antimicrobial Activity of Metal-Textile Nanohybrid with Covalent Attachment of Metal Nanoparticle on Textile"

3. 2009년, Seeing at the nanoscale Ⅶ, "Surface Analysis of Antimicrobial Metal-Textile Nanohybrid with Covalent Attachment of Metal Nanoparticle on Textile"

4. 2010년 춘계 고분자학회, "Fabrication of Cyclodextrin-Textile Hybrid via Covalent Attachment of Cyclodextrin on Cellulosic Textile"

5. 2010년, ICIT 2010, "Preparation and Characterization of Metal-Textile Hybrid with Covalent Attachment of Metal Nanoparticle on Textile"

6. 2010년 추계 고분자학회, "The Assembly of Mesoporous TiO_2 on Cellulose Textile by Epoxy Silane Coupling Agent for Preparing VOCs Protective Textile"

7. 2010년, ICBEC 2010, "Antibacterial Metal-Fiber Hybrid with Covalent Assembly of Silver and Palladium Nanoparticles on Cellulose Fibers"

8. 2011년, ATC11, "Composite Nanofiber Mat with Transition Metal Incorporated Mesoporous TiO_2 for Protective Clothing Against Chemical and Biological Warfare Agents"

9. 2012년, AMS7, "Preparation and Characterization of Silver Nanoparticle Assembled Polysulfone (PSF) Membrane"

10. 2013년 춘계고분자학회, “Preparation and Characterization of Silver-Polyvinylidene Fluoride (PVDF) Membrane Nanocomposite and Its Anti-biofouling Property”

11. 2013년 춘계 막학회, “Surface Functionalized Fluorinated UF/MF Membrane for Endowment of Fouling Resistance and Removal of Heavy Metal Ions”

12. 2013년, HKICEAS 2013, “Metal- and Inorganic- Cellulose Textile Hybrids for Biological and Chemical Protection”

13. 2014년 추계 대한화학회, “Assembly of metal and functional polymers to fluorinated ultrafiltration (UF) membranes for anti-fouling and heavy metal removal”

14. 2015년, MRS FALL MEETING, “Development of Regenerative Anti-biofouling Membrane by Thermo-Reversible Diels-Alder (DA) Reaction”